N° d'ordre : …… **Année 2020**

Université de Djillali Liabès -Sidi Bel Abbès-
Faculté de Génie Électrique
Département de Télécommunications
Laboratoire de Télécommunications et de Traitement Numérique du Signal

THESE DE DOCTORAT

Pour l'obtention du diplôme de Doctorat en Sciences

Spécialité : **Télécommunications**
Option : **Systèmes des télécommunications**

Présentée Par

DEHRI Brahim

RECONNAISSANCE DE L'ENVIRONNEMENT RADIO-MOBILE PAR LA RADIO COGNITIVE

Soutenu le : 04/11/2020, devant le jury composé de :

Mr. DJEBBARI Ali	**Pr**	**Président**	**UDL-SBA**
Mr. DJEBBAR Ahmed Bouzidi	**Pr**	**Directeur de thèse**	**UDL-SBA**
Mr. BENADDA Belkacem	**Pr**	**Examinateur**	**Université de Tlemcen**
Mr. BENAISSA Mohamed	**MCA**	**Examinateur**	**Centre Universitaire Ain Témouchent**
Mr. BOUZIANI Merahi	**Pr**	**Invité**	**UDL-SBA**

Année Universitaire 2019-2020

Dedication

I dedicate this work to

My mother

My brothers and sisters

All my friends and colleagues

All those who will recognize themselves throughout these few lines.

Acknowledgments

Praise be to Allah Almighty who gave me the strength to accomplish this work, as well as the audacity to overcome all difficulties.

I would like to express my deep and sincere gratitude to my research supervisor, **Pr. A. B. DJEBBAR**, for giving me the opportunity to do this wonderful project on the topic cognitive radio environment and providing invaluable guidance throughout this research. His dynamism, vision, sincerity and motivation have deeply inspired me.

He has taught me the methodology to carry out the research and to present my work as clearly as possible. It was a great privilege and honor to work with him and study under his guidance, I'm extremely grateful for what he has offered me. I would also like to thank him for his patience, motivation, enthusiasm, and immense knowledge. I could not imagined having a better advisor and mentor for my PhD study.

I would like to thank my fellow lab mates in the Telecommunications and Digital Processing Laboratory (LTTNS) at Djillali Liabes university, particularly **Pr. A. DJEBBARI**, the director of the LTTNS laboratory and **Mrs. L. DASSI**, laboratory engineer. I would like also to thank my research fellows **Pr. I. DAYOUB** for the stimulating discussions, for the hard work we were working together before deadlines.

I highly appreciate the jury members **Pr. DJEBBARI Ali**, **Pr. BENADDA Belkacem**, **Pr. BOUZIANI Merahi**, and **Dr. BENAISSA Mohammed** who devoted part of their precious time to examine and judge my work.

Abstract

Research in the field of cognitive radio (CR) has emerged to meet both the military's communication and the public safety sector needs. The CR often share the same requirements as civilian radio-mobile telecommunication operators.

One of the main features of a CR device is to be aware of its radio environment and to detect available bands. The objective of the research work in this doctoral thesis is to develop a blind digital modulation identification algorithm that can be used for STBC-MIMO and STBC-OFDM systems.
The modulation identification process requires four steps: 1- The extraction of higher order statistics (HOS) from the signal; 2- HOS processing (normalization and use of PCA to keep only a subset of HOS with large variance); 3- The use of Pattern Recognition tools (ANN, SVM, RF and KNN) for modulation classification; 4- The improvement of classification using a decision fusion center. The results obtained show the effectiveness of the proposed algorithm.

Keywords: Multi-carrier, Cognitive radio, spectral sounding, blind waveform identification, multiple antennas, multiple-input multiple-output systems.

Résumé

Les recherches dans le domaine de la radio cognitive (CR) ont vu le jour afin de répondre aux besoins de communication de l'armée ainsi qu'aux besoins dans les secteurs de la sécurité publique. La CR partage souvent les mêmes exigences que les opérateurs de télécommunication radio-mobile civile.

Une des principales fonctionnalités d'un dispositif de radio cognitive est de prendre conscience de son environnement radioélectrique et de détecter les bandes disponibles. L'objectif du travail effectué dans le cadre de cette thèse de doctorat est de développer un algorithme qui sera utiliser pour l'identification aveugle de modulations numériques pour les systèmes STBC-MIMO et STBC-OFDM. Le processus d'identification de modulation exige quatre étapes : 1- L'extraction des statistiques d'ordre supérieur (HOS) à partir du signal ; 2- Le traitement des HOS (normalisation et utilisation de la PCA pour ne garder qu'un sous ensemble de HOS à grande variance) ; 3- L'utilisation des outils de Pattern Recognition (ANN, SVM, RF et KNN) pour la classification de modulation ; 4- L'amélioration la classification en utilisant un centre de fusion des décisions. Les résultats obtenus montrent l'efficacité de l'algorithme proposé.

Mots Clef: Multi-porteuses, Radio cognitive, sondage spectral, identification aveugle de la forme d'onde, antennes multiple, Systèmes multiple-input multiple-output.

ملخص

ظهرت الأبحاث في مجال الراديو الادراكي أو المعرفي (CR) لتلبية كل من الاتصالات العسكرية واحتياجات قطاع السلامة العامة. غالباً ما يتشارك CR نفس المتطلبات مع مشغلي الاتصالات اللاسلكية.

تتمثل إحدى السمات الرئيسية لجهاز CR في الانتباه إلى بيئته الكهرورادیوية واكتشاف النطاقات أو الترددات المتاحة. الهدف من العمل البحثي في أطروحة الدكتوراه هذه هو تطوير خوارزمية يمكن استخدامها لمعرفة التعديل الرقمي في أنظمة STBC-MIMO وSTBC-OFDM تتطلب عملية تحديد التعديل إلى أربع خطوات: 1)- إستخدام الإشارة المقدرة لاستخراج الإحصائيات برتبة أعلى (HOS) ؛ 2)- معالجة HOS (تحسين واستخدام PCA للحفاظ على مجموعة فرعية فقط من HOS مع تباين كبير)؛ 3)- استخدام أدوات التعرف على الأشكال (ANN، SVM، RFC، و KNN) لتصنيف التعديل، 4)- تحسين التصنيف باستخدام مركز دمج التصنيفات الفرعية. تُظهِر النتائج التي تم الحصول عليها فعالية الخوارزمية المقترحة.

كلمات مفتاحية: الموجات الحاملة المتعددة، الراديو الادراكي أو المعرفي، السبر الطيفي، التحديد الأعمى لشكل الموجة، هوائيات متعددة، أنظمة متعددة المخرجات متعددة المدخلات.

Contents

3. Digital Modulation Classification in MIMO-OFDM Systems

Appendices

List of Figures

List of Tables

Mathematical notations and acronyms

Mathematical notations

- Upper (lower) bold face letters indicate matrices (column vectors).
- $[\mathbf{F}_N]_{m,n} = \frac{1}{\sqrt{N}}\exp(-2j\pi mn/N)$ is the $(N \times N)$ Fast Fourier transform (FFT) matrix.

$(\cdot)^*$	:	Complex conjugate
$(\cdot)^T$	:	Transpose
$(\cdot)^\#$	:	Pseudo-inverse
$(\cdot)^{\mathcal{H}}$	:	Hermitian
$\|\cdot\|$	:	Euclidean norm
$\|\cdot\|_F$	:	Frobenius norm
$\otimes$	:	Kronecker product
$\Re(\cdot)$	:	Real part
$\Im(\cdot)$	:	Imaginary part
$E[\cdot]$	:	Expectation
$\lceil\cdot\rceil$	:	Maximum ceiling function of scalar argument.
$\mathbf{D}_N(\mathbf{h})$	:	Diagonal matrix of $(N \times N)$ with the vector $\mathbf{h}$ its main diagonal
$\log(\cdot)$	:	Logarithm
$\ln(\cdot)$	:	Natural logarithm
N_t	:	Number of transmitting antennas.
N_r	:	Number of receiving antennas.
N_s	:	Number of STBC encoder inputs vectors.
N	:	Number of observed samples.
L	:	Number of channel coefficients (channel order)
σ_x^2	:	Variance of x
ρ	:	Correlation coefficient
φ_0	:	Phase offset
s_I	:	Phase component
s_Q	:	Quadrature component
T_s	:	Sampling period

$\mathrm{tr}(\mathbf{X})$	:	Trace of the matrice $\mathbf{X}$
$[\mathbf{A}]_{m,n}$	:	(m,n)-th entry of a matrix $\mathbf{A}$
$[\mathbf{x}]_m$	:	m-th entry of a column vector $\mathbf{x}$
$\mathbf{I}_N$	:	Identity matrix of $(N \times N)$
$\mathbf{e}_N^{(i)}$	:	i-th column of the identity matrix $\mathbf{I}_N$
$\mathbb{P}(\cdot)$	:	Probability of an event
P_i	:	Probability of Identification
P_{ci}	:	Probability of Correct Identification
P_{fa}	:	Probability of False Alarm
$S\alpha S(\cdot)$	:	Symmetrical α-Stable distribution
$\mathrm{card}(\Theta)$	:	Cardinal of Θ
α	:	Stability index
β	:	Skewness index
γ	:	Scale parameter
δ	:	Location parameter

Acronyms

ANN	:	Artificial Neural Network
ASK	:	Amplitude Shift Keying
AWGN	:	Additive White Gaussian Noise
BDMC	:	Blind Digital Modulation Classification
BER	:	Bit Error Rate
BLAST	:	Bell Labs Layered Space-Time
BP	:	Back Propagations
BPSK	:	Binary Phase Shift Keying
BSS	:	Blind Source Separation
CDF	:	Cumulative Density Function
CFO	:	Carrier Frequency Offset
CMA	:	Constant Modulus Algorithm
CP	:	Cyclic-Prefix
CR	:	Cognitive Radio
CSCG	:	Circularly Symmetric Complex Gaussian
CSI	:	Channel State Information

DMC	:	Digital Modulation Classification
DSA	:	Dynamic Spectrum Access
FDM	:	Frequency Division Multiplexing
FFT	:	Fast Fourier Transform
GSNR	:	Generalized Signal to Noise Ratio
HOC	:	Higher Order Cumulants
HOM	:	Higher Order Moments
HOS	:	Higher Order Statistical
ICI	:	Inter-Carrier Interference
IFFT	:	Inverse Fast Fourier Transform
i.i.d	:	Independent and Identically Distributed
ISI	:	Inter-Symbol Interference
KNN	:	K-Nearest Neighbors
MF	:	Myriad Filter/Filtering
MIMO	:	Multiple-Input Multiple-Output
MIMO-SC	:	Multiple-Input Multiple-Output Single-Carrier
ML	:	Maximum Likelihood
MLP	:	Multi-Layer Perceptron
MMSE	:	Minimum Mean Square Error
MSE	:	Mean Squared Error
MUSIC	:	MUltiple SIgnal Classification
OFDM	:	Orthogonal Frequency Division Multiplexing
OSI	:	Open System Interconnection
OSTBC	:	Orthogonal Space-Time Block Code/Codes/Coding
PAPR	:	Peak to Average Power Ratio
PCA	:	Principal Component Analysis
PDA	:	Personal Digital Assistant
PS	:	Primary Sources
PSK	:	Phase Shift Keying
PU	:	Primary User(s)
QAM	:	Quadrature Amplitude Modulation
QoS	:	Quality of Service
QPSK	:	Quadrature Phase Shift Keying
RFC	:	Random Forest Classifier

r.v	:	random variable(s)
SC	:	Single-Carrier
SCMA	:	Simplified Constant Modulus Algorithm
SDR	:	Software-Defined Radio
SF	:	Space-Frequency
SFBC	:	Space-Frequency Block Code/Codes/Coding
SG	:	Stochastic Gradient
SIMO	:	Single-Input Multiple-Output
SISO	:	Single-Input Single-Output
SISO-SC	:	Single-Input Single-Output Single-Carrier
SM	:	Spatial Multiplexing
SM	:	Spatial Multiplexing
SNR	:	Signal to Noise Ratio
SR	:	Software Radio
ST	:	Space-Time
STBC	:	Space-Time Block Code/Codes/Coding
STTC	:	Space-Time Trellis Code/Codes/Coding
SU	:	Secondary User
SVM	:	Support Vector Machines
VSC	:	Virtual Sub-Carriers
ZF	:	Zero-Forcing

Introduction

Research motivations

Todays, the need for more mobility and ability to share or exchange information at any time, using mobile devices (cell phones, personal digital assistant (PDA), laptops) has yield the notion of intelligent networks, or cognitive networks very widespread. This technological progress makes currently, telecommunications networks in the context of cognitive radio one of the most active domains of computer research.

The increasing on new technologies of wireless applications has considerably limited the use of the available radio spectrum, which has become a precious resource. Numerous research on the spectrum management shows that the spectrum is rarely used in totality, and that certain frequency bands of the radio spectrum are unoccupied, others less occupied and little used.

The cognitive radio (CR) is a technique to overcome this underutilization of the spectrum with which an unlicensed secondary user (SU) seeking to use idle parts of the spectrum when transmission from the licensed primary users (PU) is absent. One of the CR functions, called *spectrum detection*, allows a CR device to permanently search for free bands and to detect the spectrum holes (frequency band sufficiently free to be able to use them) [1].

Spectrum detection is an essential function for increasing the capacity of any CR system. To achieve these objectives, the CR must identify certain basic characteristics of the intercepted signal, that is: Single-carrier and multi-carriers transmission identification, identification of the coding type, and identification of the modulation type [2-3].

The digital modulation classification (DMC) process is considered an intermediate step between intercepting signals and informations retrieval. The application of DMC is found in communication systems such as spectrum monitoring, interference identification, and adaptive receivers in software-defined radio (SDR). A lot of research concerning modulation recognition methods has been proposed. They have objective to develop rapid and precise algorithms to produce acceptable results in real applications.

Previous published research on the modulation identification topic was limited to single-input single-output – single-carrier (SISO-SC) systems [4-5], and for multi-input multi-output – SC (MIMO-SC) systems [6-7]. Only a few studies deal with the modulation classification

problem for MIMO-Orthogonal Frequency Division Multiplexing (MIMO-OFDM) systems [8-9]. The contribution that we brought through this thesis is to examine the impact of the joint estimation of channel and carrier frequency offset (CFO) on the digital modulations identification for MIMO-OFDM systems operating in frequency selective channel and in the presence of impulsive noise.

The DMC problem for MIMO-OFDM systems is more difficult than in the case of MIMO-SC systems, because the OFDM technique is extremely sensitive to transmission degradations. For cognitive devices, it is highly desirable to develop a DMC algorithm, which is robust to synchronization and channel errors for MIMO-OFDM systems. In this context, we propose a low-complexity blind and semi-blind joint estimation method of MIMO channels and CFO. Furthermore, in most research, the assumption of Gaussian noise is considered. However, this assumption is not applicable in railway communications where noise is considered not Gaussian and impulsive. The existence of impulsive noise is not often taken as a working hypothesis. This is the reason why we are interested in studying this noise, and their reduction methods, and this in order to improve the performance of DMC. Contrary to Gaussian white noise, impulsive noise has a non-standard statistic; it is generally non-stationary, non-Gaussian and of very complex frequency behavior. This considerably degrades the transmission characteristics of MIMO-OFDM signal [10].

Reducing impulsive noise in the received signal is a difficult task. In this context, various studies and measures have been developed to model the heavy-tail impulsive noise. In [11], it has been proven that the symmetrical α-stable ($S\alpha S$) distribution allows it possible to model the impulsive noise generated in railway environnements. Authors in [11] - [14] address the problem of modulation detection in an impulsive environment. The method introduced in this thesis to reduce the effect of impulsive noise is based on Myriad filtering [15]. The results obtained are better and reflect the robustness of the methods proposed regarding to synchronization and MIMO channels errors, and to impulsive noise.

The existing DMC algorithms in literature can generally be classified into two categories: **1)** *Algorithms based on the criterion of maximum likelihood*: these algorithms based on likelihood consider the modulation classification problem as an inference task, where the classification decisions are taken by maximizing the likelihood function of each candidate modulation type. These algorithms characterized by a very high computational complexity, which increases significantly with MIMO antennas number [16]. **2)** *Algorithms based on features extraction*, from the received signal using a higher order statistical (HOS). These specific features extracted from the received signal in order to discriminate the candidate modulation types using a certain classifier.

Functionality-based algorithms are efficient in terms of lower computational complexity in general and more practical for real-time applications [17]. The HOS used for the features extraction, are combined with pattern recognition methods to solve the modulation identification problem. The digital modulations types concerned by the identification in this thesis are [2, 4, 8]-PSK, [4, 8]-ASK and [16, 64]-QAM. The channels considered for the simulations are multipath Rayleigh type.

Thesis contributions

The spectrum detection in radio mobile environment is the main function of CR. For this, all the parameters that could affect the performance of the detection, such as interference, frequency offsets, spatial correlations, and impulsive noise must be estimated.

The CR detection capacity is improved by identifying several characteristics contained in the received signal, that is: the number of transmitted antennas, the noise power, the channel effects, the frequency offset, the modulation and the coding type. These detected informations from the radio domain are introduced into the operational platform of CR.

In this thesis, we focus on the identification of the modulations type contained in the received signal. The main contributions of this thesis are summarized as follows:

1- Based on the extraction of HOS and on the pattern recognition methods, we were able to identify the modulation type used by MIMO system operating space-time block coding (STBC) with spatial correlation.
2- To improve the quality of the identification, it is necessary to estimate the parameters affecting the detected signal. For this, we blindly and semi-blindly estimate the frequency offset and the MIMO channels.
3- The assumption of Gaussian noise is no longer valid for developing and evaluating modulation identification algorithms used by CR devices in railway environnements. The noise generated in this environnement is of impulsive type. Impulse noise of the heavy-tails type, considered the most severe, will significantly degrade the performance of the transmission system. This noise is modeled by the symmetrical α-stable distribution. To reduce these effects, we will estimate the parameters characterizing this noise. These estimates are used to design a Myriad filter (MF). Applying the Myriad filter to the MIMO-OFDM system improves these performances.

The ultimate goal is to build a practical, robust and light classifier that must be able to identify almost all the different modulation schemes used in different telecommunications systems and

for different transmission scenarios. The modulation type and order must be recognized at the same time and without a priori information of the received signal. Processing time must be reduced to ensure real-time operating conditions.

The various studies of the DMC problem over the past decades have made a lot of progress, but never have an optimal classifier. Some algorithms require a priori information about the signal (for example, carrier frequency, signal bandwidth, baud rate, offset synchronization, etc.), others require a high signal to noise ratio (SNR) value. Some classifiers are limited to identifying a small number of modulation types; others cannot be used in real-time applications [1].

Therefore, through this thesis we were able to develop an optimal blind classifier of digital modulations used by MIMO-OFDM system, and this in a realistic environment characterized by the presence of multipath, CFO, and impulsive noise. The results obtained demonstrate the effectiveness of the proposed algorithms.

Thesis organization

This thesis is divided into three chapters. In the first chapter, we have reviewed the main characteristics defining cognitive radio. Then, the second chapter presents the techniques for digital modulations classifications in STBC-MIMO systems. Finally, the methods of digital modulations identification in MIMO-OFDM systems are studied in chapter 3.

The first chapter describes the concept of CR, its definition, its architecture, its cycle, and its possible applications.

The second chapter discusses the digital modulation identification process for spatially correlated STBC-MIMO systems. In this part, we examine the particular constraints inherent in the particular nature of radio environment, which is spatial correlation, radio channel interference, etc. The spatial correlation between the system antennas is a practical problem that could decrease the performance of the system. The extraction of HOS, i.e. the functionalities as well as their exploits by the pattern recognition algorithms allowed us to classify several modulations types with different orders.

Since the modulation classification in MIMO-OFDM systems has not been discussed previously at least to the best of our knowledge, chapter 3 proposes the blind digital modulations identification in MIMO-OFDM systems, i.e., multi-carriers or wideband systems. In order to improve identification, joint semi-blind channels and CFO estimation, and impulsive noise reduction, are necessary. The results obtained reflect the robustness of the developed algorithm to the errors introduced by channel.

List of publications and communications

☞ **Publication in an International Journal**

- B. DEHRI, M. BESSEGHIER, A. B. DJEBBAR, I. DAYOUB; *"Blind Digital Modulation Classification for STBC-OFDM System in Presence of CFO and Channels Estimation Errors*", IET Communications, vol. 13, no. 17, pp. 2827-2833, 29 October 2019.

☞ **Communications in International Conferences with Reading Committee**

- B. DEHRI, A. B. DJEBBAR, "*Performance Analysis of STBC-OFDM and SFBC-OFDM Systems*;" 1st International Conference on Networking Telecommunications, Biomedical Engineering and Applications (ICNTBA'19), Boumerdes, Algeria, November 4 – 5, 2019.
- B. DEHRI, A. B. DJEBBAR, "*Effect of Impulsive Noise Reduction on Digital Modulation Classification for STBC-OFDM Systems*," 8th International Conference On Defense Systems : Architectures and Technologies (DAT'2020), 2020, Constantine, Algeria.

☞ **National Communications**

- B. DEHRI, A. B. DJEBBAR, I. DAYOUB, *"Digital Modulation Classification with Channel Errors for MIMO-STBC System*," Oral Communication, 2nd JDGE (Deuxièmes Journées Doctorales de Génie Electrique), Sidi Bel Abbes, December 4-5, 2018.
- B. DEHRI, A. B. DJEBBAR, "*Performance Analysis of SFBC-OFDM Systems in Frequency Selective Fading Channel*," Oral Communication, 3rd JDGE (Troisièmes Journées Doctorales de Génie Electrique), Sidi Bel Abbes, December 17-18, 2019.

Chapter 1

Introduction to Cognitive Radio

Contents

1.1 Introduction

The radio spectrum is one of the most widely used natural resources around the world, and is regulated by government agencies. Most frequency bands are authorized for the long term over large geographic areas. Recent studies indicate that many portions of the licensed spectrum are not used for long periods of time or in certain geographic areas. A wider range of applications operating in unlicensed bands causes overpopulation in this band. It is increasingly difficult to find frequency spectra which can be made available either for new services or to develop an existing service [1].

Consequently, it has become necessary to find new methods for managing radio frequency resources. To this end, a new technique, called *cognitive radio*, has appeared. One of the main functions of a CR device is to become aware of its radio environment and to detect the available bands [18]. CR is an optimal solution for managing radio frequency resources. This will at some point allow unauthorized users (SU) to detect and intelligently access the unoccupied portions of spectrum or spectrum holes (see figure 1.1) i.e. which is not used by authorized users (PU).

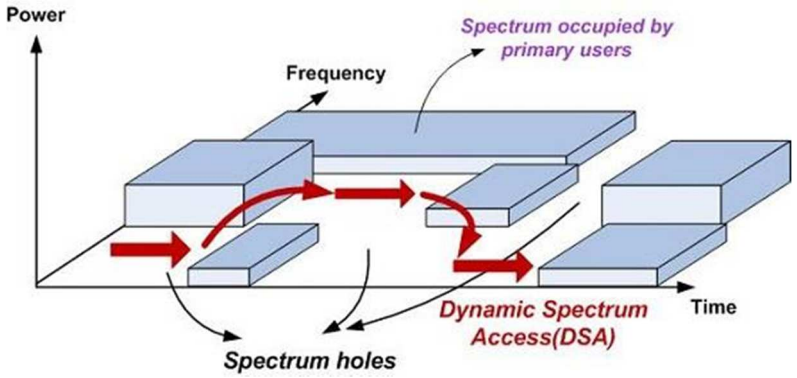

Figure 1.1- Spectrum holes concept [19].

Cognitive radio systems must also be able to recognize the different wireless networks deployed in their environment and their transmission characteristics and to be able to communicate with these networks. The identification of the some key characteristics of the signals present in the analyzed band can significantly enhance the performance at the receiver's side.

1.2 From information theory to cognitive radio

In 1948, Claude Elwood Shannon [20] invented a new theory known as "*information theory*" which has radically changed the vision of modern telecommunications. In his work, Shannon provided

in particular the answer to a fundamental telecommunications problem concerning the quantity of information transferred without errors between two nodes, which communicate in a given environment at a given time. However, the rate of information transmitted without error is naturally limited by the bandwidth of the communication environment and the signal transmission power. Therefore, if one of these three basic resources reaches its limit, we cannot effectively transmit information [21].

In this context, Joseph Mitola in his research work [18] explained that the inefficient use of radio frequency resources (in particular bandwidth) has resulted in a huge waste of these resources.

1.3 The cognitive radio definition

The "Cognition" is a process by which we acquires knowledge; it regroup the various mental processes ranging from perceptual analysis of the environment to motor control via memorization, reasoning, emotions and language.

Cognitive radio is used to describe a radio system with the ability to detect its radio frequency environment allowing it to adjust its transmission parameters in an interactive, dynamic and autonomous manner.

This capacity allows each radio device to adapt to current spectral conditions and therefore offers users more flexible, efficient and complete access to this resource. This approach can significantly improve data throughput and range of links without increasing bandwidth or transmission power. The CR also offers a balanced solution to the problem of spectrum congestion by first granting priority use to the owner of the spectrum and then allowing others to use unused portions of the spectrum [18].

1.4 Cognitive cycle

Introducing a cognitive cycle allows the CR to analyze its context and act accordingly. Many variants have been proposed [18, 22-24] but we can reduce all of them to the generic cycle presented in figure 1.2.

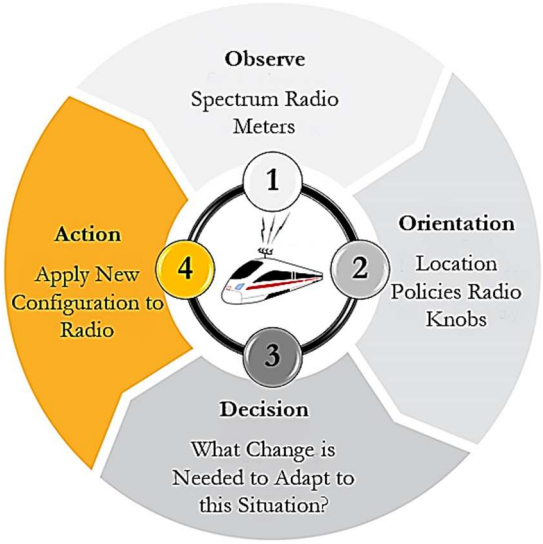

Figure 1.2- The generic cognitive cycle [25].

This cycle includes four essential capacities for any autonomous agent [26]:

- The ability to observe: The resource has sensors to collect information on its operational context.
- The ability to orient: The resource influences its environment through its actuators. The transmitted signal occupies spectral resources and the applied processing consume energy resources. The radio can reconfigure itself and thus modulate this influence according to the situation and the objectives of quality of service (QoS).
- The ability to decide: The resource exploits the information collected to identify the most suitable configuration and learn from its experiences.
- The ability to act: application of the new configuration on the radio.

1.5 The cognitive radio architecture

In the literature, there are several architectures of CR according to the studied system [1, 27-28]. Figure 1.3 represents one of these architectures [27].

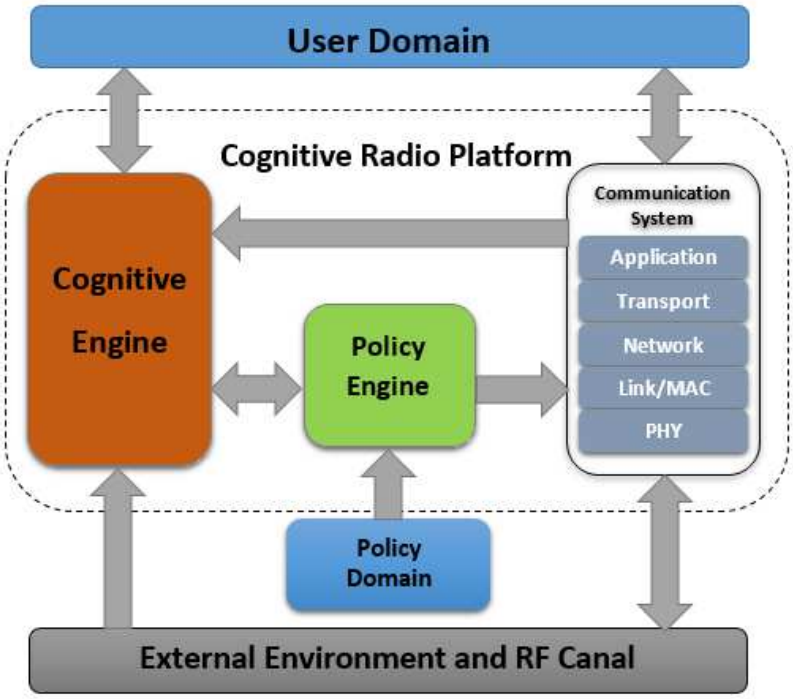

Figure 1.3- Cognitive radio architecture [28].

The functional components of this architecture are:

1. **Cognitive Engine (Intelligent part of CR):** The cognitive engine appears as the simplified open system interconnection (OSI) stack to perform the modeling, learning and optimization processes, which are required to reconfigurate the radio communication system. The cognitive engine searches for a solution to the problem in its conept space called the *objective space*. The architectural features of the reconfigurable equipment (i.e., available modulation and coding schemes, maximum amplifier power, accessible portions of the spectrum) bound this space. The information accumulated by the cognitive engine is derived from the radio environment and from the three main domains of CR architecture, namely the *user domain*, the *radio domain* and the *policy domain*.
2. **User Domain**: The user is directly concerned by the QoS provided by the radio link. The QoS is a qualitative concept taking on a different quantitative sens for each application. Real-time applications valorize low-latency communications while the efficiency of the radio link is measured in terms of throughput for non-real-time applications. The user domain transmits information relevant to the user's application and must contribute to the optimization of the cognitive engine.
3. **Radio Domain**: Radio domain information consists of radio frequency and environmental data, which could affect the system's performances such as propagation or sources of interferences. The radio environment provides the communication

medium used by the system. Its influence on communication performances depends on the developed waveform and the installed receiver. The radio link will become more effective if the signal is modulated over a wide bandwidth unless it is perturbed by one or more sources of interferences. Likewise, the QoS will be greatly degraded if radio operates in a very selective channel without a complex receiver structure. A simpler receiver would however be possible in the presence of a direct path [27].

4. **Policy Engine**: This engine receives information about the rules in the policy domain. This information helps the CR to avoid prohibited and illegal solutions and to choose the best solution among those, which respect the local regulations [1, 27].

1.6 The cognitive radio applications

Figure 1.4 represents a high-level classification of possible CR applications [1, 29].

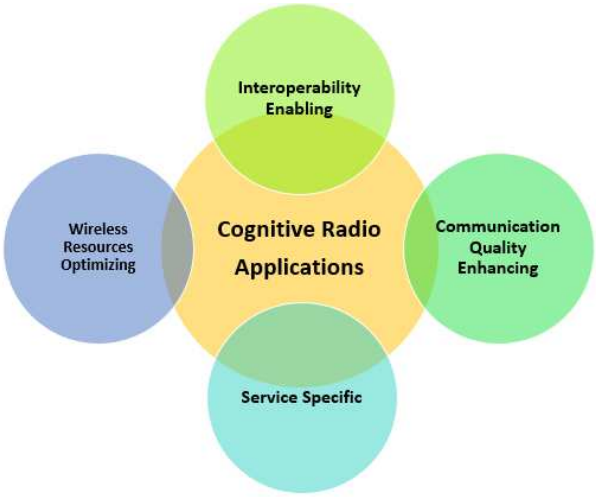

Figure 1.4- Classification of cognitive radio applications [29].

This classification is based on the relationship between each application and the cognitive concept:

1. **Wireless ressources optimization**: These resources include spectrum, power, network, hardware/software, etc.
2. **Communication quality enhancing**: For example. Improving link reliability.
3. **Interoperability enabling**: This is one of the most desirable features of CR. Interoperability allows two or more communication systems to exchange information.
4. **Service specific**: It is the services and users needs in private, public and military sectors.

In general, some targeted applications belong to different groups, for example: transmit traffic congestion information to the mobile in advance and maintain communication in disaster

situation, etc., can take advantage of applications set and they can work together to improve wireless communications [1, 29].

1.7 The cognitive radio functions

The CR includes many functions (steps) to permanently analyze the spectrum and determine the PU and SU. Figure 1.5 describes the different functions that must be integrated into the cognitive user in order to create the CR network.

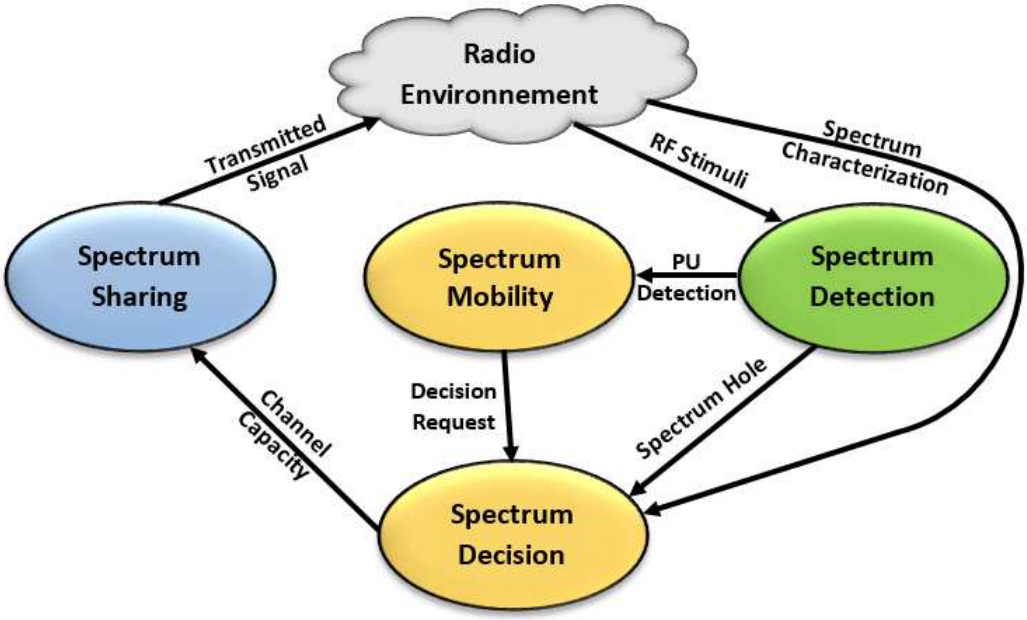

Figure 1.5- Cycle and functions of cognitive radio [30-32].

There are four main functions of CR:

1.7.1 Spectrum sensing

Spectrum sensing consists of determining the presence of PU (detection of unused spectrum or spectrum hole), and sharing the detection result with other users [32]. In particular, a CR transceiver periodically detects unused spectrum and determines the access method without interfering with the transmission of licensed data. There are two types of spectrum detection:

- *Centralized spectrum detection*: A detection controller detects the target frequency band and shares information with other nodes in the system.
- *Distributed spectrum detection*: A distributed detection consists in cooperative sensing detection that depends not only on the user's strategy but also on the strategies taken by other users, without the detection controller.

1.7.2 Spectrum management

The CR should decide on the best spectrum band to answer the QoS requirements on all available frequency bands. Therefore, spectrum management is necessary for CR with its two functions:

- *Spectrum analysis* is used to characterize different spectrum bands, which allows exploiting user requirements in terms of the spectrum band.
- *Spectrum decision* determines the data rate, transmission mode and transmission bandwidth. Then, the appropriate spectrum band is selected based on the spectrum characteristics and the user needs.

1.7.3 Spectrum sharing

The CR allocates the spectrum hole to SU when PU does not use it. This property is described as *spectrum sharing*.

- *Underly spectrum sharing*: is the availability of access to the radio spectrum with a minimum transmission power so that the temperature of the interference above the preset thresholds is not increased [33].
- *Overlay spectrum sharing*: In this technique, unlicensed users can use a spectrum band for a fraction of time where licensed users underuse this band.

1.7.4 Spectrum mobility

This process allows the SU to change its operating frequency. CR networks try to use the spectrum dynamically by allowing radio terminals to operate in the best available frequency band, to maintain transparent communication requirements during the transition to a better frequency [34].

1.8 From software radio to cognitive radio

In 1995, Joseph Mitola proposed a new concept called *Software Radio* (SR) [35]. This concept allows equipments to communicate with any radio communication standard, without changing any hardware component and only by modifying the integrated software. This technology, which may seem very simple at first, not only introduces many new advantages, but also raises many technological challenges. Mitola understood the necessity to integrate, simultaneously intelligence into the network and equipment in order to respond the user needs and resource constraints, resulting in increased spectral efficiency. That is why he proposed the idea of CR [18].

1.9 Conclusion

The purpose of this chapter was to introduce the concept of cognitive radio. Indeed, a detailed description of the CR and these characteristics in terms of its architecture, these functions and these applications. CR permit to the transmission system to become aware of its radio frequency environment, and therefore to seize opportunities by detecting spectrum holes to improve spectral efficiency.

The objective of the CR is to give a communication system the ability to make these types of decisions independently. It is even highly desirable that our telecommunications devices can intelligently execute this reasoning precisely.

This intelligence allows the equipment to choose the best conditions to meet their communication needs. The choice ideally implies a real-time change of the transmission parameters, or even a change of standard. To do this optimally, Mitola has shown that an SR. should achieve real-time change. He concluded that CR would be more effective if supported by SR technology.

In Chapter 2, the techniques used in digital modulation classification in STBC-MIMO systems will be studied.

Chapter 2

Digital Modulation Classification in STBC-MIMO Systems

Contents

2.1 Introduction

In the signal processing, the source separation is used to extract initial signals from a mixture of several signals detected by a receiver (SU). According to the context (the signal's type, the channel's propagation type, the receiver's type, etc.) there exist different methods of sources separations.

Therefore, waveform identification or waveform knowledge is very beneficial for CR devices. In this chapter, the transmission characteristics identified by the CR device including the identification of the number of transmit antennas and the recognition of the modulation used for the transmission process. The important contribution in this chapter consists in the development of a blind modulation identification algorithm for STBC-MIMO systems spatially correlated and in the presence of channel estimation errors [7, 36].

We will start by mathematically formulating the signal transmitted in baseband for the MIMO system, and the STBC-MIMO system. Next, we contribute the digital modulation identification algorithm in STBC-MIMO systems, and we finish by providing and explaining the results of the simulations.

2.2 Basic principles of modulation

The aim of the modulation process is to transfer a signal (whether it is analog or digital) over a channel to a given destination. The data are carried by a radio frequency carrier in the form of a sinusoid called *carrier wave*. A modulated carrier wave has the following form:

$$\begin{aligned} s(t) = &\quad a(t)\cdot\cos\left(2\pi f_c t+\varphi(t)\right)\\ = &\quad \Re\left\{a(t)\cdot\exp\left(j\left(2\pi f_c t+\varphi(t)\right)\right)\right\}\\ = &\quad \Re\left\{a(t)\cdot\exp\left(j\varphi(t)\right)\cdot\exp(j2\pi f_c t)\right\}\\ = &\quad \Re\left\{b(t)\cdot\exp(j2\pi f_c t)\right\} \end{aligned} \tag{2.1}$$

where $a(t)$ is the signal amplitude, $\varphi(t)$ is his phase, f_c is the carrier frequency, and the function $b(t)=\Re\left\{a(t)\cdot\exp\left(j\varphi(t)\right)\right\}$ is the baseband signal.

Carrier-wave based modulation is the process of varying one or more properties of the carrier signal, with a modulating signal that typically contains information to be transmitted. In addition, the signal is transmitted at a given frequency, which may be different for different users. There are different modulation types modifying different parameters of the carrier including [37]:

- Amplitude Shift Keying (ASK),
- Phase Shift Keying (PSK),
- Quadrature Amplitude Modulation (QAM),

We note n the number of bits per binary symbol. Therefore, we have $M = 2^n$ possible symbols. To simplify the writing of modulated signals, we model the bit stream by independent and identically distributed (i.i.d) random variables (r.v). In addition, we will admit that the bits are equiprobable, i.e., the probability of occurrence of a "0" or a "1" equals to $\frac{1}{2}$. For the amplitude $a(t)$, we assume without loss of generality that the symbol's constellation is normalized, i.e the average energy of the symbols is unitary ($E[|s|^2] = 1$).

2.2.1 ASK modulation

The ASK modulation includes manipulating the amplitude of a carrier according of the baseband signal (see figure 2.1). The general expression of the modulated signal written as:

$$\begin{aligned} s(t) &= \sum_m \alpha_m g_{T_x}(t - mT)\cos(2\pi f_c t) \\ &= s_I(t)\cos(2\pi f_c t) \end{aligned} \tag{2.2}$$

where the function $g_{T_x}(t)$ is the impulse response filter of the pulse shaping at the transmitter. The signal $s_I(t)$ changes the amplitude of the carrier $p(t) = \cos(2\pi f_c t)$. We will take a priori an alphabet $\alpha_m \in \{\pm m\alpha | m = 1,\ 3, \dots, (M-1)\}$.

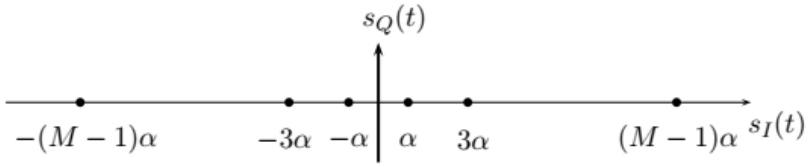

Figure 2.1- M-ASK modulation constellation.

2.2.2 PSK modulation

The PSK modulation includes manipulating the phase of a carrier according of the baseband signal (see figure 2.2). The general expression of the digitally modulated phase signal written as:

$$\begin{aligned} s(t) &= \sum_m \cos(2\pi f_c t + \alpha_m)\, g_{T_x}(t - mT) \\ &= s_I(t)\cos(2\pi f_c t) - s_Q(t)\sin(2\pi f_c t) \end{aligned} \tag{2.3}$$

The signal $s_I(t)$ changes the amplitude of the carrier $\cos(2\pi f_c t)$, while the signal $s_Q(t)$ changes the amplitude of the carrier $\sin(2\pi f_c t)$. We call the first carrier the *carrier in phase*, and the second the *carrier in quadrature*. We can take a priori an alphabet $\alpha_m \in \left\{\varphi_0 + \frac{2\pi m}{M} | m = 0, 1, \dots, (M-1)\right\}$ where φ_0 is the phase offset. In the following, we consider some special cases of PSK:

- *Binary-PSK (BPSK) modulation*: with this modulation type, each symbol could indicate two states ($M = 2$), one bit per symbol (0 or 1), and two different phases ($\alpha_0 = 0, \alpha_1 = \pi$ with $\varphi_0 = 0$).
- *Quadrature-PSK (QPSK) modulation*: is a simple extension of the BPSK by adding two additional phases ($\alpha_0 = \frac{\pi}{4}, \alpha_1 = \frac{3\pi}{4}, \alpha_2 = \frac{-3\pi}{4}, \alpha_3 = \frac{-\pi}{4}$ with $\varphi_0 = \frac{\pi}{4}$). Each symbol could indicate four states ($M = 4$), two bits per symbol (00, 01, 11 ou 10).

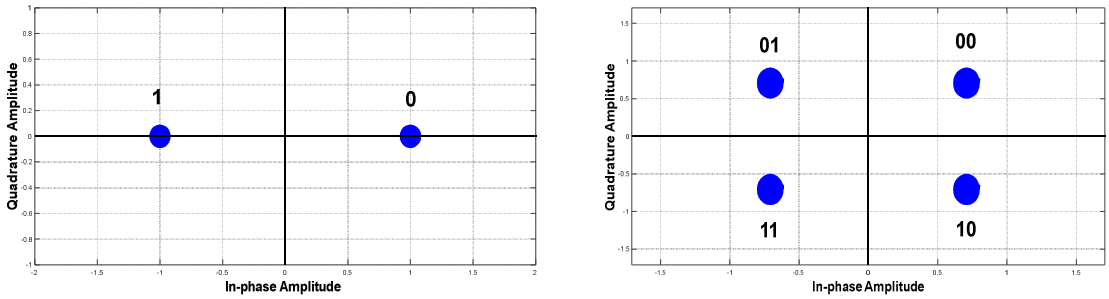

BPSK **QPSK**

Figure 2.2- M-PSK modulation constellation ($M = 2, 4$).

2.2.3 QAM modulation

The ASK and PSK modulations can be combined to create QAM modulation. In the same way as QPSK, the signal with QAM can be represented as a combination of components in phase and in quadrature (see figure 2.3), but the constellation points are distributed on all the area of the constellation diagram rather than on the circle as for M-PSK. This is achieved by amplitude modulation at several levels of each component. The M-QAM signal can be written as follows:

$$\begin{aligned} s(t) &= \sum_m \alpha_m \cos(2\pi f_c t + \beta_m)\, g_{T_x}(t - mT) \\ &= s_I(t)\cos(2\pi f_c t) - s_Q(t)\sin(2\pi f_c t) \end{aligned} \quad (2.4)$$

As for phase modulation, $s_I(t)$ and $s_Q(t)$ modify the amplitude of the carrier in phase and in quadrature, respectively.

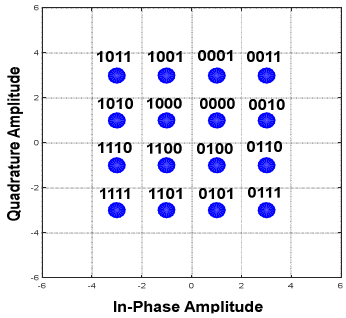

Figure 2.3- M-QAM modulation constellation ($M = 16$).

2.3 MIMO system

The technological development of wireless communications depends on many technologies such as the large-scale implementation of integrated circuits, energy storage, and antennas, etc. The MIMO technology has been one of the major contributions in the wireless communications domain for several decades until today. The spatial diversity created by MIMO systems increases capacity, and the transmission rate. On the other hand, MIMO systems permit to combat the fading of multipath channel (see figure 2.4).

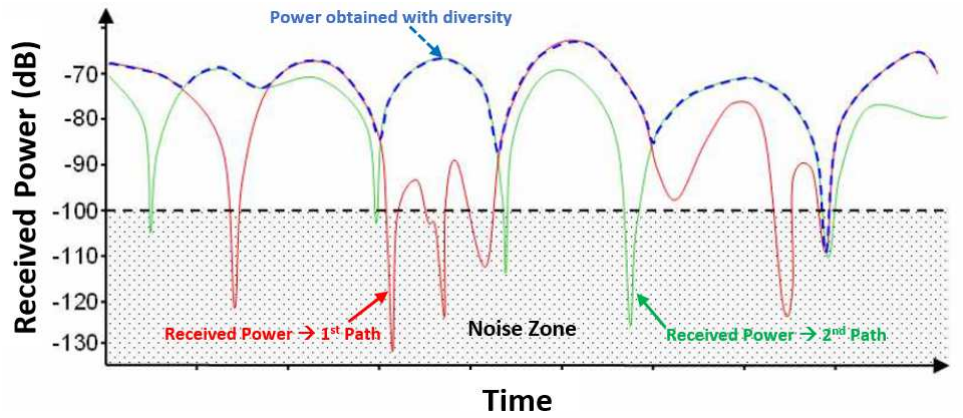

Figure 2.4- Principle of improving the power level at receiver by the antennas diversity effect [38].

2.3.1 MIMO techniques

MIMO techniques are designed to improve significantly the performance of wireless mobile communications. These techniques use multiple antennas on transmission and/or reception in order to improve the quality of the SNR and/or the communication capacity. A MIMO system can provide two types of gain; a gain in spatial diversity and a gain in spatial multiplexing:

- **Spatial diversity**: The same signal is transmitted simultaneously on different transmitting antennas. Several copies of the transmitted signal pass through different

independent propagation paths with flat fading. At the receiver, the signals received on each of the receiving antennas are then re-phased and summed coherently. In a MIMO system with N_t transmit antennas and N_r receiving antennas, the maximum diversity gain is $(N_t \cdot N_r)$, assuming that the path gains between each pair of transmit-receive antennas are i.i.d [38]. Smart antenna techniques [39], Alamouti coding [40] and space-time (ST) codes [41] are well-known spatial diversity techniques. Spatial diversity techniques improve the reliability of communication in fading channels, eliminating the effects of fading thus increasing the transmission SNR. For these techniques to be effective, the MIMO subchannels must be decorrelated (independent).

- **Spatial multiplexing:** If spatial diversity is a way of eliminating fading, spatial multiplexing is a way of exploiting this fading to increase the transmission rate. The MIMO systems can achieve orthogonal sub channels between the transmitters and receivers antennas through a rich scattering environment and consequently increase the data rate. The signals received on the receiving antennas are combined to reconstruct the original signal. In a MIMO system with N_t transmitting antennas and N_r receiving antennas, for a high SNR, Foschini [42] and Telatar [43] have shown that the channel capacity increases linearly with $m = \min(N_t, N_r)$, if the sub-channel gains are i.i.d. BLAST (Bell Labs Layered Space-Time) technique [42] is a spatial multiplexing technique. As for MIMO diversity, the propagation subchannels must be decorrelated.

2.3.2 An overview of a MIMO system

With the assumption that the MIMO paths are not correlated, the MIMO channels have a higher capacity compared to the SISO channels [44].

First, we consider a narrowband MIMO channel with N_t transmit antennas at the PU side, and we assume that there are $N_r \geq 1$ antennas at the CR mobile terminal (SU). The SU receiver detects multiple primary sources (PS) where the PS is the signal of a PU.

Let $T_s = {}^{1}/_{f_s}$ the sampling period. The signal received at a sampling time T_s at the n_r-th antenna is written as:

$$y_{n_r}(nT_s) = \tilde{s}_{n_r}(nT_s) + \eta_{n_r}(nT_s) \tag{2.5}$$

where $\tilde{s}_{n_r}(nT_s)$ is the superposition of the possible simpled PS signals including the effects of path-loss, multi-path fading and time dispersion, and $\eta_{n_r}(nT_s)$ is the noise. To simplify the notation, let $y_{n_r}(n) \triangleq y_{n_r}(nT_s)$, $\tilde{s}_{n_r}(n) \triangleq \tilde{s}_{n_r}(nT_s)$, and $\eta_{n_r}(n) \triangleq \eta_{n_r}(nT_s)$ [1].

In presence of N_t primary sources ($1 \leq n_t \leq N_t$), the signal received by the n_r-th antenna is written as:

$$y_{n_r}(n) = \sum_{n_t=1}^{N_t} \sum_{l=0}^{L-1} h_{n_r,n_t}(n,l) s_{n_t}(n-l) + \eta_{n_r}(n), \quad n = 1,2,.... \tag{2.6}$$

where $s_{n_t}(n)$ is the n-th symbol transimitted by the n_t-th primary sources, L is the number of the channel coefficients, also called *channel order*, between PU and each antenna of SU, and $h_{n_r,n_t}(n,l)$ is the $(l+1)$-th coefficient of the channel impulse response between n_t-th transmitted antenna of a PU and the n_r-th received antenna of a SU at instant n. The MIMO system is expressed in matrix form as:

$$\underbrace{\begin{bmatrix} y_1(n) \\ y_2(n) \\ \vdots \\ y_{N_r}(n) \end{bmatrix}}_{=\mathbf{y}(n)} = \underbrace{\begin{bmatrix} \mathbf{h}_{1,1}(n) & \mathbf{h}_{1,2}(n) & \cdots & \mathbf{h}_{1,N_t}(n) \\ \mathbf{h}_{2,1}(n) & \mathbf{h}_{2,2}(n) & \cdots & \mathbf{h}_{2,N_t}(n) \\ \vdots & \vdots & \vdots & \vdots \\ \mathbf{h}_{N_r,1}(n) & \mathbf{h}_{N_r,2}(n) & \cdots & \mathbf{h}_{N_r,N_t}(n) \end{bmatrix}}_{=\mathbf{H}(n)} \mathbf{s}(n) + \underbrace{\begin{bmatrix} \eta_1(n) \\ \eta_2(n) \\ \vdots \\ \eta_{N_r}(n) \end{bmatrix}}_{=\boldsymbol{\eta}(n)}, \quad n = 1,2,... \tag{2.7}$$

where $\mathbf{s}(n) = \left[s_1(n), \dots, s_1(n-L+1), \dots, s_{N_t}(n), \dots, s_{N_t}(n-L+1)\right]^T$. The vector $\mathbf{h}_{n_r,n_t}(n) = \left[h_{n_r,n_t}(n,0), \dots, h_{n_r,n_t}(n,L-1)\right]$ represents the channel coefficients between the n_t-th transmitted antenna of a PU and the n_r-th received antenna of a SU at instant n.

Let us consider N consecutive samples and define the corresponding signal/noise vectors:

$$\begin{cases} \mathbf{y}_N(n) = \left[y_1(n), \dots, y_1(n-N+1), \dots, y_{N_r}(n), \dots, y_{N_r}(n-N+1)\right]^T \\ \mathbf{s}_N(n) = \left[\mathbf{s}_1^T(n), \dots, \mathbf{s}_{N_t}^T(n)\right]^T \\ \boldsymbol{\eta}_N(n) = \left[\eta_1(n), \dots, \eta_1(n-N+1), \dots, \eta_{N_r}(n), \dots, \eta_{N_r}(n-N+1)\right]^T \end{cases}$$

where $\mathbf{s}_{n_t}(n) = \left[s_{n_t}(n), s_{n_t}(n-1), \dots, s_{n_t}(n-L-N+1)\right]^T$. The signal model is expressed in matrix form as:

$$\mathbf{y}_N(n) = \mathbf{H}_N(n)\mathbf{s}_N(n) + \boldsymbol{\eta}_N(n) \tag{2.8}$$

where $\mathbf{H}_N$ is a matrix of $N_r N \times N_t(L+N)$ written as :

$$\mathbf{H}_N(n) = \begin{bmatrix} \mathbf{H}_{1,1}(n) & \mathbf{H}_{1,2}(n) & \cdots & \mathbf{H}_{1,N_t}(n) \\ \mathbf{H}_{2,1}(n) & \mathbf{H}_{2,2}(n) & \cdots & \mathbf{H}_{2,N_t}(n) \\ \vdots & \vdots & \ddots & \vdots \\ \mathbf{H}_{N_r,1}(n) & \mathbf{H}_{N_r,2}(n) & \cdots & \mathbf{H}_{N_r,N_t}(n) \end{bmatrix}$$

where the matrix $\mathbf{H}_{n_r,n_t}$ of $N \times (L+N)$ is defined by:

$$\mathbf{H}_{n_r,n_t} = \begin{bmatrix} \mathbf{h}_{n_r,n_t}(n) & \mathbf{0} & \cdots & \mathbf{0} \\ \mathbf{0} & \mathbf{h}_{n_r,n_t}(n-1) & \ddots & \vdots \\ \vdots & \ddots & \ddots & \mathbf{0} \\ \mathbf{0} & \cdots & \mathbf{0} & \mathbf{h}_{n_r,n_t}(n-N+1) \end{bmatrix}$$

In the rest of this thesis, we assume that $\boldsymbol{\eta}(n)$ is an additive white Gaussian noise (AWGN) vector with zero mean and variance σ_η^2.

The SNR is the ratio of the average received signal power from PU to the average receiver noise power, that is:

$$\text{SNR} = \frac{E[\|\mathbf{y}(n) - \boldsymbol{\eta}(n)\|^2]}{E[\|\boldsymbol{\eta}(n)\|^2]} \tag{2.9}$$

In general, modeling a MIMO channel can be applied to evaluate correctly the performance of a given system and to create the exemplary channels. The precise channel model obtained will allow us to understand it and also to make precise hypotheses on the system conception.

The purpose of the following subsection is to evaluate the performance of a MIMO system with correlated channels.

2.3.3 Spatial correlation models

Different correlative models have been proposed for MIMO such as the Kronecker model, and the exponential model. We focus on the first model in this thesis.

The spatially correlated MIMO channels are modeled by the Kronecker model [45]. To reduce the complexity of analysis, this channel model assumes that the spatial correlations between the receiving antennas are independent of the correlations between the transmitting antennas. Under this hypothesis, we show that the Kronecker model is given by:

$$\mathbf{H} = \mathbf{R}_r^{1/2} \mathbf{H}_w \mathbf{R}_t^{1/2} \tag{2.10}$$

where $\mathbf{R}_t$ of $(N_t \times N_t)$ and $\mathbf{R}_r$ of $(N_r \times N_r)$, are the emission and reception correlation matrices, respectively. $\mathbf{H}_w$ of $(N_r \times N_t)$ is a matrix containing a circularly symmetric complex Gaussian (CSCG) and i.i.d variables with zero mean and variance equal to unity. The equivalent Kronecker model describing the total correlation of the channel $\mathbf{R}_H$ perhaps express by the Kronecker product "⊗" of the correlation matrices $\mathbf{R}_t$ and $\mathbf{R}_r$ [46]:

$$\mathbf{R}_H = \mathbf{R}_t \otimes \mathbf{R}_r \tag{2.11}$$

The two matrices $\mathbf{R}_t$ and $\mathbf{R}_r$ are expressed, respectively, by the transmit correlation coefficient ρ_t and the receive correlation coefficient ρ_r:

$$\begin{cases} [\mathbf{R}_t]_{i,j} = \rho_t^{|i-j|}, & i,j = 1,\dots,N_t \\ [\mathbf{R}_r]_{i,j} = \rho_r^{|i-j|}, & i,j = 1,\dots,N_r \end{cases} \tag{2.12}$$

The correlation matrices can be presented by the exponential correlation model, which was introduced in [46], and developed in [47]. This model defines the elements of the correlation matrix $\mathbf{R}$ by a single coefficient:

$$[\mathbf{R}]_{i,j} = \begin{cases} \rho^{j-i}, & i \le j \\ [\mathbf{R}_w]_{ji}^*, & i > j \end{cases} \tag{2.13}$$

where $|\rho| < 1$ and $\mathbf{R}_w = \mathbf{H}_w \mathbf{H}_w^{\mathcal{H}}$. The curves in figure 2.5 show the cumulative distribution function (CDF) versus the capacity of a correlated MIMO system.

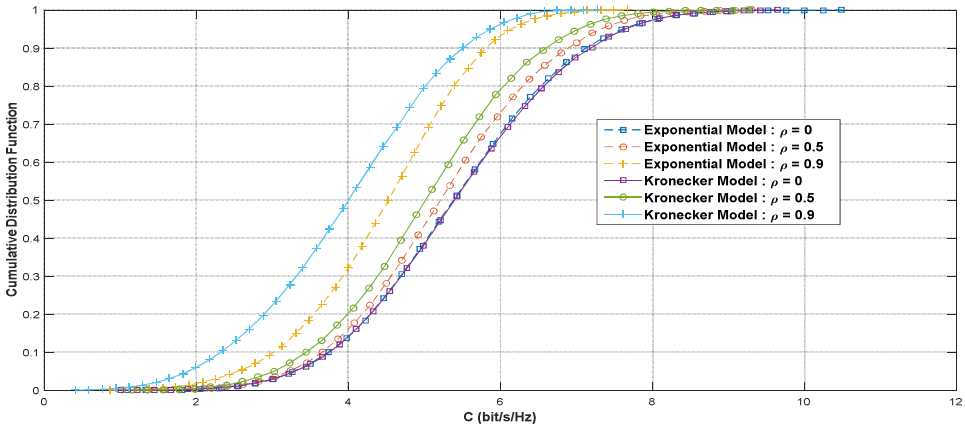

Figure 2.5- CDF versus the channel capacity using the Kronecker model and the exponential model, for different correlation coefficients. $\rho_t = \rho_r = \rho$. $N_t = 2, N_r = 2$. SNR=10dB. BPSK modulation.

2.4 Space-time coding

Hoping to reduce the exponential complexity of the decoder used in Space-Time Trellis Coding (STTC) [48], Alamouti [40] proposed a simple scheme of space-time diversity at the transmitter side, subsequently extended by Tarokh and *al.* [49], in order to forming a new class of space-time codes called *space-time block coding*. According to Tarokh [49], STBC codes can be seen as an orthogonal design and a linear application, which applied to the complex vector of information data symbols $\mathbf{s}_i \triangleq \left[s_{iK}, s_{iK+1}, \dots, s_{(i+1)K-1}\right]^T$ gives in the output the matrix $\mathcal{G}_c(\mathbf{s}_i)$ of $U \times N_t$ where U is the length of the code STBC and K being the length of the data vector before coding. This matrix should satisfy the following orthogonality property:

$$\mathcal{G}_c^{\mathcal{H}} \mathcal{G}_c = \|\mathbf{s}_i\|_2^2 \mathbf{I}_{N_t \times N_t} \tag{2.14}$$

The most studied criterion [48] when designing STBC codes is diversity. This diversity can be characterized by the number of independent detectable paths at the receiver side for each transmitted symbol. In addition, it also depends on the number of antennas at the transmitter and receiver. The objective of using STBC is to achieve maximum diversity gain with the smallest number of antennas. The rate of an STBC code, R, represents the number of coded symbols transmitted per symbol period, and defined by $R = {}^{K}/_{U}$. Also, U represents the number of symbol periods (or the time-slots) that the receiver must wait before starting to decode the symbols coded from the same matrix $\mathcal{G}_c$. In summary, STBC codes are designed to:

- Maximize the rate of the code,
- Minimize the number of antennas,
- Maximize the gain of diversity.

Table 2.1 shows three types of STBC code, which are the most, used in the literature.

Table 2.1. Different types of STBC code with different rate.

Alamouti ($\mathcal{G}_{Al}$) [40]	OSTBC3 ($\mathcal{G}_3$) [41, 49]	OSTBC4 ($\mathcal{G}_4$) [41, 49]
$\begin{bmatrix} s_0 & s_1 \\ -s_1^* & s_0^* \end{bmatrix}$	$\begin{bmatrix} s_0 & s_1 & s_2 \\ -s_1 & s_0 & -s_3 \\ -s_2 & s_3 & s_0 \\ -s_3 & -s_2 & s_1 \\ s_0^* & s_1^* & s_2^* \\ -s_1^* & s_0^* & -s_3^* \\ -s_2^* & s_3^* & s_0^* \\ -s_3^* & -s_2^* & s_1^* \end{bmatrix}$	$\begin{bmatrix} s_0 & s_1 & s_2 & s_3 \\ -s_1 & s_0 & -s_3 & s_2 \\ -s_2 & s_3 & s_0 & -s_1 \\ -s_3 & -s_2 & s_1 & s_0 \\ s_0^* & s_1^* & s_2^* & s_3^* \\ -s_1^* & s_0^* & -s_3^* & s_2^* \\ -s_2^* & s_3^* & s_0^* & -s_1^* \\ -s_3^* & -s_2^* & s_1^* & s_0^* \end{bmatrix}$
$N_t = 2, K = 2, U = 2$	$N_t = 3, K = 4, U = 8$	$N_t = 4, K = 4, U = 8$

A comparison is presented in figure 2.6, in terms of bit error rate (BER) between different STBC codes (Alamouti, Orthogonal-STBC3 (OSTBC3), and Orthogonal-STBC4 (OSTBC4)) and spatial multiplexing (SM). The Rayleigh fading channel for two types of QPSK and 16QAM modulation.

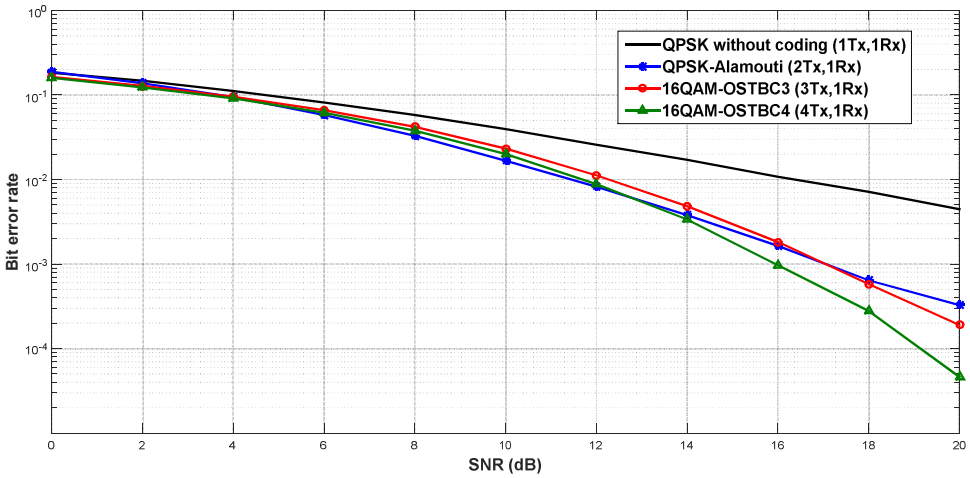

Figure 2.6- BER versus SNR, of STBC coding in a Rayleigh fading channel for two types of modulation.

Note that antennas gain increases SNR, while diversity gain reduces fading.

2.4.1 A special case: Alamouti coding

STBC coding of Alamouti type [40] is characterized by two transmitting antennas ($N_t = 2$) and $N_r \geq 1$ receiving antennas, so $K = U = 2$.

To transmit b bits, we use a modulation technique that maps the b bits according to a real or complex constellation (QAM ou PSK …etc.,) to generate data symbols. The Alamouti coder divides the data stream into several substreams. Each substream is composed of two consecutive symbols. Therefore, the coder processes two successive symbols of the constellation at the same time ($\mathbf{s}_i \triangleq [s_{2i}, s_{2i+1}]^T$), such that s_{2i} and s_{2i+1} are sent, simultaneously, during a first time-slot ($u = 1$), by the two transmitting antennas $n_t = 1$ and $n_t = 2$, respectively. During the second time slot ($u = 2$), the encoder sends, simultaneously, the symbols $(-s_{2i+1}^*)$ and s_{2i}^* to the antennas $n_t = 1$ and $n_t = 2$, respectively. The data matrix after STBC coding corresponding to the symbols $[s_{2i}, s_{2i+1}]$ is defined as:

$$\mathcal{G}_{Al}(\mathbf{s}_i) = \begin{bmatrix} s_{2i} & s_{2i+1} \\ -s_{2i+1}^* & s_{2i}^* \end{bmatrix} \tag{2.15}$$

This code provides a total diversity equal to $2N_r$. The decoding used is based on the maximum likelihood algorithm. The results obtained are much higher than that obtained using a single antenna [20], see figures 2.6 and 2.7.

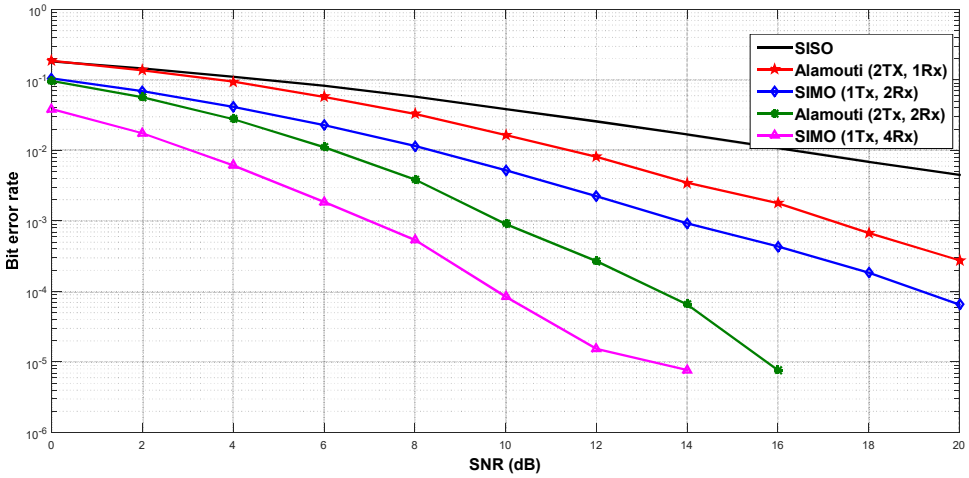

Figure 2.7- BER versus SNR, using Alamouti coding and a Single-Input Multiple-Output (SIMO) system in a Rayleigh fading channel with QPSK modulation.

We can introduce another form of STBC(N_t, K, U) coding, where the ST coder generates matrix blocks of size $U \times N_t$ using the following expression [50-51] :

$$\mathcal{G}_c(\mathbf{s}_i) = \left[\mathbf{A}_1\underline{\mathbf{s}_i}, \mathbf{A}_2\underline{\mathbf{s}_i}, \dots, \mathbf{A}_U\underline{\mathbf{s}_i}\right]^T \tag{2.16}$$

where $\underline{\mathbf{s}_i} = \left[\Re[s_{iK}], \Re[s_{iK+1}], \dots, \Re\left[s_{(i+1)K-1}\right], \Im[s_{iK}], \Im[s_{iK+1}], \dots, \Im\left[s_{(i+1)K-1}\right]\right]^T$.

We take an example of Alamouti coding (STBC(2,2,2)), the two coding matrices written as:

$$\begin{cases} \mathbf{A}_1 = \begin{bmatrix} 1 & 0 & j & 0 \\ 0 & 1 & 0 & j \end{bmatrix} \\ \mathbf{A}_2 = \begin{bmatrix} 0 & -1 & 0 & j \\ 1 & 0 & -j & 0 \end{bmatrix} \end{cases}$$

2.5 Digital modulation classification algorithm

In this section, we will study the problem of blind identification or classification of several types of digital modulations from a mixture of received signals, for STBC-MIMO system using a correlated and noisy channel.

A structure for blind-DMC (BDMC) for a transmission system using the STBC-MIMO technique is given in figure 2.8.

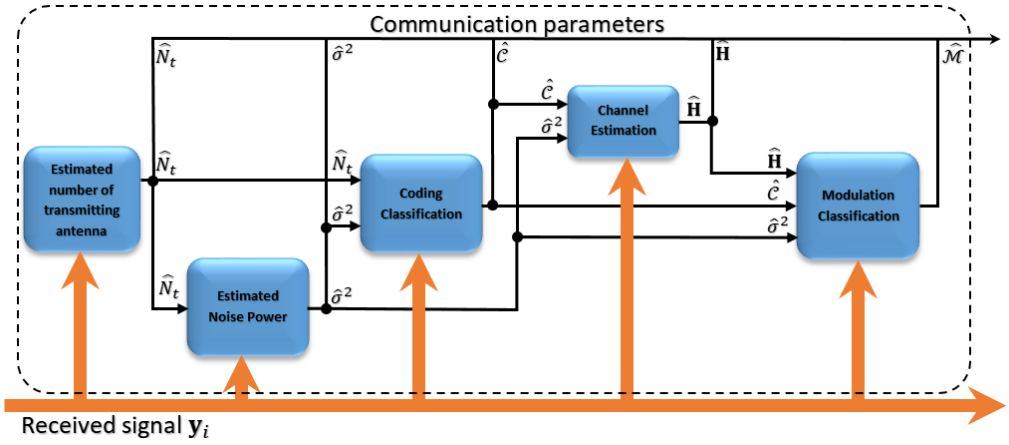

Figure 2.8- Structure of a blind digital modulation classification process in STBC-MIMO system.

To identify the parameters of an unknown received signal, we propose to estimate at first the number of transmitting antennas. This estimate limits the number of possible codes. Then we estimate the noise power $\hat{\sigma}_\eta^2$. After that, the recognition of the communication coding $\hat{\mathcal{C}}$ is performed, then a channel estimation technique $\widehat{\mathbf{H}}$ is employed. At the end, we determine the modulation $\widehat{\mathcal{M}}$ of the transmitted symbols.

2.5.1 Basic model of modulation identification for STBC-MIMO systems

A block diagram of a blind modulation identification in STBC-MIMO system with N_t transmit antennas and N_r receiver antennas ($N_r \geq N_t$) is illustrated in figure 2.9.

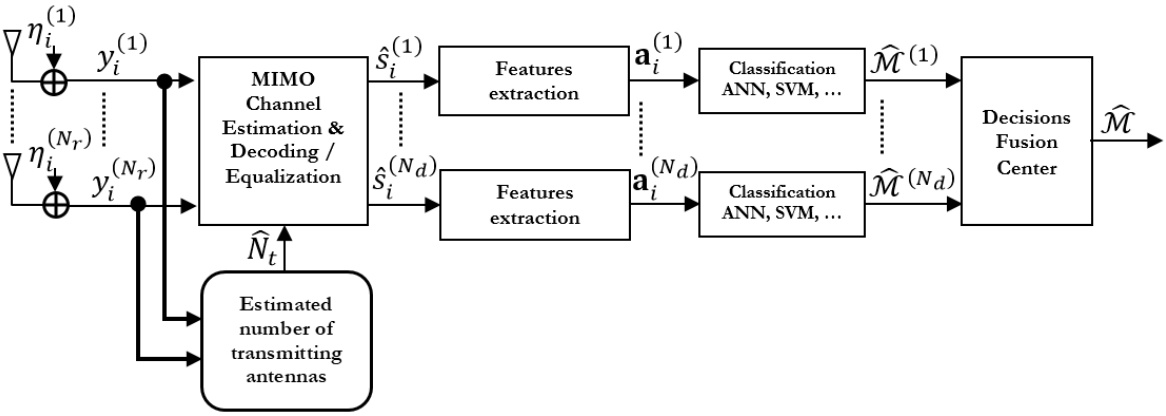

Figure 2.9- A block diagram of the modulation identification process at the receiver [7, 36].

By applying an STBC coding to the complex vector of data $\mathbf{s}_i$ of size $(K \times 1)$, we construct a matrix $\mathbf{X}_i$ of size $(N_t \times U)$ as follows:

$$\mathbf{X}_i = \mathcal{G}_c^T(\mathbf{s}_i) \tag{2.17}$$

The entries of $\mathbf{X}_i$ are linear combinations of the elements of $\mathbf{s}_i$ and their conjugates. The source symbols $\mathbf{X}_i$ are assumed i.i.d.

The channel is considered quasi-static. The received signal vector at time u for i-th block is written:

$$\mathbf{y}_{i,u} = \mathbf{H}\mathbf{x}_{i,u} + \boldsymbol{\eta}_{i,u} \tag{2.18}$$

with:

$$\begin{cases} \mathbf{y}_{i,u} = \left[y_{iU+u}^{(1)}, y_{iU+u}^{(2)}, \dots, y_{iU+u}^{(N_r)}\right]^T : \text{ received signal vector ;} \\ \mathbf{x}_{i,u} = \left[x_{iU+u}^{(1)}, x_{iU+u}^{(2)}, \dots, x_{iU+u}^{(N_t)}\right]^T : \text{transmitted source signal vector ;} \\ \boldsymbol{\eta}_{i,u} = \left[\eta_{iU+u}^{(1)}, \eta_{iU+u}^{(2)}, \dots, \eta_{iU+u}^{(N_r)}\right]^T : \text{AWGN vector, where } \boldsymbol{\eta}(k) \sim \mathcal{N}\left(0, \sigma_\eta^2 \mathbf{I}_{N_r}\right); \end{cases}$$

And the MIMO channel matrix $\mathbf{H}$ of $(N_r \times N_t)$ is considered complex and spatially correlated:

$$\mathbf{H} \triangleq \begin{bmatrix} h^{(1,1)} & h^{(1,2)} & \dots & h^{(1,N_t)} \\ h^{(2,1)} & h^{(2,2)} & \dots & h^{(2,N_t)} \\ \vdots & \vdots & \vdots & \vdots \\ h^{(N_r,1)} & h^{(N_r,2)} & \dots & h^{(N_r,N_t)} \end{bmatrix}$$

For the i-th block, the matrix form of the received signal is written:

$$\mathbf{Y}_i = \mathbf{H}\mathbf{X}_i + \mathbf{W}_i \tag{2.19}$$

where:

$$\mathbf{Y}_i \triangleq \begin{bmatrix} y_{iU+1}^{(1)} & y_{iU+2}^{(1)} & \dots & y_{(i+1)U}^{(1)} \\ y_{iU+1}^{(2)} & y_{iU+2}^{(2)} & \dots & y_{(i+1)U}^{(2)} \\ \vdots & \vdots & \vdots & \vdots \\ y_{iU+1}^{(N_r)} & y_{iU+2}^{(N_r)} & \dots & y_{(i+1)U}^{(N_r)} \end{bmatrix} = \begin{bmatrix} \mathbf{y}_i^{(1)} \\ \mathbf{y}_i^{(2)} \\ \vdots \\ \mathbf{y}_i^{(N_r)} \end{bmatrix};$$

$$\mathbf{X}_i \triangleq \begin{bmatrix} x_{iU+1}^{(1)} & x_{iU+2}^{(1)} & \dots & x_{(i+1)U}^{(1)} \\ x_{iU+1}^{(2)} & x_{iU+2}^{(2)} & \dots & x_{(i+1)U}^{(2)} \\ \vdots & \vdots & \vdots & \vdots \\ x_{iU+1}^{(N_t)} & x_{iU+2}^{(N_t)} & \dots & x_{(i+1)U}^{(N_t)} \end{bmatrix} = \begin{bmatrix} \mathbf{x}_i^{(1)} \\ \mathbf{x}_i^{(2)} \\ \vdots \\ \mathbf{x}_i^{(N_t)} \end{bmatrix};$$

$$\mathbf{W}_i \triangleq \begin{bmatrix} \eta_{iU+1}^{(1)} & \eta_{iU+2}^{(1)} & \dots & \eta_{(i+1)U}^{(1)} \\ \eta_{iU+1}^{(2)} & \eta_{iU+2}^{(2)} & \dots & \eta_{(i+1)U}^{(2)} \\ \vdots & \vdots & \vdots & \vdots \\ \eta_{iU+1}^{(N_r)} & \eta_{iU+2}^{(N_r)} & \dots & \eta_{(i+1)U}^{(N_r)} \end{bmatrix} = \begin{bmatrix} \boldsymbol{\eta}_i^{(1)} \\ \boldsymbol{\eta}_i^{(2)} \\ \vdots \\ \boldsymbol{\eta}_i^{(N_r)} \end{bmatrix};$$

2.5.2 Additive Gaussian noise model

In probability theory and statistics, the Gaussian distribution is one of the most suitable probability distributions for modeling generated processes by the superposition of many independent effects (this is the case of thermal noise). Additive noise resulting from the superimposition of several i.i.d random signals different from the useful signal. We assume that the average noise power is the same on the different receiving antennas and that the noise is spatially independent. The second order statistics of a Gaussian noise are equal to $E\left[\boldsymbol{\eta}_i \boldsymbol{\eta}_i^{\mathcal{H}}\right] = \sigma_\eta^2 \mathbf{I}_{N_r}$, where σ_η^2 is the average noise power on each receiving antenna, and $\boldsymbol{\eta}_i = \left[\eta_i^{(1)}, \eta_i^{(2)}, \dots, \eta_i^{(N_r)}\right]^T$. Then, the probability density of the noise vector $\boldsymbol{\eta}_i$ is given by the relation:

$$f(\boldsymbol{\eta}_i) = \frac{1}{\left(2\pi\sigma_\eta^2\right)^{N_r/2}} \exp\left(-\frac{1}{2\sigma_\eta^2}\|\boldsymbol{\eta}_i\|^2\right) \tag{2.20}$$

In general, a system designed according to the Gaussian hypothesis will produce serious performance degradations when the noise statistics are based on heavy-tails models [52].

2.5.3 Estimated number of transmitting antennas

In a non-cooperative context, the number of transmitting antennas is unknown information to the receiver, which must blind estimated from the received samples [53].

Most of estimating methods for the antennas number available in the literature approximate the distribution of transmitted signals by the Gaussian distribution. Generally, this approximation motivated by two reasons [53-56]:

- The received samples on each antenna are composed of a mixture of several i.i.d random variables and of Gaussian additive noise.
- The Gaussian distribution is relatively simple to manipulate because its statistics of first order (mean) and second order (covariance matrix) fully describe it.

Therefore, the method chosen in our work is a sequential test. This method based on second order statistics. The technique for estimating the number of transmitting antennas consists in maximizing the probability of obtaining the samples $\mathbf{Y}$ relative to the antennas number q [53, 56-57]. This probability is called the *likelihood function* of the parameter q and is denoted by $\Lambda[\mathbf{Y}|q]$. When the transmitted signals are Gaussian, the logarithm of the likelihood function expressed in the form [58]:

$$\log(\Lambda[\mathbf{Y}|q]) = N(N_r - q).\log\left(\frac{\left(\prod_{n_x=q+1}^{N_r}\hat{\lambda}_{n_x}\right)^{\frac{1}{N_r-q}}}{\frac{1}{N_r-q}\sum_{n_x=q+1}^{N_r}\hat{\lambda}_{n_x}}\right) \quad (2.21)$$

The term in parentheses corresponds to the ratio of the geometric mean and the arithmetic mean of the smallest $(N_r - q)$ eigenvalues $\hat{\lambda}_{n_x}$. In the case where the $(N_r - q)$ smaller eigenvalues are equal, we will have $\log(\Lambda[\mathbf{Y}|q]) = 0$. In practice, a possible detecting method of the antennas number consists to achieve a sequential hypothesis test. By initializing the value q to 0, the estimated antennas number corresponds to the first value q for which $\log(\Lambda[\mathbf{Y}|q]) \approx 0$. The nullity test of likelihood function can be performed by a threshold detector. When the function $\log(\Lambda[\mathbf{Y}|q])$ is approximately zero, the distribution of the statistic $-2\log(\Lambda[\mathbf{Y}|q]) \leq \gamma_q$ follows a χ^2 law of degree $(Q-q)^2 - 1$ [59]. The detection threshold of the test, noted γ_q, is then set from a probability of false alarm ($\mathrm{P_{fa}} = 10^{-3}$) and the estimated antennas number, $\widehat{N}_t$, corresponds to the first value of q respecting $-2\log(\Lambda[\mathbf{Y}|q]) \leq \gamma_q$. To illustrate the principle of the test, figure 2.10 presents the value of the statistic $-2\log(\Lambda[\mathbf{Y}|q])$ and the detection threshold for a MIMO communication ($N_r = 5, N_t = 2$). The first index q for which the statistic $-2\log(\Lambda[\mathbf{Y}|q])$ is less than the threshold, here $\mathbf{2}$, corresponds to the number of transmitting antennas.

The detection method by sequential hypothesis test makes it possible to identify between $\mathbf{0}$ and $N_r - 1$ transmitting antennas. Its use requires fixing a detection threshold based on the probability of false alarm.

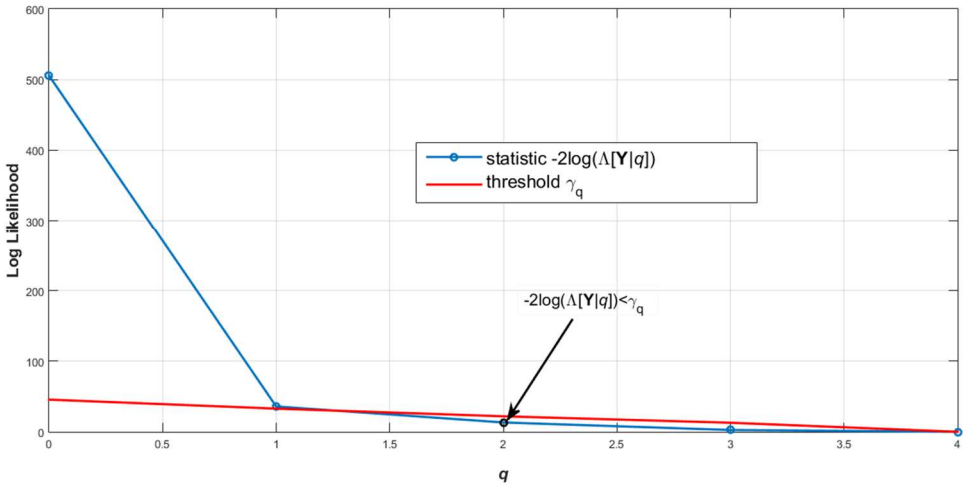

Figure 2.10- Detection of antennas number by sequential test. Example for a MIMO system ($N_r = 5, N_t = 2$), with $N = 512$, and $\mathrm{SNR_{dB}} = 0\mathrm{dB}$.

2.5.4 Equalization algorithms in MIMO

In this section, we present the equalization algorithms that are used in our study:

2.5.4.1 ZF algorithm

The Zero-Forcing (ZF) technique applied to remove some ambiguity from the received symbols. This technique consists in applying an equalization matrix $\mathbf{G_{ZF}}$ on the received vector $\mathbf{y}_i$ [38]. This matrix $\mathbf{G_{ZF}}$ is defined by:

$$\mathbf{G_{ZF}} = \mathbf{H}^{\#} = (\mathbf{H}^{\mathcal{H}}\mathbf{H})^{-1}\mathbf{H}^{\mathcal{H}} \tag{2.22}$$

where $\mathbf{H}^{\#}$ is the pseudo-inverse of the channel matrix $\mathbf{H}$. The transmitted signal is estimated by:

$$\hat{\mathbf{s}}_i = \mathbf{G_{ZF}}\mathbf{y}_i = \mathbf{s}_i + (\mathbf{H}^{\mathcal{H}}\mathbf{H})^{-1}\mathbf{H}^{\mathcal{H}}\boldsymbol{\eta}_i \tag{2.23}$$

Here we assume perfect channel state information (CSI) at the receiver side (semi-blind classifier). The ZF equalization is usually increases the noise level. This is the reason why we have considered another equalizer type.

2.5.4.2 MMSE algorithm

The Minimum Mean Square Error (MMSE) technique searches a matrix $\mathbf{G_{MMSE}}$, which minimizes the mean square error between the transmitted signal $\mathbf{s}_i$ and an equalized version of the received signal $\mathbf{y}_i$ [60]:

$$\varepsilon^2 = E[(\mathbf{s}_i - \mathbf{G_{MMSE}}\mathbf{y}_i)^{\mathcal{H}}(\mathbf{s}_i - \mathbf{G_{MMSE}}\mathbf{y}_i)] \tag{2.24}$$

The linear solution of MMSE is given by:

$$\hat{\mathbf{s}}_i = \mathbf{G_{MMSE}}\mathbf{y}_i = \left(\sigma_\eta^2\mathbf{I}_{N_t} + \mathbf{H}^{\mathcal{H}}\mathbf{H}\right)^{-1}\mathbf{H}^{\mathcal{H}}\mathbf{y}_i \tag{2.25}$$

The MMSE equalizer can minimize the global error caused by noise and mutual interference between received signals [60].

Figure 2.11 shows the BERs of both the MMSE and ZF equalizers along with the Maximum Likelihood (ML) detector, and this for STBC-MIMO system using QPSK modulation and operating in Rayleigh fading channel.

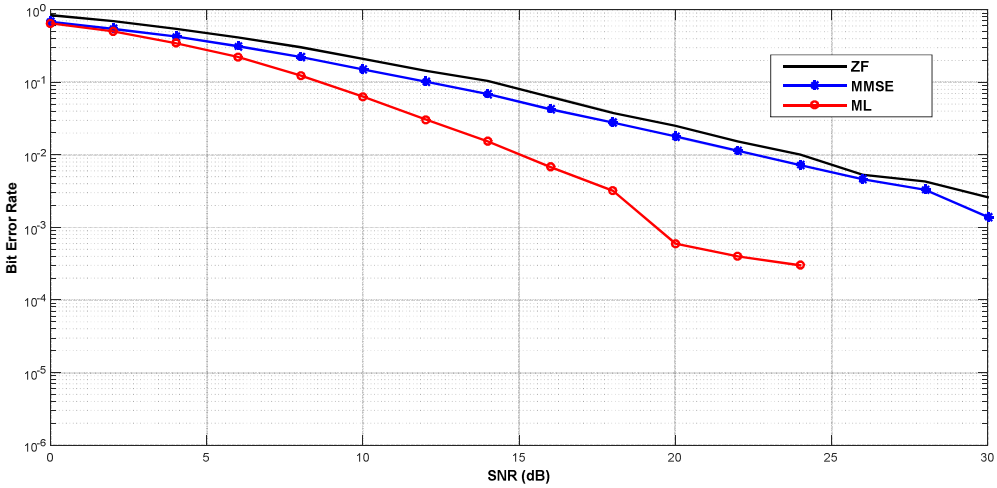

Figure 2.11- BER versus SNR of the ZF and MMSE equalizers and the ML detector for STBC-MIMO system with a configuration (2×2) and QPSK modulation. Fading channel is Rayleigh type.

In the three previous cases, we assume that CSI is available at the receiver. Otherwise, channel estimation must be performed. In this chapter, we will study the impact of channel estimation errors on the performance of the modulation identification process. Therefore, we model the estimated channel as follows:

$$\widehat{\mathbf{H}} = \mathbf{H} + \sigma_e \mathbf{H}_w \tag{2.26}$$

where the elements of $\mathbf{H}_w$ are i.i.d and CSCG variables with zero mean and variance equal to unity, and σ_e^2 represents the variance of channel estimation error.

2.5.4.3 SCMA algorithm

Other types of equalization algorithms exist in the literature; inspired by Blind Source Separation (BSS) algorithms [61-62]. Among these methods, we used a simplified method of the Constant Modulus Algorithm (CMA) called *Simplified-CMA* (SCMA). This algorithm is designed for blind separation and recovery of source symbols (without CSI). Using an equalization matrix $\mathbf{V}$ of size $(N_r \times N_t)$, where $\mathbf{V} = [\mathbf{v}_1, \mathbf{v}_2, \dots, \mathbf{v}_{N_t}]$, we have:

$$\mathbf{z}(i) = \mathbf{V}^{\mathcal{H}}\mathbf{y}_i = \mathbf{V}^{\mathcal{H}}\mathbf{H}\mathbf{s}_i + \mathbf{V}^{\mathcal{H}}\boldsymbol{\eta}_i \tag{2.27}$$

The transmitted symbols $\mathbf{s}_i$ are determined using a permutation matrix $\mathbf{P}$ and a diagonal matrix $\mathbf{\Lambda}$ as follows:

$$\mathbf{G} = \mathbf{V}^{\mathcal{H}}\mathbf{H} = \mathbf{P}\mathbf{\Lambda} \tag{2.28}$$

Indeed, the SCMA criterion uses only one dimension, for example the real part (or the imaginary part) of signal. The SCMA based on the minimization of the following cost function:

$$\begin{cases} \mathbf{J}_{\text{SCMA}}(\mathbf{V}) = \sum_{n_t=1}^{N_t} E\left[\left(\Re\left(z_{n_t}(i)\right)^2 - R\right)^2\right] \\ \text{Subject to : } \mathbf{V}^{\mathcal{H}}\mathbf{V} = \mathbf{I}_{N_t} \end{cases} \tag{2.29}$$

where $R = \frac{E[\Re(z(i))^4]}{E[\Re(z(i))^2]}$ is the dispersion constant. SCMA implemented using the stochastic gradient (SG) algorithm. The equalization update equation is obtained by calculating the gradient of $\mathbf{J}_{\text{SCMA}}$ as follows:

$$\tilde{\mathbf{v}}_{n_t}(i) = \tilde{\mathbf{v}}_{n_t}(i-1) - \varphi_i \epsilon_i \underline{\mathbf{y}}_i \tag{2.30}$$

where φ_i is the SG step size, $\epsilon_i = \left(\Re\left(z_{n_t}(i)\right)^2 - R\right)\Re\left(z_{n_t}(i)\right)$ is the error signal, and $\underline{\mathbf{y}}_i$ is the pre-whitened received signal [63].

2.5.5 Features extraction

One of the important aspects of modulation identification is the selection of the proper features using a HOS from the received signal. Previous works have shown that higher order cumulants (HOC) and higher order moments (HOM) of the received signal are among the best candidates for modulation recognition in SISO and MIMO systems [7, 36, 4, 64-65]. The HOM of a signal "x" is defined by [66]:

$$\boldsymbol{\mu}_{ab}(x) = E[x^{a-b}(x^*)^b] \tag{2.31}$$

where a is the moment order with $0 \leq b \leq a$. The cumulans order "a" of the zero-mean signal "x" is defined by [7]:

$$\boldsymbol{\kappa}_{ab}(x) = Cum\left[\underbrace{x, \ldots, x}_{a-b}, \underbrace{x^*, \ldots, x^*}_{b}\right] \tag{2.32}$$

The relationship between moments and cumulants can be expressed as:

$$\boldsymbol{\kappa}(x_1, \dots, x_a) = \sum_{\Phi}(\varepsilon - 1)!\,(-1)^{(\varepsilon-1)} \prod_{v\in\Phi} E[\prod_{i\in v} x_i] \tag{2.33}$$

where Φ runs through the list of all partitions of $\{1, \dots, a\}$, v runs through the list of all the blocks of the partition Φ, and ε is the number of elements in the partition Φ.

Based on equation (2.33), the moments estimation leads to estimate the cumulants. We can estimate the moments of a signal x with N samples, as:

$$\boldsymbol{\mu}_{ab}(x) = \frac{1}{N}\sum_{n=1}^{N} x_n^{a-b}(x_n^*)^b \tag{2.34}$$

For a complex signal, the estimate of cumulants can be defined as indicated in appendix A. The common self-normalized HOS of order "a", are defined by [66]:

$$\begin{cases} \widetilde{\boldsymbol{\mu}}_{ab} = \frac{\boldsymbol{\mu}_{ab}}{\boldsymbol{\mu}_{21}^{a/2}} \\ \widetilde{\boldsymbol{\kappa}}_{ab} = \frac{\boldsymbol{\kappa}_{ab}}{\boldsymbol{\kappa}_{21}^{a/2}} \end{cases} \tag{2.35}$$

The decision rule for digital modulation using HOS is described in table 2.2, where we assume that the constellations are normalized to have a unity energy ($\boldsymbol{\kappa}_{21} = 1$). We have M ordered hypotheses so that $\boldsymbol{\mu}_1 < \boldsymbol{\mu}_2 < \cdots < \boldsymbol{\mu}_M$. In addition, and for simplicity, we consider that all the variances are equal ($\sigma_1^2 = \sigma_2^2 = \cdots = \sigma_M^2$). In this case, the decision rule based on the choice of hypothesis H verifying [4]:

$$\left(\frac{\boldsymbol{\mu}_{k-1}+\boldsymbol{\mu}_k}{2}\right) \le H < \left(\frac{\boldsymbol{\mu}_k+\boldsymbol{\mu}_{k+1}}{2}\right) \; avec : \begin{cases} \boldsymbol{\mu}_0 = -\infty \\ \boldsymbol{\mu}_{M+1} = +\infty \end{cases} \tag{2.36}$$

Table 2.2. The decision rule based on HOS of order "4" and "6".

	4th HOS : $H = \lvert\widetilde{\boldsymbol{\kappa}}_{40}\rvert$	**6th HOS : $H = \lvert\widetilde{\boldsymbol{\kappa}}_{61}\rvert$**
$\boldsymbol{\Theta_1} = \{\mathbf{BPSK, QPSK, 8PSK}\}$	$\begin{cases} H < 0.5 \Rightarrow \text{8PSK} \\ 0.5 \le H < 1.5 \Rightarrow \text{QPSK} \\ 1.5 \le H \Rightarrow \text{BPSK} \end{cases}$	$\begin{cases} H < 2 \Rightarrow \text{8PSK} \\ 2 \le H < 10 \Rightarrow \text{QPSK} \\ 10 \le H \Rightarrow \text{BPSK} \end{cases}$
$\boldsymbol{\Theta_2} = \begin{Bmatrix} \mathbf{BPSK, QPSK, 8PSK, 4ASK,} \\ \mathbf{8ASK, 16QAM, 64QAM} \end{Bmatrix}$	$\begin{cases} H < 0.31 \Rightarrow \text{8PSK} \\ 0.31 \le H < 0.65 \Rightarrow \text{64QAM} \\ 0.65 \le H < 0.84 \Rightarrow \text{16QAM} \\ 0.84 \le H < 1.12 \Rightarrow \text{QPSK} \\ 1.12 \le H < 1.3 \Rightarrow \text{8ASK} \\ 1.3 \le H < 1.68 \Rightarrow \text{4ASK} \\ 1.68 \le H \Rightarrow \text{BPSK} \end{cases}$	$\begin{cases} H < 0.9 \Rightarrow \text{8PSK} \\ 0.9 \le H < 1.94 \Rightarrow \text{64QAM} \\ 1.94 \le H < 3.04 \Rightarrow \text{16QAM} \\ 3.04 \le H < 5.59 \Rightarrow \text{QPSK} \\ 5.59 \le H < 7.75 \Rightarrow \text{8ASK} \\ 7.75 \le H < 12.16 \Rightarrow \text{4ASK} \\ 12.16 \le H \Rightarrow \text{BPSK} \end{cases}$

To improve the accuracy of identification model, all input and output parameters have been normalized to ensure that they have a zero-mean and variance equal to unity.

2.5.6 Normalization of features

Accelerating the learning process of the classifiers and improving the accuracy of identification can be achieved by normalizing the extracted features (HOS) to ensure that they are zero-mean and unity-variance. Then, we use principal component analysis (PCA) to choose an optimal subset from the uncorrelated extracted HOS.

The PCA allows to select an optimal subset of HOS to improve the identification process [7]. The PCA technique is a standard technique for preprocessing and visualizing high dimension data. The PCA is a linear transformation, which orthogonalizes the data components and reduces the dimensionality (the size of variation) [67]. Therefore, the other components tend to be highly correlated and can be neglected with minimal loss of information.

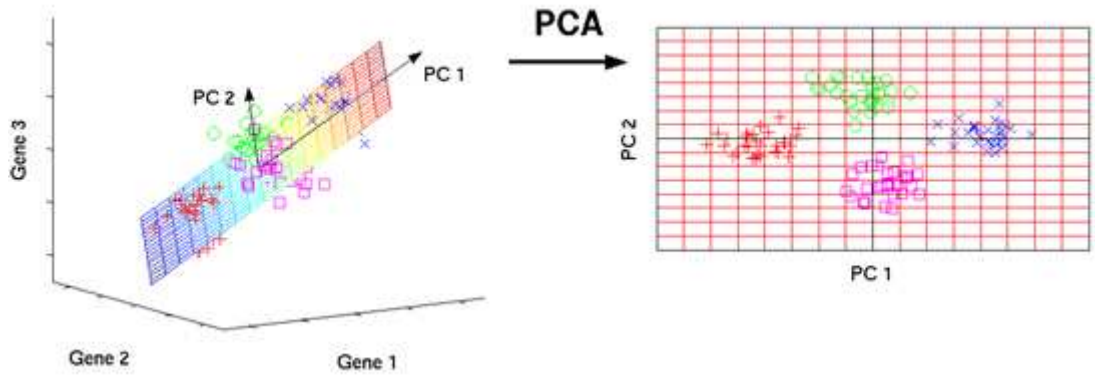

Figure 2.12- A three-dimensional dataset (gene) transformed into a two-dimensional subspace using the PCA algorithm [67].

After selecting the subset with greater variance, the final classification process started.

2.5.7 Comparison of classification methods

The pattern recognition approach is used to solve the problem of modulations identification. This section is consecrated to the study of different classification algorithms such as: Multilayer artificial neural networks (ANN), Support Vector Machines (SVM), Random Forest Classifier (RFC), and K-nearest neighbors (KNN). For digital modulation identification in STBC-MIMO system, these classifiers use three steps:

1- The preprocessing of the signal at the input of the classifiers: Extracts and normalizes the optimal features for each realization of the received signal ;
2- Training and learning phase to adjust the classifier parameters ;

3- Test phase which evaluates the performance of the classification with real signals in order to achieve a final decision about the modulation type of transmitted signal ;

According to figure 2.9, a banc of classifiers of the same type is used to identify the N_d processed signals $\left[\mathbf{a}_i^{(1)}, \dots, \mathbf{a}_i^{(N_d)}\right]$ where $N_d = (K \text{ or } N_t \text{ or } N_r)$. The modulation type in the candidates pool $\Theta = \{\text{BPSK}, \text{QPSK}, \text{8PSK}, \text{4ASK}, \text{8ASK}, \text{16QAM}, \text{64QAM}\}$ is determined by the $\mathcal{T}$-dimension HOS vector defined by $\mathbf{a}_i^{(n_d)} = \left[M_{p_1 q_1}, C_{p_1 q_1}, \dots, M_{p_\mathcal{T} q_\mathcal{T}}, C_{p_\mathcal{T} q_\mathcal{T}}\right]^T$ and represented by the label N_i for each processed signal. These vectors are then used by the classifier bank to give the decisions $\left[\widehat{\mathcal{M}}^{(1)}, \dots, \widehat{\mathcal{M}}^{(N_d)}\right]$. These decisions are used by the decisions fusion block to generate the final decision $\widehat{\mathcal{M}}$.

2.5.7.1 ANN classifier

The multi-layer perceptron (MLP) used in the modulations identification is a linear classifier based on a neural network with back propagations (BP), composed of several layers: an input layer, an output layer, and one or more hidden layers. Each layer consists of a variable number of neurons, and a transfer function for each neuron. The neurons of the output layer always correspond to the outputs of the system.

The inputs of MLP ($\mathbf{a}_i^{(n_d)}$) propage from layer to another and combine at the output layers. The MLP can be expressed by the following equation:

$$y_k = \phi_k\left(\sum_{i=1}^{q} w_{ki}\, \phi_i\left(\sum_{j=1}^{p} w_{ij} a_j\right)\right) \tag{2.37}$$

where y_k is the output of the MLP network, $\phi_i(\cdot)$ is the activation function of the i-th neuron, w_{ij} is the link weighting between the neuron « j » and the neuron « i », and $a_j \in \mathbf{a}^{(n_d)}$ is the j-th input feature of the HOS features set [68]. A visual illustration of an MLP network is given in figure 2.13.

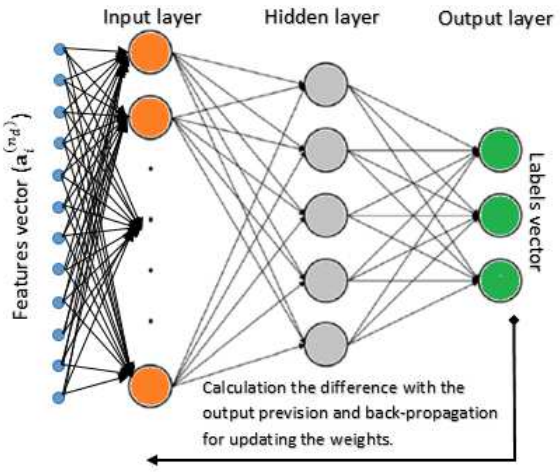

Figure 2.13- Multilayer back-propagation neuron network.

The weights training method of w_{ij} adopted for this MLP is back propagations. This algorithm adjusts the weights through an iterative process by calculating the variation of each weight with respect to the error function E [69]. For example, the mean squared error (MSE) function give the equation:

$$\frac{\delta \mathrm{E}}{\delta w_{ij}} = \frac{\delta \mathrm{E}}{\delta y_i}\frac{\delta y_i}{\delta u_i}\frac{\delta u_i}{\delta w_{ij}} \tag{2.38}$$

where y_i is the output, and u_i is the inputs weighted sum of i-th neuron. The weight value adjusted using the gradient descent approach as follows:

$$w_{ij}(t+1) = w_{ij}(t) - \varepsilon \frac{\delta \mathrm{E}}{\delta w_{ij}} \tag{2.39}$$

where ε is the learning rate that dictates the convergence speed. With a high learning rate, the convergence is faster. However, this is done with a risk of oscillation. On the other hand, with a low learning rate, many additional iterations will be necessary to attain convergence.

The use of ANN classifier goes through two phases: a learning phase, which allows adjusting the weights of neurons. In order to properly adjust the weights of the neurons, learning should relate to a large number of HOS vectors and to all associated modulation schemes, in order to achieve acceptable decision precision, while taking into account different parameters of transmission [7, 70-71].

The features subset $\mathbf{a}_i^{(n_d)}$ lets starter the test process in order to obtain the desired modulation $\widehat{\mathcal{M}}^{(n_d)}$ for the n_d-th branch. The selection of ANN parameters is based on the

choice of structure, which offers the best precision of the probability for making a correct decision in the test phase.

2.5.7.2 SVM classifier

SVM constitute the best-known form of methods based on the use of so-called *kernel function*, which allow optimal binary separation by supervised learning data. The simplest example of a kernel function is the linear kernel, which defined by the equation:

$$\mathcal{K}(\mathbf{x}_i, \mathbf{x}_j) = \mathbf{x}_i^T \mathbf{x}_j \tag{2.40}$$

The SVM method inspired by the statistical learning theory of Vladimir N. Vapnik [72-73]. This method based on the existence of a linear classifier in an appropriate space. If there is a two-class classification problem, $\boldsymbol{\Theta} = \{\mathcal{M}(m), \mathcal{M}(n)\}$, then, the solution is obtained by using the sign of $h(a)$, as shown in the equation:

$$\widehat{\mathcal{M}} = \begin{cases} \mathcal{M}(m) / \ h(a) = \mathbf{a}_i^T \boldsymbol{w} + w_0 \geq 0 \\ \mathcal{M}(n) / \ h(a) = \mathbf{a}_i^T \boldsymbol{w} + w_0 < 0 \end{cases} \tag{2.41}$$

where w_0 is a constant, $\mathbf{a}_i$ is the HOS features vector at the classifier input, and $\boldsymbol{w}$ is the weights vector (or the normal vector of the hyperplane, see figure 2.14) to optimize. The weight is obtained by considering a training samples set $\{\mathbf{a}_i, N_i\}_{i=1}^{N_{tot}}$, with $N_i \in \{-1, +1\}$ a target value also called the binary *class label* corresponding to sample $\mathbf{a}_i$ and N_{tot} is the total number of realizations for the candidates pool $\boldsymbol{\Theta}$. For linearly separable samples, the optimal hyperplane can be found by solving the following optimization problem [74]:

$$\begin{gathered} \text{Minimize } \mathcal{Q}(\boldsymbol{w}, w_0, \mathfrak{L}_i) = \frac{1}{2} \boldsymbol{w}^T \boldsymbol{w} + C \sum_{i=1}^{N_{tot}} \mathfrak{L}_i \\ \text{Subject to } \ N_i(\mathcal{K}(\mathbf{a}_i, \boldsymbol{w}) + w_0) \geq 1 - \mathfrak{L}_i \end{gathered} \tag{2.42}$$

where $\mathfrak{L}_i \geq 0$ are the Lagrange multiplicative variables, and « C » is the margin parameter that determines the arrangement between maximizing the margin and minimizing the classification error. The cost function $\mathcal{Q}$ is minimized compared to $\boldsymbol{w}$, and maximized or reduced according to the sign of $\sum_{i=1}^{N_{tot}} \mathfrak{L}_i$.

SVMs are also called *large-margin separators* because their objective is to find the optimal classification hyperplane as a decision surface that maximizes the margin between classes in a large dimension space. The margin is the distance between the separation border and the closest samples, also called *support vectors*. A maximum margin allows obtain a smaller dimension, which ensures good performances in generalization.

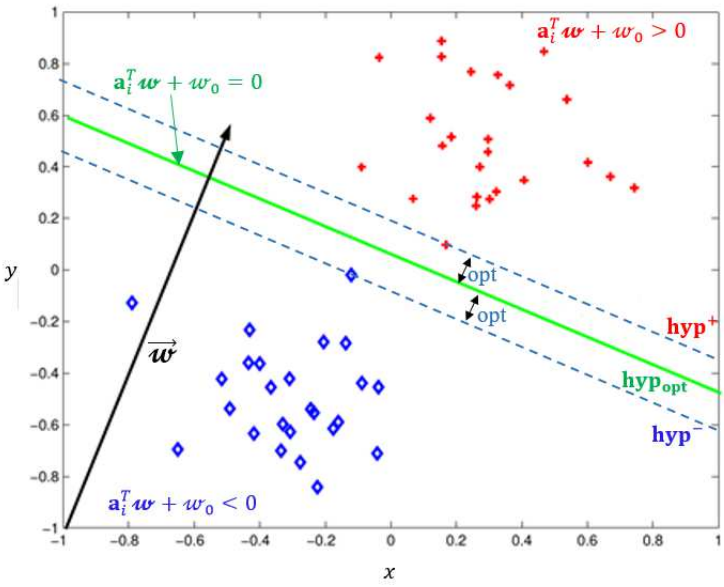

Figure 2.14- Optimal hyperplane of SVM binary classification.

By ensuring these conditions, the learning model of SVM classifier provides accurate classification results and test-ready in order to validate unlabeled data samples.

SVMs are considered easier to deploy compared to neural networks. The main advantage of SVM is its remarkable performances using large data. However, they are slow in convergence and memory intensive when it comes to process large datasets.

A linear SVM classifier algorithm

Input: N_{tot} vectors of the HOS features set derived from each candidate modulation $\boldsymbol{\Theta} = \{\mathcal{M}(1), \mathcal{M}(2)\}$, an observed vector $\mathbf{a}^{(n_d)}$ with extracted feautures for the n_d-th branch.

Step 1 : **Initialization** of weight $\boldsymbol{w}$, w_0

Step 2 : **Repeat**

Step 3 : **Update** the weights via equation (2.42) using the function $\mathcal{Q}$.

Step 4 : **Until** the maximum number of iterations is reached.

Step 5 : $\mathbf{a}_i^T\boldsymbol{w} + w_0$ is calculated.

Step 6 : **If** $\mathbf{a}_i^T\boldsymbol{w} + w_0 \geq 0$, $\mathcal{M}(1)$ is given as classification decision $\widehat{\mathcal{M}}$

Step 7 : **If** $\mathbf{a}_i^T\boldsymbol{w} + w_0 < 0$, $\mathcal{M}(2)$ is given as classification decision $\widehat{\mathcal{M}}$

Output $\widehat{\mathcal{M}}$

2.5.7.3 RFC algorithm

The classification based on random forest algorithm is a learning methodology based on a samples set [75]. The main steps of this algorithm are as follows:

1. Forming the training sample subset by N_{tot} HOS vectors $\mathbf{a}_i^{(n_d)}$, in order to obtain the desired label N_i. n_f out of N_{tot} samples are selected, and $\epsilon_1, \ldots, \epsilon_n$ are the samples seeds generated and assigned to n tree nodes.
2. Random selection of features: t_f out of $\mathcal{T}$ features are randomly selected, from the above samples subsets, as the training samples for RFC, and are assigned to each tree nodes (see figure 2.15).
3. Estimation of errors: Every decision tree of RFC is not growing until the percentage of the classification purity in each node achieves the desired growth or a given layer. After that, one decision tree in the random forest is generated.
4. Complete growth of the decision tree: Repeat the above steps, until achieving an optimal classification and the RFC with n trees is eventually established.

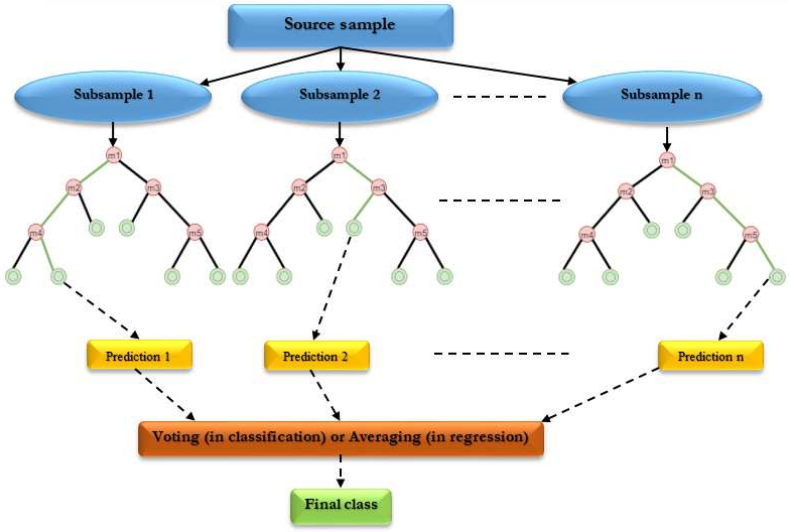

Figure 2.15- Architecture of RFC classification model.

2.5.7.4 KNN classifier

Another supervised algorithm studied in this section. It is a KNN algorithm, which the performance depends on the number of neighbors "K", the distance type used, and the data representation space.

KNN is a simple learning and non-parametric method for classification. Despite the simplicity of this algorithm, it works very well and is constitutes an important reference method.

The KNN classifier requires a metric « $\mathcal{D}$ » and a positive integer "K" [76]. However, KNN is slower to classify new data, since it must launch and completely treat their process for each new input data.

The learning samples set $\{\mathbf{a}_i, N_i\}_{i=1}^{N_{tot}}$ is displayed on an initial space of dimension « $\mathcal{D}$ ». The principle of the supervised selection algorithm is to extract a subset of "K" features among all features set, allowing to classifying this labeled data. The obtained KNN classifier model is used to calculate the distance (for example, Euclidean distance) between unlabeled input samples from "K" neighboring samples. KNNs are found and a voting scheme used to find the most common neighbor label. The class with the maximum number of neighbors is considered the class of the test sample (see figure 2.16).

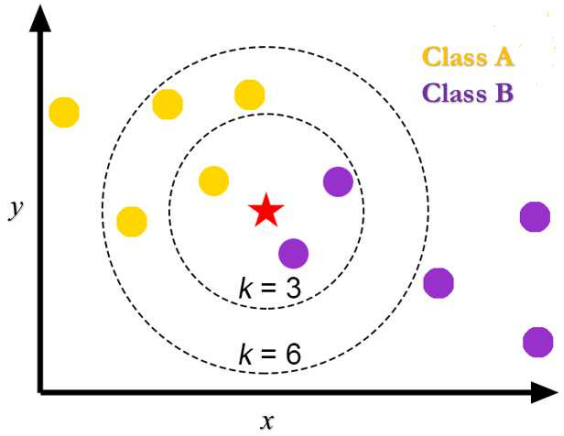

Figure 2.16- K-nearest neighbors method.

With the KNN classifier, the Euclidean distance metric is a simple and easy-to-implement method for calculating distances in a multidimensional input space [77-78]. The Euclidean distance between two points in a space is the length of the line between them. In Cartesian coordinates, if p_d and q_d are two points of the Euclidean space $\mathcal{D}$, the distance between p_d and q_d is given by:

$$d_E = \sqrt{\sum_{d=1}^{\mathcal{D}} (q_d - p_d)^2} \tag{2.43}$$

The outputs of the classifiers are combined in the decision fusion center in order to improve the precision of the identification and the final decision.

2.5.8 Decisions fusion center

Since there are multiple antennas at the receiver, it is possible for them to cooperate to achieve higher identification reliability. The modulation scheme of each stream among N_d processed

streams is identified independently and all the decision vectors are jointly processed to take a final decision. We call this cooperative identification scheme as *decisions fusion*. The final decision is taken by combining the decision vectors and applying the "M-out-of-N_d" decision fusion rule, i.e., a certain modulation scheme is identified when it is decided on M classifier among the N_d classifiers [7, 36].

Suppose that the decisions are independent, the total probability of the modulation identification scheme is given by:

$$\mathbb{P} = \sum_{k=M}^{N_d} \binom{N_d}{k} P_{n_d}^k \left(1 - P_{n_d}\right)^{N_d - k} \tag{2.44}$$

where $\binom{N_d}{k} = \frac{N_d!}{k!(N_d-k)!}$, and P_{n_d} is the detection probability for each individual classifier. Here, we consider that the probability of identification is identical for all the decision branches ($P_{n_d} = \frac{1}{N_d}$), which all the classifiers are identical and the N_d processed signals are statistically identical. Note that the M-out-of-N_d decision fusion rule includes different logics:

1. **Logical OR:** The cooperative detection performance with this fusion rule can be evaluated by taking $M = 1$ in the equation (2.44) :

$$\mathbb{P}_{\mathrm{OR}} = 1 - \left(1 - P_{n_d}\right)^{N_d} \tag{2.45}$$

2. **The majority:** The fusion is based on a majority rule. The cooperative detection performance with this fusion rule can be evaluated by taking $M = \left\lceil \frac{N_d}{2} \right\rceil$ in equation (2.44), where $\lceil \cdot \rceil$ denotes the ceiling function:

$$\mathbb{P}_{\mathrm{MAJ}} = \sum_{k=\left\lceil \frac{N_d}{2} \right\rceil}^{N_d} \binom{N_d}{k} P_{n_d}^k \left(1 - P_{n_d}\right)^{N_d - k} \tag{2.46}$$

3. **Logical AND:** The decision at the fusion center is calculated by the logical "AND". The cooperative detection performance with this fusion rule can be evaluated by taking $M = N_d$ in equation (2.44):

$$\mathbb{P}_{\mathrm{AND}} = P_{n_d}^{N_d} \tag{2.47}$$

When the decision vectors do not fit the decisions fusion rule, the final decision is rejected.

2.6 Simulation results

The objective of these simulations is to evaluate our classification method in order to identify the modulation schemes. The algorithm studied has been checked and validated to identify the different modulation schemes in the pool $\boldsymbol{\Theta} = \{\text{BPSK}, \text{QPSK}, \text{8PSK}, \text{4ASK}, \text{8ASK}, \text{16QAM}, \text{64QAM}\}$. We assume that the N_d branches are equiprobable.

In these simulations, we consider the different configurations written below:

- Antennas configuration : $N_t = 2$ and $N_r = 4$;
- Alamouti coding : $N_t = 2, K = 2, U = 2$;
- Number of symbols : $N = 512$ i.i.d symbols ;
- All results are based on **1000** Monte Carlo trials for each modulation scheme i.e. $N_{iter} = 7000$ Monte Carlo trials in total for $\boldsymbol{\Theta}$;

The probability of identification is given in percentage and is estimated by:

$$\mathrm{P}_i = \frac{N_c}{N_{iter}} \times 100 \tag{2.48}$$

where N_c is giving by:

$$N_c = \sum_{\widehat{\mathcal{M}}_m \in \Theta} N_{\widehat{\mathcal{M}}_m} \tag{2.49}$$

where $N_{\widehat{\mathcal{M}}_m}$ is the number of decisions for which each modulation in the pool Θ is correctly identified.

The probability of correct identification $\mathrm{P_{ci}}$, is evaluated by the modulation classification process, and is given in percentage by:

$$\mathrm{P_{ci}} = \frac{1}{\mathrm{card}(\Theta)} \sum_m \mathbb{P}\left(\widehat{\mathcal{M}} = \mathcal{M}_m | \mathcal{M}_m\right) \times 100 \tag{2.50}$$

where $\mathbb{P}(\cdot)$ is the probability of an event, the $\mathrm{card}(\Theta)$ is the modulation pool cardinal of Θ, and $\widehat{\mathcal{M}}$ is the estimated modulation scheme.

The performance of the identification is also confirmed by the probability of false alarm $\mathrm{P_{fa}}$, and is evaluated in percentage by:

$$\mathrm{P_{fa}} = \frac{1}{\mathrm{card}(\Theta)} \sum_m \mathbb{P}\left(\widehat{\mathcal{M}} = \mathcal{M}_m | \mathcal{M}_n\right)_{,m \neq n} \times 100 \tag{2.51}$$

Since OSTBC decouples the space-time channel into parallel scalar channels each with SNR considered in our simulations is defined as [79]:

$$\mathrm{SNR_{dB}} = 10\log_{10}\left(\frac{1}{R}\frac{\rho^2}{N_t}\frac{\sigma_s^2}{\sigma_\eta^2}\|\mathbf{H}\|^2\right) \tag{2.52}$$

where σ_s^2 is the average power of the samples on each antenna, σ_η^2 is the noise power, N_t number of transmitting antennas, ρ^2 is a constant used to control the transmit power, and $\|\mathbf{H}\|$ is the channel matrix norm. We assume that the transmit power is equal to one for each antenna (hence $\rho^2 = N_t$).

We define the minimum required SNR for close to optimal modulation identification, $\mathrm{SNR_{min}}$ by $\frac{\mathrm{P}_i(\infty)-\mathrm{P}_i(\mathrm{SNR}>\mathrm{SNR_{min}})}{\mathrm{P}_i(\infty)} < \epsilon$, where normally, $\epsilon = 0.01$ and $\mathrm{P}_i(\infty) = 100\%$ [7].

In the following, we present the simulation results of the two proposed algorithms ZF-DMC and SCMA-DMC.

2.6.1 Performances of antenna correlation

In this section, we evaluate the behavior of the radio channel in the digital modulations classification in the presence of spatial correlation at the transmitter and receiver side. We consider the case where the channel matrix is modeled by the Kronecker model as indicated in equation 2.10, where $\mathbf{H}_w \sim \mathcal{CN}\left(\mathbf{0}_{N_r\times N_t}, \mathbf{I}_{N_r} \otimes \mathbf{I}_{N_t}\right)$, we conclude that $\mathbf{H} \sim \mathcal{CN}\left(\mathbf{0}_{N_r\times N_t}, \mathbf{R}_{N_r} \otimes \mathbf{R}_{N_t}\right)$ [1, 7]. Here, we will consider the presence of both spatial correlation on transmission and on reception with $|\rho| = |\rho_t| = |\rho_r|$. These coefficients are parameters used to adjust the level of spatial correlation.

Figure 2.17 examines the identification performance of modulations in the presence of spatial correlation. As noted, performance degrades as correlation increases.

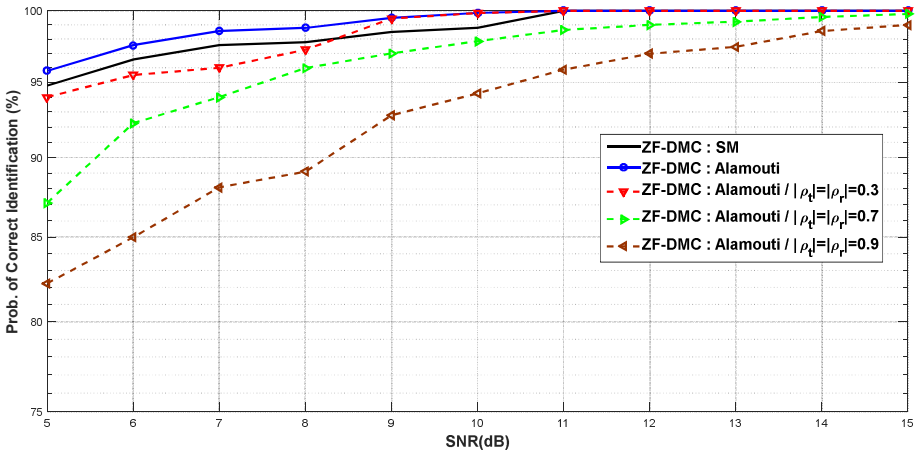

Figure 2.17- Probability of identification versus SNR for ZF-DMC with the Kronecker correlation model.

The $\mathrm{SNR_{min}}$ of the modulation identification via the spatially uncorrelated MIMO channel is 8.7dB, while the $\mathrm{SNR_{min}}$ is 9dB and 12dB when $|\rho t| = |\rho r| = 0.3$ and $|\rho t| = |\rho r| = 0.7$. In addition, the $\mathrm{SNR_{min}}$ of the modulation identification is 15dB when $|\rho t| = |\rho r| = 0.9$. The results found indicate that when $|\rho| \rightarrow 1$, the performance degrades quickly.

2.6.2 Performances of equalization and channel estimation error

In the ZF algorithm, the modulation identification is considered semi-blind, assuming that the perfect CSI at the receiver. However, the ZF equalizer could be considered blind using the channel estimation error. On the other hand, the SCMA equalizer is used to blindly separate MIMO sources and the identification is considered blind. The objectives of this simulation are:

- Compare the identification of different schemes in the blind and semi-blind case in order to show the influence of channel mixing on the probability of modulation identification.
- Examine the impact of channel estimation error on modulation recognition rather than on the estimation process. An incorrect channel estimate is modeled in equation (2.26).

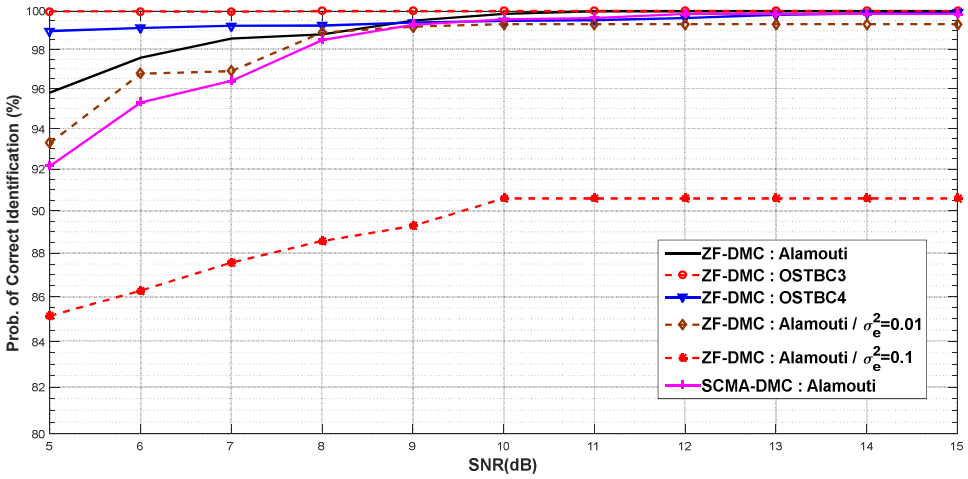

Figure 2.18- Probability of identification versus SNR for two equalization methods with channel estimation errors.

From figure 2.18, we noticed that the ZF-DMC algorithm offers the best performance when perfect CSI is assumed. However, the proposed ZF-DMC algorithm is sensitive to channel estimation errors. It should be noted that, the presence of an incorrect channel estimate causes a rapid performance degradation when the error variance $\sigma_e^2 \geq 0.1$. Also, this erroneous estimation leads to an upper bound of the probability of correct recognition ($< 100\%$) contrary to the perfect CSI case. This upper bound decreases as σ_e^2 increases. To solve this problem, the

blind SCMA-DMC algorithm was proposed. This algorithm solved the upper bound problem without any CSI knowledge. However, the SCMA-DMC requires a higher SNR to obtain the same performance as ZF-DMC when the perfect CSI is assumed [1, 7, 65].

2.6.3 Probability of correct identification and probability of false alarm

The detection thresholds for each digital modulation processed is based on the probability of correct identification P_{ci} and the probability of false alarm P_{fa} (see equations 2.50 and 2.51). In this study, we examine P_{ci} and P_{fa} separately for each modulation scheme instead of calculating the average probability P_i for all the schemes. To answer the requirements of our detection system, the typical values of P_{fa} must be between **1%** and **10%** for $SNR_{dB} \geq 5dB$.

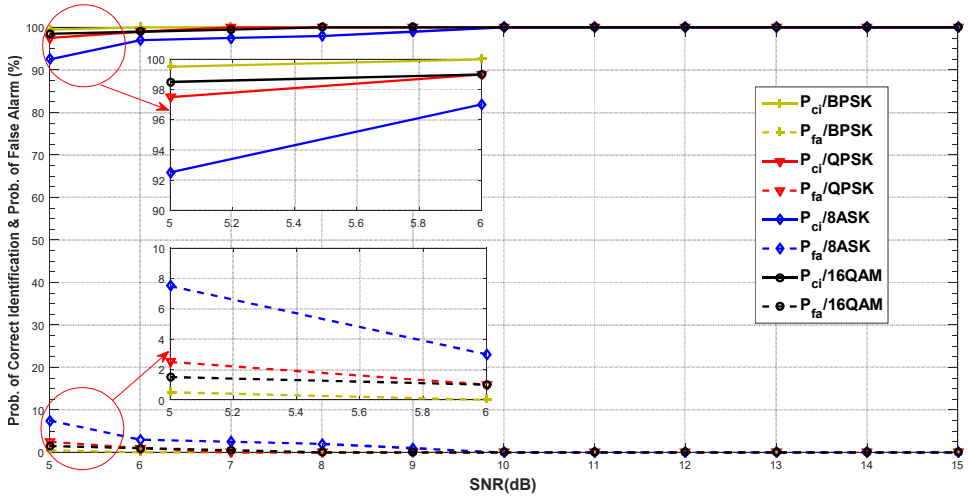

Figure 2.19- P_{ci} and P_{fa} versus SNR for each modulation scheme, ZF-DMC algorithm.

According to figure 2.19, when the SNR is relatively low, the BPSK modulation has a higher P_{ci} and a lower P_{fa} compared to the other modulations.

2.7 Conclusion

In the second part, we are interested in the problems of recognition of the various parameters of the transmitted signal as a supervised classification problem. The supervised algorithms are applied on labeled databases. The DMC process studied here is proposed for STBC-MIMO systems spatially correlated and based on HOS subsystem as a features extraction and the neural network as a classification subsystem.

The simulation results show that the ZF-DMC algorithm using a ZF equalizer is less complex compared to the SCMA-DMC algorithm. The ZF-DMC algorithm shows better results if there is perfect CSI. The SCMA-DMI algorithm blindly separates the symbols and provides

a better estimate without any CSI knowledge. The proposed algorithms are examined through correlated STBC-MIMO channels and their ability to identify different digital modulation schemes is confirmed with great precision.

The robustness of these algorithms to synchronization errors, and to frequency offset in STBC-MIMO system is the subject of future work.

Chapter 3

Digital Modulation Classification in MIMO-OFDM Systems

Sommaire

3.1 Introduction

MIMO systems represent an important role in the development of future broadband wireless communications, because they offer improved channel capacity compared to SISO systems. By using MIMO techniques, the effects of selective fading channel can be considerably reduced. However, Inter-Symbol Interference (ISI) generated in a frequency selective channel results in serious performance degradation. To overcome this disadvantage, the OFDM system is used, firstly for its simplicity of equalization and on the other hand to increase the spectral efficiency.

In order to recover the transmitted symbols from an observed noisy mixture at the CR receiver side in MIMO-OFDM system, recognition of the digital modulation type is necessary. This improves the capacity of the CR system to allow it to select the appropriate demodulation process.

Various modulation classification algorithms have been proposed for MIMO-SC systems [6-7]. Only a few research works deal with the modulation classification problem for MIMO-OFDM systems.

In [17], an algorithm based on the SVM classifier using HOCs as discriminating features is reported. Furthermore, the DMC algorithm based on the approximate Bayesian inference adopting the Dirichlet model is proposed in [9], which allow obtaining a better classification performance with a higher computational complexity.

In this chapter, we treat the DMC algorithm in MIMO-OFDM systems. The deployment of our identification method in MIMO-OFDM systems is more difficult than the case of MIMO-SC systems, because the OFDM technique is extremely sensitive to transmission degradations (the problem of symbols synchronization) [80].

Also, the different transmitters do not share the same equipment, which causes frequency offsets between the different transmitters. Indeed, if they are not compensated, the subcarriers are no longer orthogonal and the performance of the receivers is degraded [81]. In order to increase system capacity, we use blind and semi-blind techniques to jointly estimate the CFO and channels.

In addition to channel fading and the synchronization problem, the MIMO-OFDM signal is distorted by the presence of AWGN noise, which is the most widely employed noise model in the literature. Indeed, in the majority of research papers, the hypothesis of Gaussian noise is considered. However, this hypothesis is not applicable in railway communications which exhibit non-Gaussian and impulsive noise. Impulsive noise is described as one or more repetitive or no

repetitive pulses with the random duration and the occurrence. This degrade severely the transmission characteristics of OFDM signal [10]. In this context, various studies and measurements have guided to the reality that the impulsive noise is a heavy-tailed. Our objective is the mitigation of the impulsive noise present in the received STBC-OFDM signal, which consequently ameliorates the DMC process. To achieve this goal, we estimate the impulsive noise parameters, and then implement the Myriad filter (MF) in the STBC-OFDM receiver.

In order to obtain the estimates of transmitted signal we decode the received filtered signal. After that, a HOS calculation is done to extract features followed by pattern recognition process (ANN, SVM, KNN or RFC). Outputs of this step are jointly processed, in a decisions fusion center, to decide about the used modulation. The proposed algorithm is robust and allows it possible to identify the different parameters of radio signal in more complicated scenarios with a comparatively lower computational complexity. The algorithms used address the DMC problem in MIMO-OFDM systems using the Alamouti matrix for ST coding and SF (space-frequency) coding.

In the rest of this chapter, we discuss the OFDM modulation technique, followed by the basic concepts of STBC-OFDM and SFBC-OFDM systems. In each MIMO-OFDM system, we describe the different processes proposed for our DMC algorithm. The chapter ends with conclusion and perspectives on future projects.

3.2 OFDM techniques

OFDM modulation is an extension of the Frequency Division Multiplexing (FDM) technique. The basic idea of FDM is to divide the bandwidth into many narrow sub-bands and use a large number of parallel narrow-band subcarriers to transfer information [82]. The main advantage of FDM is its robustness against:

- *Frequency selective fading*: Each subcarrier treaty with flat fading rather than frequency selective fading like a broadband carrier.
- *Narrowband interference*: Narrow band interference will affect only one or two subcarriers of the set of subcarriers. The other subcarriers will not be affected by the interference.

The OFDM technique is a multi-carrier modulation whose available frequency band is divided into several orthogonal subcarriers thus authorizing a certain overlap between the sub-bands, allowing to increase the spectral efficiency. Interference between the subcarriers is eliminated due to the orthogonality between them; this contributes helps to reducing the implementation complexity of the transmitter and the receiver [83-85]. The bands occupied by the subcarriers

are very narrow, therefore considered flat compared to the interferences introduced by the channel, and can be easily equalized.

The spacing of the subcarriers is carefully selected so that each carrier is located on all the crossing points of other carrier spectrum and the power spectrum of each subchannel is relatively coherent [86].

To write this technique mathematically, we assume a symbol $\tilde{s}_{k,i}$ sent on the k-th subcarrier at time iT. So the signal transmitted in baseband is written as [87]:

$$s_m = \frac{1}{\sqrt{N}} \sum_{k=0}^{N-1} \sum_i \tilde{s}_{k,i} g[m - iN] e^{j2\pi \frac{km}{N}} \tag{3.1}$$

where N is the number of subcarriers and the function $g[m]$ is given by :

$$g[m] = \begin{cases} 1 & 0 \leq m < N \\ 0 & \text{sinon} \end{cases} \tag{3.2}$$

In a perfect channel, the reconstruction of the transmitted symbols is assured by the condition of orthogonality:

$$\sum_m g[m - iN] g[m - i'N] e^{j2\pi \frac{km}{N}} e^{j2\pi \frac{k'm}{N}} = \delta_{k,k'} \delta_{i,i'} \tag{3.3}$$

The expression of equation (3.1) can be easily and effectively obtained using the inverse fast Fourier transform (IFFT). Thus, the IFFT algorithm is applied to each vector $\tilde{\mathbf{s}}_i = \left[\tilde{s}_{0,i}, \tilde{s}_{1,i}, \dots, \tilde{s}_{N-1,i}\right]^T$ which is called a *symbol OFDM*.

When the signal is transmitted over a frequency-selective channel, we will observe an interference between the symbols of the same block (Inter-Carrier Interference (ICI)), but also between the symbols from two successive OFDM symbols (ISI).

The OFDM orthogonality is lost due to the appearance of ISI. To reduce this problem, a first solution consists in extending the number of subcarriers N, to increase the OFDM symbol duration. The second solution is to insert a guard interval or cyclic prefix (CP), greater than or equal to the maximum channel spread ($N_{cp} \gg L$) [88].

The guard interval contains a copy of the last symbols of a block; we can also delete ISI from the same block. At the reception, the CP is first deleted, then an fast Fourier transform (FFT) operation is applied to the remaining symbols.

3.3 STBC-OFDM system model

In general in OFDM modulation, all N subcarriers are modulated using data symbols ($N = N_s$), but in certain situations (semi-blind system) some subcarriers among the N are assigned to N_p non-zero pilots symbols. Only N_e ($N_e = N_s + N_p$) from N subcarriers are used, the remaining $(N_{vsc} = N - N_e)$ subcarriers represent the virtual subcarriers (VSC), where $N = N_s + N_p + N_{vsc}$. The pilot symbols are known at the transmitter and receiver side and are used for the joint channel and CFO estimation. The pilot symbols can be distributed over several consecutive OFDM symbols.

In this project, we consider a wireless OFDM system employing an STBC architecture with N_t and N_r transmit and receiver antennas, respectively. The data and pilot symbol streams $\boldsymbol{S}$ and $\boldsymbol{P}$ are collected into N_b blocks $\{\mathbf{s}_{iN_b+m}\}_{m=0}^{N_b-1}$ of length N_s and $\{\mathbf{p}_{iN_b+m}\}_{m=0}^{N_b-1}$ of length N_p, respectively. N_b is the number of the inputs of the STBC encoder. Each block constituted N_b data symbol vectors, $\mathbf{s}_{i,m} = \left[s_{i,m}(0), s_{i,m}(1), \dots, s_{i,m}(N_s - 1)\right]^T$ and N_b pilots symbol vectors, $\mathbf{p}_{i,m} = \left[p_{i,m}(0), p_{i,m}(1), \dots, p_{i,m}(N_p - 1)\right]^T$. Data and pilot symbols are randomly and independently drawn from well-defined modulation scheme. STBC encoder maps the vectors $\mathbf{s}_i$ and $\mathbf{p}_i$ in space and time coding matrices $\mathbf{C} = \mathcal{G}_{Al}^T(\mathbf{s}_i)$ and $\mathbf{B} = \mathcal{G}_{Al}^T(\mathbf{p}_i)$ of size $N_t N_s \times U$ and $N_t N_p \times U$ respectively, to be transmitted from N_t antennas during U time slots per block [89] :

$$\begin{cases} \mathcal{G}_{Al}^T(\{\mathbf{s}_{2i+m}\}_{m=0}^1) = \begin{bmatrix} \mathbf{c}_{2i}^{(1)} & \mathbf{c}_{2i+1}^{(1)} \\ \mathbf{c}_{2i}^{(2)} & \mathbf{c}_{2i+1}^{(2)} \end{bmatrix} = \begin{bmatrix} \mathbf{s}_{2i} & -\mathbf{s}_{2i+1}^* \\ \mathbf{s}_{2i+1} & \mathbf{s}_{2i}^* \end{bmatrix} \\ \mathcal{G}_{Al}^T(\{\mathbf{p}_{2i+m}\}_{m=0}^1) = \begin{bmatrix} \mathbf{b}_{2i}^{(1)} & \mathbf{b}_{2i+1}^{(1)} \\ \mathbf{b}_{2i}^{(2)} & \mathbf{b}_{2i+1}^{(2)} \end{bmatrix} = \begin{bmatrix} \mathbf{p}_{2i} & -\mathbf{p}_{2i+1}^* \\ \mathbf{p}_{2i+1} & \mathbf{p}_{2i}^* \end{bmatrix} \end{cases} \tag{3.4}$$

After that, $\mathbf{C}$ and $\mathbf{B}$ are multiplexed into one matrix of size $N_t N_e \times U$. Each element of the multiplexed matrix, namely $\left\{\tilde{\mathbf{v}}_{iU+u}^{(n_t)}\right\}_{u\in\{0,\dots,U-1\}}^{n_t\in\{1,\dots,N_t\}}$ of length N_e can be written as :

$$\tilde{\mathbf{v}}_{i,u}^{(n_t)} = \boldsymbol{\mathcal{Q}}_{N_e}^{\alpha} \mathbf{c}_{i,u}^{(n_t)} + \boldsymbol{\mathcal{Q}}_{N_e}^{\beta} \mathbf{b}_{i,u}^{(n_t)} \tag{3.5}$$

where $\boldsymbol{Q}_{N_e}^{\alpha}$, $\boldsymbol{Q}_{N_e}^{\beta}$ are $(N_e \times N_s)$ and $(N_e \times N_p)$, permutation matrices, and are selected to be mutually orthogonal. They are formed from the columns of the identity matrix $\mathbf{I}_{N_e}$ as follows [90]:

$$\begin{cases} \boldsymbol{Q}_{N_e}^{\alpha} = \mathbf{I}_{N_e}\{\boldsymbol{i}_{\alpha}\} = \left[\mathbf{e}_{N_e}^{(\alpha_1)}, \mathbf{e}_{N_e}^{(\alpha_2)}, \dots, \mathbf{e}_{N_e}^{(\alpha_{N_s})}\right] \\ \boldsymbol{Q}_{N_e}^{\beta} = \mathbf{I}_{N_e}\{\boldsymbol{i}_{\beta}\} = \left[\mathbf{e}_{N_e}^{(\beta_1)}, \mathbf{e}_{N_e}^{(\beta_2)}, \dots, \mathbf{e}_{N_e}^{(\beta_{N_p})}\right] \end{cases}$$

where $\boldsymbol{i}_{\beta} = \{\beta_1 \dots \beta_{N_p}\}$ and $\boldsymbol{i}_{\alpha} = \{\alpha_1 \dots \alpha_{N_s}\}$ are the indexes of pilot tones and subcarriers carrying data symbols, respectively. N_{vsc} virtual subcarriers are added to $\tilde{\mathbf{v}}_{i,u}^{(n_t)}$ to form the vector $\bar{\mathbf{v}}_{i,u}^{(n_t)}$. Next, N-points of $(\mathbf{F}_N^{\mathcal{H}})$, is applied to the vector $\bar{\mathbf{v}}_{i,u}^{(n_t)}$ and a CP is inserted by multiplication with an appropriate matrix $\mathbf{T}_{cp} = \left[\mathbf{I}_{N_{cp}\times N}^T, \mathbf{I}_N^T\right]^T$.

The i-th ST block is generated as shown on the figure 3.1.

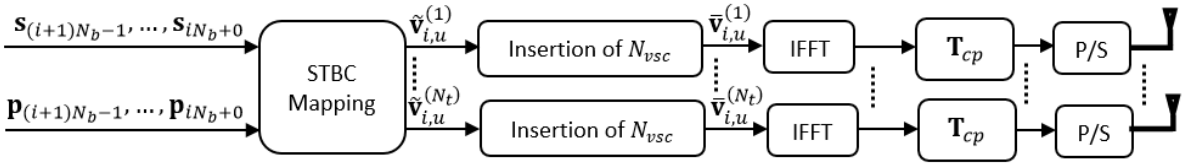

Figure 3.1- Discrete-time-equivalent baseband model of STBC-OFDM block transmission systems.

The resulting signal sent through N_t antennas and received by N_r antennas passes through a Rayleigh fading channel. $h^{(n_r,n_t)}(l)$ with $l \in [0, L-1]$ denotes the L channel coefficient between the n_t-th transmit antenna and the n_r-th receive antenna.

At the receiver side, the condition of orthogonality between the subcarriers will be restored by removing the CP. Using the appropriate matrix $\mathbf{R}_{cp} = \left[\mathbf{0}_{N\times N_{cp}}, \mathbf{I}_N\right]$, to remove the CP from the received signal.

We assume that the synchronization between the oscillators of the transmitter and the receiver is perfect (absence of CFO), the i-th received signal by the n_r-th antenna is written in the following form:

$$\mathbf{y}_{i,u}^{(n_r)} = \frac{1}{\sqrt{N_e}} \sum_{n_t=1}^{N_t} \widetilde{\mathbf{H}}^{(n_r,n_t)} \mathbf{F}_N^{\mathcal{H}} \bar{\mathbf{v}}_{i,u}^{(n_t)} + \boldsymbol{\eta}_{i,u}^{(n_r)} \tag{3.6}$$

where $\boldsymbol{\eta}_{i,u}^{(n_r)} = \left[\eta_i^{(n_r)}(uN), \ldots, \eta_i^{(n_r)}(uN+N-1)\right]^T$ is an $(N \times 1)$ additive zero-mean white circularly complex Gaussian noise vector with variance $\sigma_\eta^2\, \mathbf{I}_N$; i.e. $\boldsymbol{\eta}_{i,u}^{(n_r)} \sim \mathcal{CN}\left(0, \sigma_\eta^2\, \mathbf{I}_N\right)$. $\widetilde{\mathbf{H}}^{(n_r,n_t)} = \mathbf{R}_{cp}\mathbf{H}^{(n_r,n_t)}\mathbf{T}_{cp}$ is a $(N \times N)$ circulant matrix and $\mathbf{H}^{(n_r,n_t)}$ is a $\left(N_q \times N_q\right)$ lower triangular Toeplitz matrix with $N_q = N + N_{cp}$. The First column $\mathbf{H}^{(n_r,n_t)}$ is $\left[h^{(n_r,n_t)}(0), \ldots, h^{(n_r,n_t)}(L-1), 0, \ldots, 0\right]^T$.

To simplify our input–output relationship in equation (3.6), we can use the property of diagonal matrix $\mathbf{D}_N\left(\tilde{\mathbf{h}}^{(n_r,n_t)}\right) = \mathbf{F}_N \widetilde{\mathbf{H}}^{(n_r,n_t)} \mathbf{F}_N^{\mathcal{H}}$, where:

$$\begin{cases} \tilde{\mathbf{h}}^{(n_r,n_t)} \coloneqq \left[\tilde{h}^{(n_r,n_t)}(0), \ldots, \tilde{h}^{(n_r,n_t)}(2\pi\,(N-1)/N)\right]^T \\ \tilde{h}^{(n_r,n_t)}(2\pi\, n/N) \coloneqq \sum_0^{L-1} h^{(n_r,n_t)}(l) e^{(-j2\pi ln/N)} \end{cases}$$

The $\tilde{h}^{(n_r,n_t)}$ denoting the (n_r, n_t)-th channel's frequency-response values. Equation (3.6) can be rewritten now as:

$$\mathbf{y}_{i,u}^{(n_r)} = \frac{1}{\sqrt{N_e}} \mathbf{F}_N^{\mathcal{H}} \sum_{n_t=1}^{N_t} \mathbf{D}_N\left(\bar{\mathbf{v}}_{i,u}^{(n_t)}\right) \tilde{\mathbf{h}}^{(n_r,n_t)} + \boldsymbol{\eta}_{i,u}^{(n_r)} \tag{3.7}$$

Where:

$$\begin{cases} \tilde{\mathbf{h}}^{(n_r,n_t)} = \boldsymbol{\Gamma}_N \mathbf{h}^{(n_r,n_t)} \\ \boldsymbol{\Gamma}_N = [\mathbf{f}_0^L, \mathbf{f}_1^L, \ldots, \mathbf{f}_{N-1}^L]^{\mathcal{H}} \\ \mathbf{f}_n^L = [1, \exp(j2\pi n/N), \ldots, \exp(j2\pi n(L-1)/N)]^T \end{cases}$$

At each receiving antenna, the restored OFDM symbol is given to the FFT block to be demodulated. The signal at the output of the FFT is written:

$$\tilde{\mathbf{y}}_{i,u}^{(n_r)} = \frac{1}{N_e} \sum_{n_t=1}^{N_t} \mathbf{D}_N\left(\bar{\mathbf{v}}_{i,u}^{(n_t)}\right) \tilde{\mathbf{h}}^{(n_r,n_t)} + \tilde{\boldsymbol{\eta}}_{i,u}^{(n_r)} \tag{3.8}$$

From equation (3.8), the transmitted signal can be easily decoded by applying a simple equalization to the FFT output.

Despite their advantages, OFDM has two weaknesses that must be taken into account, that is:

- The OFDM is sensitive to frequency offsets due to the destruction of orthogonality. Pollet et *al.* [91] have shown that multi-carrier systems are much more sensitive to frequency offsets than single-carrier systems. They gave a relationship that determines the degradation in terms of SNR [92] :

$$D_{\mathrm{db}} \approx \frac{10\pi^2}{3\ln 10}\left(1-\frac{1}{N}\right)^2 (1+\mathrm{SNR}_{\mathrm{without-cfo}})\omega_0^2 \tag{3.9}$$

where ω_0 is the normalized frequency offset. The frequency offsets looks like noise, which degrades the SNR in the absence of the CFO ($\mathrm{SNR}_{\mathrm{without-cfo}}$).

- The OFDM is sensitive to the non-linearities of the amplifiers. The signal may have a very high peak to average power ratio (PAPR), causing saturation of the analog blocks [93].

3.3.1 DMC in STBC-OFDM systems

In this section, we solve the DMC problem in MIMO-OFDM system. The STBC encoder of Alamouti type is used to code information symbols. The information symbols are chosen from the different modulation schemes grouped in a pool $\Theta = \{\mathrm{QPSK}, 16\mathrm{QAM}\}$. The features extraction is done by HOS subsytem, and then classified by different classifiers to solve the modulation identification problem (see figure 3.2).

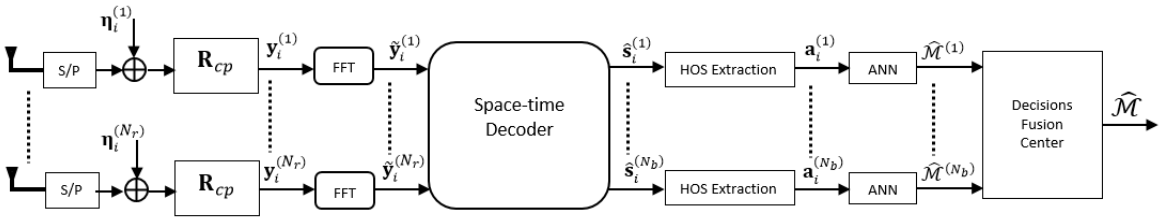

Figure 3.2- Discrete-time-equivalent baseband model of the DMC method in STBC-OFDM system.

Figure 3.3 shows the effect of the number of received antennas (N_r) on the probability of correct modulation identification $\mathrm{P_{ci}}$ for all classifiers. We remark that all classifiers showed slightly more stable results. Indeed, we observe that $\mathrm{P_{ci}}$ improves, in a progressive way, as the SNR values increase and as the number of received antennas N_r increases from 2 to 4.

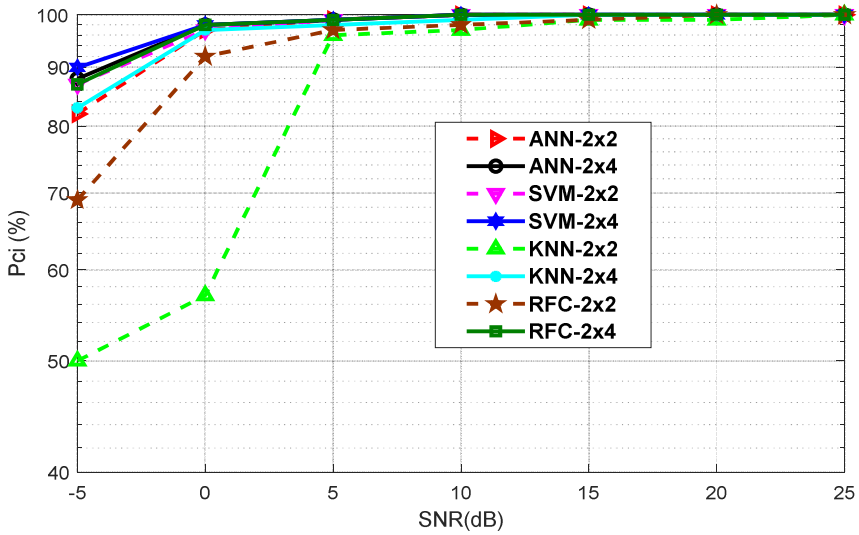

Figure 3.3- Probability of correct identification versus SNR in STBC-OFDM system for different antennas configurations. $N = 64$.

For (2x4), antennas configuration, the classification accuracies of ANN, SVM and RFC exhibited rather similar performances, and displayed significant higher accuracies at least by 4% than KNN at $\mathrm{SNR_{dB}} = -5\ \mathrm{dB}$.

However, for (2x2) antennas configuration, notably lower accuracies, at $\mathrm{SNR_{dB}} = -5\ \mathrm{dB}$, were observed using ANN, RFC and KNN by 5%, 18% and 37% respectively than SVM. SVM perform better than ANN for large range of SNR. This is due to the robustness of the SVM training step, which yields a better accuracy compared to other classifiers training step.

The improvement in performance achieved by increasing the number of receiving antennas beyond "2" antennas is due to the enhancement of the spatial diversity gain at the receiver, which leads to an increased the number of received samples.

For $\mathrm{SNR_{dB}} < 5\ \mathrm{dB}$ demonstrates the need for RFC and KNN of a number of received antennas greater than "2" ($N_r > 2$) to achieve the same performance as SVM and ANN for $N_r = 2$.

Figure 3.4 compares the probability of correct modulation identification of the considered classifiers for different values of OFDM symbol length N. The classification accuracies improve as N increases from 64 to 512. This is due to the improvement in time diversity of the received signal, which ameliorates the channels estimation and consequently the probability of correct identification.

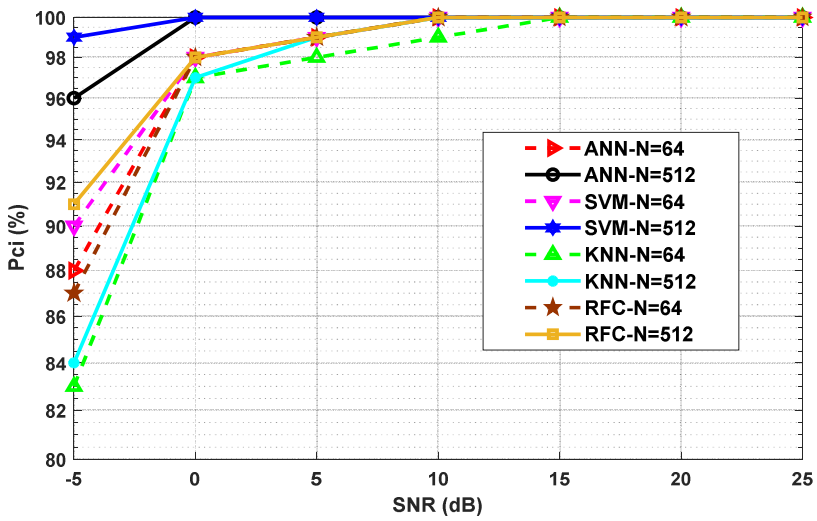

Figure 3.4- Probability of correct identification versus SNR in STBC-OFDM system for different values of N. $N_t = 2, N_r = 4$.

On the other hand, increasing the number of realizations from 50 to 500 leads to a large set of HOS trials and the associated modulation in training phase, which improves the probability of correct identification for all classifiers.

3.3.2 DMC in STBC-OFDM systems with channels and CFO estimation

In this section, we propose a robust blind-DMC (BDMC) algorithm for the MIMO-OFDM system based on STBC coding in the presence of CFO and channel estimation errors.

The Alamouti coding will be used to code information data and pilot symbols. The joint estimation of the CFO and the channels is based on the MUSIC (Multiple Signal Classification) algorithm and is also relies on a pilot symbols design model [94].

In the absence of CFO, the FFT of $\mathbf{y}_{i,u}^{(n_r)}$, makes the frequency selective channel equivalent to a set of flat fading sub-channels. However, in presence of CFO, the orthogonality among subcarriers is destroyed and even the FFT operation cannot diagonalize the channel. This frequency deviation of the received signal is caused by the Doppler effect, which introduces a phase and quadrature offset between the transmitted and received symbols. This is manifested by a rotation in the modulation constellation as shown in figure 3.5 [95]. This offset may also be due to the mismatch between the generated frequencies by oscillators on transmission and on reception [94].

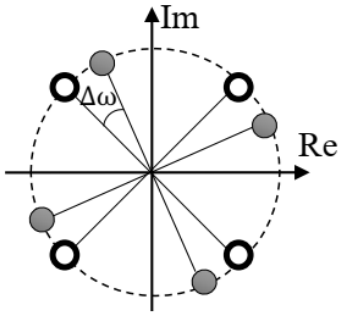

Figure 3.5- Rotation of the modulation constellation due to the CFO [94].

We have assumed that the frequency offset is the same for all reception antennas. This is true, for example, in the case where the frequency offset is mainly due to the difference in generated frequencies by the local transmit and receive oscillators [90, 94]. The value of the frequency offset is less than half the subcarriers spacing ($|\omega_0| \leq \pi$).

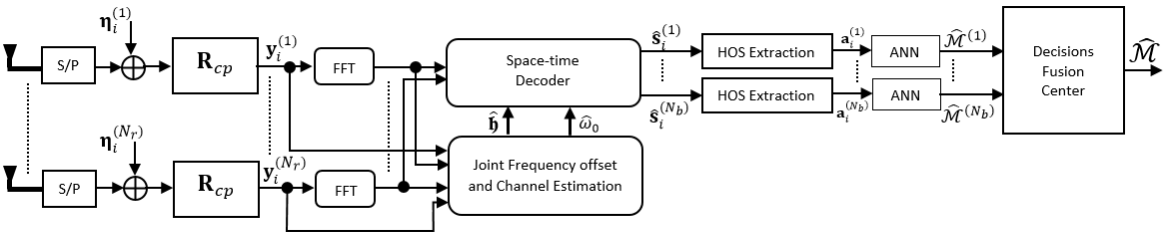

Figure 3.6- Discrete-time baseband model of the BDMC method with joint CFO and channel estimation in STBC-OFDM system.

In the presence of the frequency offset, equation (3.7) becomes:

$$\mathbf{y}_{i,u}^{(n_r)} = \frac{1}{\sqrt{N_e}} e^{j\omega_0(UiN_q+N_{cp})} \mathbf{D}_N^{(u)}(\omega_0) \mathbf{F}_N^{\mathcal{H}} \sum_{n_t=1}^{N_t} \mathbf{D}_N\left(\bar{\mathbf{v}}_{i,u}^{(n_t)}\right) \tilde{\mathbf{h}}^{(n_r,n_t)} + \boldsymbol{\eta}_{i,u}^{(n_r)} \qquad (3.10)$$

where $\mathbf{D}_N^{(u)}(\omega_0)$ is a diagonal matrix defined as $\mathbf{D}_N^{(u)}(\omega_0) = diag\left(e^{juN_q\omega_0}, \dots, e^{(j(uN_q+N-1)\omega_0)}\right)$.

with matrix notation equation (3.10) becomes :

$$\mathbf{y}_i^{(n_r)} = \frac{1}{\sqrt{N_e}} e^{j\omega_0(UiN_q+N_{cp})} \mathbb{D}_N(\omega_0)\left(\mathbb{F}_p^{\mathcal{H}} \mathbb{P}_i \mathbb{J}_p + \mathbb{F}_d^{\mathcal{H}} \mathbb{S}_i \mathbb{J}_d\right) \mathfrak{h}^{(n_r)} + \boldsymbol{\eta}_i^{(n_r)} \qquad (3.11)$$

where $\boldsymbol{\eta}_i^{(n_r)} = [\left(\boldsymbol{\eta}_{i,0}^{(n_r)}\right)^T, \dots, \left(\boldsymbol{\eta}_{i,U-1}^{(n_r)}\right)^T]^T$, $\mathfrak{h}^{(n_r)} = [\mathbf{h}^{(n_r,1)}, \dots, \mathbf{h}^{(n_r,N_t)}]^T$,

$$\begin{cases} \mathbb{F}_p^{\mathcal{H}} = \mathbf{I}_U \otimes \left(\mathbf{F}_N^{\mathcal{H}} \boldsymbol{\mathcal{Q}}_N^{\beta}\right) \\ \mathbb{F}_d^{\mathcal{H}} = \mathbf{I}_U \otimes \left(\mathbf{F}_N^{\mathcal{H}} \boldsymbol{\mathcal{Q}}_N^{\alpha}\right) \\ \mathbb{J}_p = \mathbf{I}_{N_t} \otimes \boldsymbol{\Gamma}_{N_p} \\ \mathbb{J}_d = \mathbf{I}_{N_t} \otimes \boldsymbol{\Gamma}_{N_d} \\ \boldsymbol{\Gamma}_{N_p} = \left[\mathbf{f}_{\beta_1}^L, \mathbf{f}_{\beta_2}^L, \dots, \mathbf{f}_{\beta_{N_p}}^L\right]^{\mathcal{H}} \\ \boldsymbol{\Gamma}_{N_d} = \left[\mathbf{f}_{\alpha_1}^L, \mathbf{f}_{\alpha_2}^L, \dots, \mathbf{f}_{\alpha_{N_d}}^L\right]^{\mathcal{H}} \end{cases},$$

and

$$\begin{cases} \mathbb{S}_i = \begin{bmatrix} \mathbf{D}_{N_d}\left(\mathbf{c}_{i,0}^{(1)}\right) & \dots & \mathbf{D}_{N_d}\left(\mathbf{c}_{i,0}^{(N_t)}\right) \\ \vdots & \ddots & \vdots \\ \mathbf{D}_{N_d}\left(\mathbf{c}_{i,U-1}^{(1)}\right) & \dots & \mathbf{D}_{N_d}\left(\mathbf{c}_{i,U-1}^{(N_t)}\right) \end{bmatrix} \\ \mathbb{P}_i = \begin{bmatrix} \mathbf{D}_{N_p}\left(\mathbf{b}_{i,0}^{(1)}\right) & \dots & \mathbf{D}_{N_p}\left(\mathbf{b}_{i,0}^{(N_t)}\right) \\ \vdots & \ddots & \vdots \\ \mathbf{D}_{N_p}\left(\mathbf{b}_{i,U-1}^{(1)}\right) & \dots & \mathbf{D}_{N_p}\left(\mathbf{b}_{i,U-1}^{(N_t)}\right) \end{bmatrix} \end{cases}$$

As mentioned above, OFDM is very sensitive to synchronization errors resulting in the appearance of interference between the subcarriers. Therefore, it is necessary to correctly estimate and correct these errors jointly with the channels estimation in order to allow a consistent equalization of the received signal. In the general case, the estimation algorithm can be combined with algorithms based on VSC to extend the acquisition range.

In the following, we propose blind and semi-blind algorithms to jointly estimate the CFO and the channels in STBC-OFDM systems.

3.3.2.1 Channels' estimation method

After compensation of the received signal with the estimated value of CFO "$\widehat{\omega}_0$" using a diagonal matrix $\mathbb{D}_N^{\mathcal{H}}(\widehat{\omega}_0)$ in equation (3.11), and multiplication by the FFT of the pilot symbols $\mathbb{F}_p$, we obtain the following equality :

$$e^{-j\widehat{\omega}_0(UiN_q+N_{cp})}\mathbb{F}_p\mathbb{D}_N^{\mathcal{H}}(\widehat{\omega}_0)\mathbf{y}_i^{(n_r)} = \frac{N}{\sqrt{N_e}}\mathbb{P}_i\mathbb{J}_p\mathfrak{h}^{(n_r)} + \mathbf{w}_i^{(n_r,p)} \tag{3.12}$$

where $\mathbf{w}_i^{(n_r,p)} = e^{-j\widehat{\omega}_0(UiN_q+N_{cp})}\mathbb{F}_p\mathbb{D}_N^{\mathcal{H}}(\widehat{\omega}_0)\boldsymbol{\eta}_i^{(n_r)}$.

The estimations of the channels should be the solution that set to zero the gradient with respect to $\mathfrak{h}^{(n_r)}$ of the following quadratic cost function:

$$\mathbf{j}_{\mathbb{P}}^{(n_r)}\left(\mathfrak{h}^{(n_r)}\right) = \sum_{i=0}^{N_i-1} \left\| e^{-j\widehat{\omega}_0(UiN_q+N_{cp})}\mathbb{F}_p\mathbb{D}_N^{\mathcal{H}}(\widehat{\omega}_0)\mathbf{y}_i^{(n_r)} - \frac{N}{\sqrt{N_e}}\mathbb{P}_i\mathbb{J}_p\mathfrak{h}^{(n_r)} \right\|^2 \quad (3.13)$$

By exploiting the STBC orthogonal signaling at a block level and the orthogonality between subcarriers of OFDM system, the estimations of the channels $\widehat{\mathfrak{h}}^{(n_r)}$ given by:

$$\widehat{\mathfrak{h}}^{(n_r)} = \frac{\sqrt{N_e}}{2N} e^{-j\widehat{\omega}_0(UiN_q+N_{cp})}\mathbb{J}_p^{\#}\mathbb{P}_i^{\mathcal{H}}\mathbb{F}_p\mathbb{D}_N^{\mathcal{H}}(\widehat{\omega}_0)\mathbf{y}_i^{(n_r)} \quad (3.14)$$

The MSE for MIMO channels estimator, used as performance measures, is defined by:

$$\mathrm{MSE}_{\mathrm{Channel}} = \frac{1}{N_c N_r N_t}\sum_{j=1}^{N_c}\sum_{n_r=1}^{N_r}\sum_{n_t=1}^{N_t}\left\|\hat{h}_j^{(n_r,n_t)} - h^{(n_r,n_t)}\right\|^2 \quad (3.15)$$

where N_c is the Monte Carlo trials.

3.3.2.2 CFO estimation methods

The CFO estimation is calculated by considering the pilot symbols and virtual subcarriers.

A. Pilots based CFO estimation

Substituting the estimated channels $\widehat{\mathfrak{h}}^{(n_r)}$ obtained in equation (3.14) into equation (3.13), we derive the training based cost function for CFO estimation as:

$$\mathbf{j}_{\mathbb{P}}^{(n_r)}(\omega_0) = \sum_{i=0}^{N_i-1}\left\| e^{-j\omega_0(UiN_q+N_{cp})}\boldsymbol{\Phi}\mathbb{F}_p\mathbb{D}_N^{\mathcal{H}}(\omega_0)\mathbf{y}_i^{(n_r)}\right\|^2 \quad (3.16)$$

where $\boldsymbol{\Phi} = \left(\mathbf{I}_{UN_p} - \frac{1}{2}\mathbb{P}_i\mathbb{J}_p\mathbb{J}_p^{\#}\mathbb{P}_i^{\mathcal{H}}\right)$.

For all received antennas "N_r" and all source blocks "N_i", the cost function given by equation (3.16) becomes:

$$\mathbf{j}_{\mathbb{P}}(\omega_0) = \mathrm{tr}\left(\mathbb{Y}^{\mathcal{H}}\mathbb{D}_N(\omega_0)\boldsymbol{\Omega}_{\mathbb{P}}\mathbb{D}_N^{\mathcal{H}}(\omega_0)\mathbb{Y}\right) \quad (3.17)$$

where $\boldsymbol{\Omega}_{\mathbb{P}} = \mathbb{F}_p^{\mathcal{H}}\boldsymbol{\Phi}^{\mathcal{H}}\boldsymbol{\Phi}\mathbb{F}_p$, $\mathbb{Y} = \left[\mathbb{Y}^{(1)}, \ldots \mathbb{Y}^{(N_r)}\right]$, $\mathbb{Y}^{(n_r)} = \left[\mathbf{y}_0^{(n_r)} \ldots \mathbf{y}_{N_i-1}^{(n_r)}\right]$, and $\mathbf{y}_i^{(n_r)} = \left[y_{i,0}^{(n_r)}, \ldots, y_{i,UN-1}^{(n_r)}\right]^T$. The CFO estimate can be obtained by minimizing the cost function in the equation (3.17) as:

$$\widehat{\omega}_0 = \underset{\omega_0}{\operatorname{argmin}}\{\mathbf{j}_{\mathbb{P}}(\omega_0)\} \tag{3.18}$$

B. Blind CFO estimation

After compensation of the received signal with the estimated CFO, and after multiplication by the FFT of VSCs, $\mathbb{F}_z$ (demodulation), we obtain:

$$e^{-j\omega_0(UiN_q+N_{cp})}\mathbb{F}_z\mathbb{D}_N^{\mathcal{H}}(\omega_0)\mathbf{y}_i^{(n_r)} = \mathbf{w}_i^{(n_r,z)} \tag{3.19}$$

For all received antennas "N_r" and all source blocks "N_i", the estimated CFO results from the minimization of the following cost function:

$$\mathbf{j}_{\mathbb{Z}}(\omega_0) = \operatorname{tr}\left(\mathbb{Y}^{\mathcal{H}}\mathbb{D}_N(\omega_0)\mathbf{\Omega}_{\mathbb{Z}}\mathbb{D}_N^{\mathcal{H}}(\omega_0)\mathbb{Y}\right) \tag{3.20}$$

where $\mathbf{\Omega}_{\mathbb{Z}} = \mathbb{F}_z^{\mathcal{H}}\mathbb{F}_z$ et $\mathbb{F}_z^{\mathcal{H}} = \mathbf{I}_U \otimes \left(\mathbf{F}_N^{\mathcal{H}}\boldsymbol{Q}_N^{\gamma}\right)$ with $\boldsymbol{Q}_N^{\gamma} = \mathbf{I}_N\{\boldsymbol{i}_{\gamma}\} = \left[\mathbf{e}_N^{(\gamma_1)}, \dots, \mathbf{e}_N^{(\gamma_{N_{vsc}})}\right]$.

C. Semi-blind CFO estimation

In this method, the CFO estimate is calculated by considering the pilot symbols and the VSCs. To refine our CFO estimation algorithms, we propose to combine the cost functions based on pilots and virtual subcarriers, which gives the following cost function:

$$\mathbf{j}_{(\mathbb{P},\mathbb{Z})}(\omega_0) = \operatorname{tr}\left(\mathbb{Y}^{\mathcal{H}}\mathbb{D}_N(\omega_0)\mathbf{\Omega}_{(\mathbb{P},\mathbb{Z})}\mathbb{D}_N^{\mathcal{H}}(\omega_0)\mathbb{Y}\right) \tag{3.21}$$

where $\mathbf{\Omega}_{(\mathbb{P},\mathbb{Z})} = \mathbf{\Omega}_{\mathbb{P}} + \mathbf{\Omega}_{\mathbb{Z}}$.

The training, blind and semi-blind CFO estimates is obtained by minimization according to ω_0 the cost functions $\mathbf{j}_{\mathbb{P}}(\omega_0)$, $\mathbf{j}_{\mathbb{Z}}(\omega_0)$ and $\mathbf{j}_{(\mathbb{P},\mathbb{Z})}(\omega_0)$ respectively.

After compensation of the received signal by the estimated CFO, and multiplication by the FFT of the data symbols, $\mathbb{F}_d$, we obtained:

$$e^{-j\omega_0(UiN_q+N_{cp})}\mathbb{F}_d\mathbb{D}_N^{\mathcal{H}}(\omega_0)\mathbf{y}_i^{(n_r)} = \frac{N}{\sqrt{N_e}}\mathbb{S}_i\mathbb{J}_d\mathbf{\mathfrak{h}}^{(n_r)} + \mathbf{w}_i^{(n_r,d)} \tag{3.22}$$

where $\mathbf{w}_i^{(n_r,d)} = e^{-j\hat{\omega}_0(UiN_q+N_{cp})}\mathbb{F}_d\mathbb{D}_N^{\mathcal{H}}(\omega_0)\mathbf{\eta}_i^{(n_r)}$.

The MSE for CFO estimator, used as performance measures, is defined by:

$$\mathrm{MSE}_{\mathrm{CFO}} = \frac{1}{N_c N_r} \sum_{j=1}^{N_c} \left\| \hat{\omega}_{0,j} - \omega_{0,j} \right\|^2 \tag{3.23}$$

In figures 3.7 and 3.8, we depicted the CFO and channels MSE of the joint semi-blind estimators versus SNR in MIMO system. As it can be seen from figure 3.7, changing the number of modulation types does not affect the MSE of the CFO in presence of Gaussian noise. From figure 3.8, we observe that the MSE of channels degrades when considering estimated CFO compared to the exact estimation of CFO.

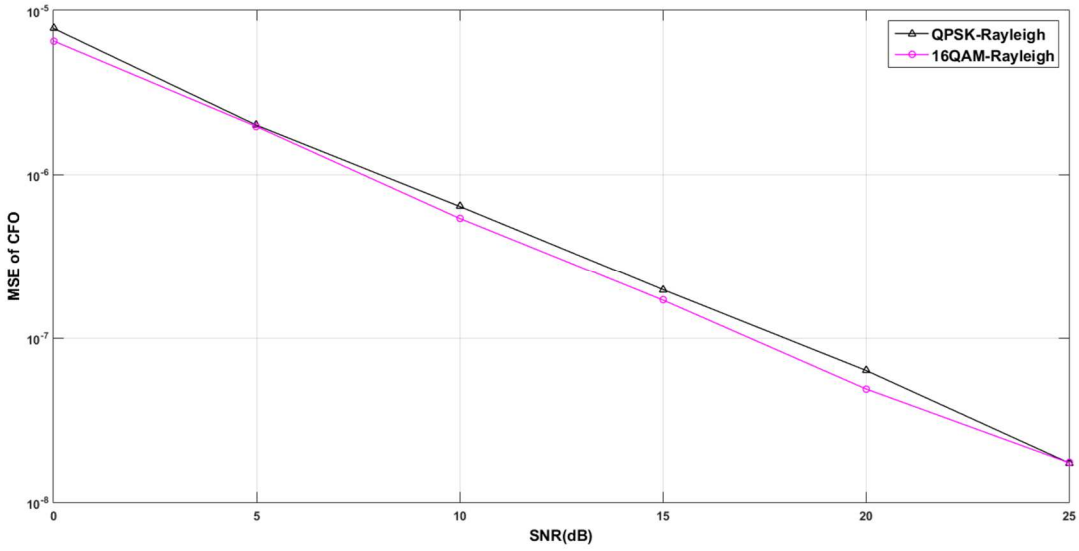

Figure 3.7- MSE of semi-blind CFO estimator versus SNR in STBC-OFDM system. $N = 64$, $N_t = 2, N_r = 2$.

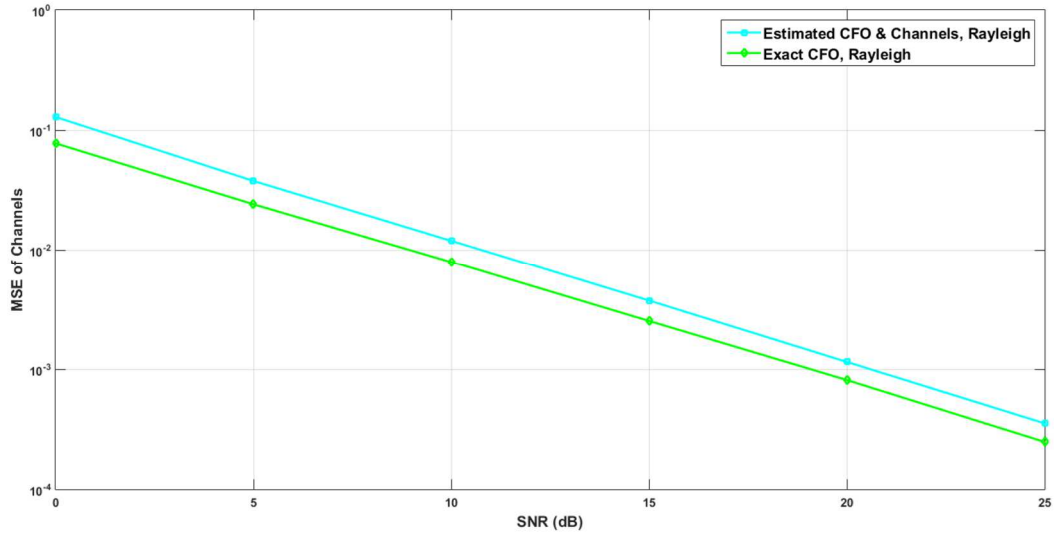

Figure 3.8- MSE of semi-blind channels estimator versus SNR in STBC-OFDM system. $N = 64$, $N_t = 2, N_r = 2, \mathcal{M} = \mathrm{QPSK}$.

To improve the reception quality of information data, channel equalization should be used. Indeed, in the case of Alamouti coding, we applied a frequency equalization matrix to the received signal from equation (3.22) in order to estimate the data vectors $\hat{\mathbf{s}}_{2i}$ et $\hat{\mathbf{s}}_{2i+1}$. The equalization matrix $\mathbb{G}_h^{(n_r)}$ is defined by:

$$\mathbb{G}_h^{(n_r)} = \begin{bmatrix} \mathbf{D}_N\left(\mathbf{\Gamma}_{N_d}\mathbf{h}^{(n_r,1)}\right) & \mathbf{D}_N\left(\mathbf{\Gamma}_{N_d}\mathbf{h}^{(n_r,2)}\right) \\ \mathbf{D}_N^{\mathcal{H}}\left(\mathbf{\Gamma}_{N_d}\mathbf{h}^{(n_r,2)}\right) & -\mathbf{D}_N^{\mathcal{H}}\left(\mathbf{\Gamma}_{N_d}\mathbf{h}^{(n_r,1)}\right) \end{bmatrix} \tag{3.24}$$

To prove the performance of our DMC algorithm in STBC-OFDM system in the presence of CFO and the channels estimation errors, we consider a MIMO system with $N_t = 2$, $N_r = 4$ using Alamouti coding. The number of estimation blocks is fixed at $N_i = 10$. The probability of correct identification $\mathrm{P_{ci}}$ is used as performance measures. The sub-carriers number of OFDM system is fixed at $N = 64$, where $N_{vsc} = 15$ subcarriers are considered to be VSCs, $N_p = 9$ subcarriers are used by pilot symbols and $N_s = 40$ subcarriers for information symbols.

In all simulations, the channel coefficients are assumed to be independent and Gaussian with zero-means and unit-variances. The channels order is fixed at $L = 5$. La longueur du CP is taken equal to $N_{cp} = L + 1$.

The noise at each receiving antenna is spatially decorrelated complex white Gaussian noise with zero-mean and variance equal to σ_η^2. The data symbols are chosen from the modulation constellations in the pool $\Theta = \{\mathrm{QPSK}, 16\mathrm{QAM}\}$.

In figure 3.9, we depicted the effects of estimation errors of CFO and channels on $\mathrm{P_{ci}}$.

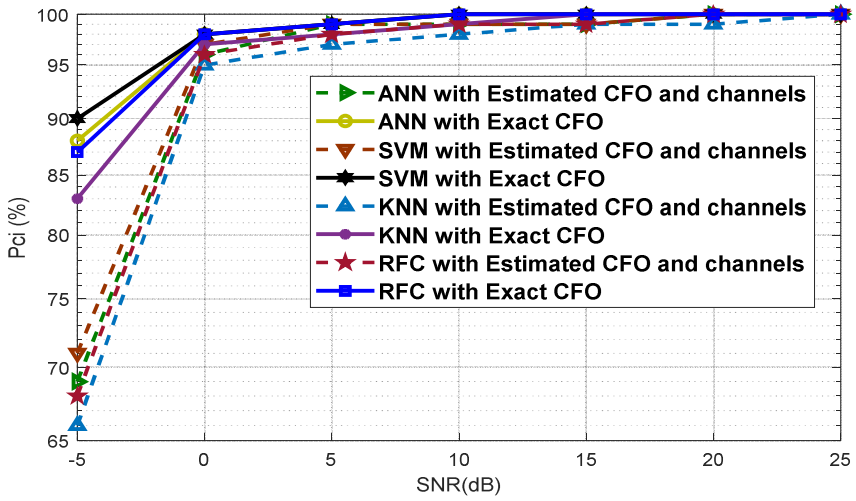

Figure 3.9- Probability of correct identification versus SNR in STBC-OFDM system with CFO and channels estimation errors. $N_t = 2$, $N_r = 4$, et $N = 64$.

As it can be seen, for SNR in the range $\mathrm{SNR_{dB}} \in [-5,0]$, the accuracies of the classifiers increase when the exact values of channels and CFO are used comparatively to the case of presence of estimation errors of CFO and channels. However, the classification accuracies of all classifiers, without and with estimated CFO and channels, exhibited rather similar results for $\mathrm{SNR_{dB}} \geq 0$. The use of $N_r = 4$ receiver antennas has contributed to this improvement in classification accuracies.

3.3.3 DMC in STBC-OFDM systems with impulsive noise

The performance of communication systems does not depend only on the channel characteristics and the used transmission techniques, but also on the nature of the additive noise and its statistical properties. Indeed, in the majority of researchs, the hypothesis of Gaussian noise is considered. However, this hypothesis is not applicable in railway communications which exhibit non-Gaussian and impulsive noise [52].

Our objective in this section is the mitigation of the impulsive noise present in the received STBC-OFDM signal, which consequently ameliorates the DMC process. To achieve this goal, we estimate the impulsive noise parameters, and then implement the Myriad filter (MF) in the STBC-OFDM receiver, as shown in figure 3.10.

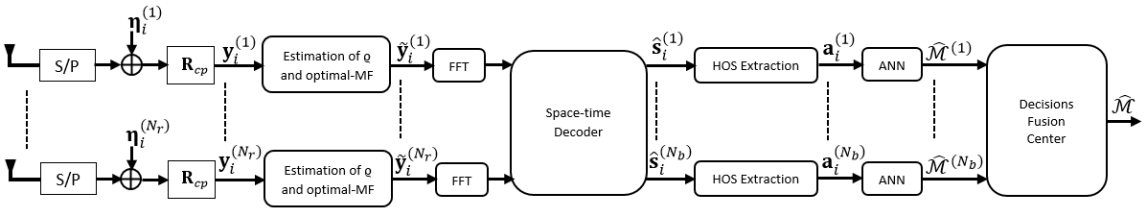

Figure 3.10- DMC for STBC-OFDM system in impulsive noise environment.

To obtain a better clarification of the environment at the receiver side, we propose an identification process composed of four subsystems: (1) Subsystem for the reduction of impulsive noise based on the optimal Myriad filter (optimal-MF), (2) Subsystem for the features extraction using HOS estimates, (3) Subsystem for pattern recognition using the differents classifiers, (4) The decisions fusion center.

3.3.3.1 Impulsive noise model

Impulse noises type are generally present in the form of elementary pulses of high amplitude, superimposed on white Gaussian noise (see figure 3.11).

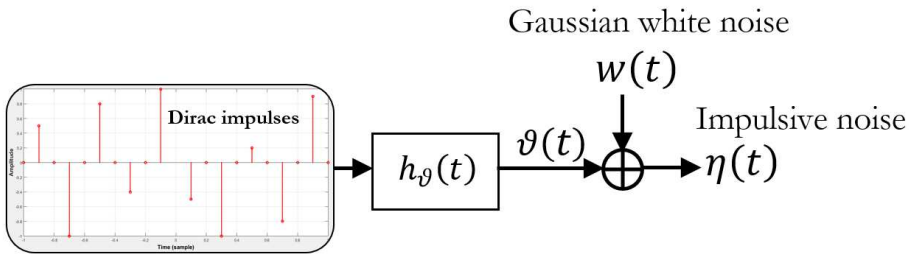

Figure 3.11- Example of generating impulsive noise system.

The impulsive phenomenon manifested by high peaks for short periods. Several models of non-Gaussian impulsive noise exist in the literature. Typical examples include atmospheric radio noise, telephone line noise, electromagnetic interference in train environments, and multi-user interference in mobile communication systems [96-97].

The main characteristics of impulsive noise are described by the α-stable distribution. This distribution is a class of probability distributions, which generalize the normal distribution, allowing heavy-tails and skewness [98-99].

An α-stable distribution is totally determined by four parameters [100]:

1. **Stability index** $(0 < \alpha \leq 2)$: This parameter controls the tails heaviness of the stable density and, therefore, the impulsivity of the stable process (i.e., lower α, implies heavier tails). The value $\alpha = 2$, corresponds to normal distribution, then for $\alpha = 1$, the α-stable process corresponds to Cauchy distribution. For these two values of α, closed form expressions exist for α-stable but for other values of α, this closed form expression does not exist.
2. **Skewness index** $(-1 \leq \beta \leq 1)$: This parameter controls the symmetry of stable distribution, and specifies whether the distribution is asymmetric to the right $(\beta > 0)$ or left $(\beta < 0)$. If $\beta = 0$, then the distribution is symmetrical and noted by $S\alpha S$ (this is the case with normal distribution).
3. **Scale parameter** $(\gamma > 0)$: A measure of dispersion which determines the spread of the distribution around its location parameter δ. For normal distribution, γ is half the variance.
4. **Location parameter** $(-\infty < \delta < +\infty)$: This parameter represents the average when $1 < \alpha \leq 2$, and the median when $0 < \alpha \leq 1$.

In the majority of cases, the stable distribution S_α is also defined by its characteristic function as follow:

$$\Phi_\alpha(t) = E[\exp(jt\mathbf{x})] = \begin{cases} \exp(j\delta t - \gamma|t|^\alpha[1 + j\beta\kappa(t,\alpha)\text{sign}(t)]), \alpha \neq 1 \\ \exp(j\delta t - \gamma|t|[1 + j\beta\kappa(t,\alpha)\text{sign}(t)]), \quad \alpha = 1 \end{cases} \tag{3.23}$$

where $\mathbf{x} \sim S_\alpha(\beta, \gamma, \delta)$, and:

$$\kappa(t,\alpha) = \begin{cases} \tan\frac{\pi\alpha}{2}, \alpha \neq 1 \\ \frac{2}{\pi}\ln|t|, \alpha = 1 \end{cases}$$

When the stable distribution is symmetrical $(\beta = 0)$, the characteristic function in equation (3.23) reduced to :

$$\Phi_\alpha(t) = \exp(j\delta t - \gamma|t|^\alpha) \tag{3.24}$$

The symmetrical α-stable process is noted by $S\alpha S_\alpha(\gamma, \delta)$. The heavy-tails impulsive noise introduced in equation (3.24) has a symmetrical α-stable distribution around zero, i.e. with $\mathbf{x} \sim S\alpha S_\alpha(\gamma_\mathbf{x}, 0)$, where the noise components are assumed and have the same characteristic parameter "α" (see figure 3.12).

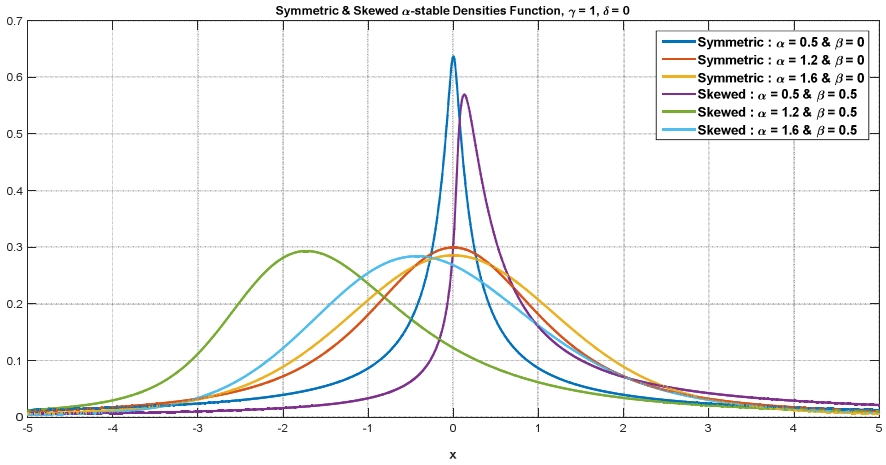

Figure 3.12- The α-stables density function.

The noise considered in this paper is defined as follow:

$$\boldsymbol{\eta}_{i,u}^{(n_r)} = \mathbf{w}_{i,u}^{(n_r)} + \boldsymbol{\vartheta}_{i,u}^{(n_r)} \tag{3.25}$$

where $\mathbf{w}_{i,u}^{(n_r)}$ is an additive white Gaussian noise vector with zero-mean and variance equal to $\sigma_\mathbf{w}^2\, \mathbf{I}_N$; i.e. $\mathbf{w}_{i,u}^{(n_r)} \sim \mathcal{CN}(0, \sigma_\mathbf{w}^2\, \mathbf{I}_N)$, and $\boldsymbol{\vartheta}_{i,u}^{(n_r)}$ is an additive impulsive-noise vector.

Without the pilot symbols, equation (3.7) can be rewritten as:

$$\mathbf{y}_{i,u}^{(n_r)} = \frac{1}{\sqrt{N}} \mathbf{F}_N^{\mathcal{H}} \sum_{n_t=1}^{N_t} \mathbf{D}_N\left(\tilde{\mathbf{h}}^{(n_r,n_t)}\right) \bar{\mathbf{c}}_{i,u}^{(n_t)} + \boldsymbol{\eta}_{i,u}^{(n_r)} \tag{3.26}$$

For all time-slots at n_r-th received antenna, equation (3.26) becomes:

$$\mathbb{y}_i^{(n_r)} = \frac{1}{\sqrt{N_d}} \mathbb{F}_{N_d}^{\mathcal{H}} \mathbb{H}^{(n_r)} \mathbb{s}_i + \mathbb{m}_i^{(n_r)} \tag{3.27}$$

where

$$\begin{cases} \mathbb{y}_i^{(n_r)} = [\left(\mathbf{y}_{i,0}^{(n_r)}\right)^T, \left(\mathbf{y}_{i,1}^{(n_r)}\right)^{\mathcal{H}}, \dots, \left(\mathbf{y}_{i,U-2}^{(n_r)}\right)^T, \left(\mathbf{y}_{i,U-1}^{(n_r)}\right)^{\mathcal{H}}]^T \\ \mathbb{m}_i^{(n_r)} = [\left(\boldsymbol{\eta}_{i,0}^{(n_r)}\right)^T, \left(\boldsymbol{\eta}_{i,1}^{(n_r)}\right)^{\mathcal{H}}, \dots, \left(\boldsymbol{\eta}_{i,U-2}^{(n_r)}\right)^T, \left(\boldsymbol{\eta}_{i,U-1}^{(n_r)}\right)^{\mathcal{H}}]^T \\ \mathbb{s}_i = \left[\mathbf{s}_{iN_b+0}^T, \dots, \mathbf{s}_{(i+1)N_b-1}^T\right]^T \\ \mathbb{F}_{N_d}^{\mathcal{H}} = \mathbf{I}_U \otimes \mathbf{F}_{N_d}^{\mathcal{H}} \end{cases}$$

In this project, we adopt the method used in [101-102] to model $\boldsymbol{\vartheta}_i^{(n_r)}$($\vartheta_i \sim S\alpha S_\alpha(\gamma_0^\alpha, \mathbf{0}_d)$, and generate an isotropic process $S\alpha S_\alpha$ of dimension d. The formula for the equivalent isotropic multidimensional process using for numerical simulations is α-stable with characteristic function:

$$\Phi_\alpha(\mathbf{u}) = \exp(j\mathbf{u}^T\boldsymbol{\delta} - \gamma_0^\alpha |\mathbf{u}|^\alpha) \tag{3.28}$$

where

$$\begin{cases} \mathbf{x} = a^{1/2}\mathbf{v} + \boldsymbol{\delta} \\ a \sim S\alpha_{/2}\left(1, 2\gamma_0^2\left(\cos(\pi\,\alpha/4)^{2/\alpha}\right)^{2/\alpha}, 0\right) \\ \gamma = \gamma_0^\alpha, \text{with } \gamma_0 > 0 \\ \mathbf{v} = [\Re(v), \Im(v)]^T \text{ with } v \sim \mathcal{CN}(0,2), \\ \forall \mathbf{u} \in \mathbb{R}^d \end{cases}$$

3.3.3.2 Impulsive noise mitigation (optimal-MF)

At the receiver, the usual filtering techniques for a signal tainted by impulsive noise are no longer reliable. This section presented a blind method to reduce the impact of impulsive noise on the received signal.

Two impulsive noise mitigation domains for OFDM systems are considered in literature [103-104]. In [103], the impulsive noise mitigation methods are implemented in the frequency-domain with the consideration of the channel estimation. However, the method in [104] consider the mitigation in the time-domain.

In this work, we focus on blind filtering of impulsive noise using MF in the time-domain as explained in the figure 3.10 [11, 102, 105].

Given an observed signal $\mathbf{y}_i^{(n_r)}$ at n_r-th received antenna, to be filtered by MF [102]. For a set of samples $\left\{y_i^{(n_r)}(k)\right\}_{k=0}^{K-1}$, this filter is defined by the value ε that minimizes the following cost function $\varphi(\cdot)$:

$$\hat{\varepsilon} = \arg\min_{\varepsilon} \sum_{k=0}^{K-1} \varphi\left(y_i^{(n_r)}(k) - \varepsilon\right) \tag{3.29}$$

For a MF, $\varphi(x) = \ln(\varrho^2 + x^2)$. Reconsidering this cost function, the MF is thus defined as:

$$\begin{aligned} \hat{\varepsilon} &= \mathrm{MF}\left\{\varrho;\ y_i^{(n_r)}(0), y_i^{(n_r)}(1), \ldots, y_i^{(n_r)}(K-1)\right\} \\ &= \arg\min_{\varepsilon} \prod_{k=1}^{K}\left(\varrho^2 + \left(y_i^{(n_r)}(k) - \varepsilon\right)^2\right) \end{aligned} \tag{3.30}$$

where $\varrho > 0$ is the linearity parameter of the MF. As mentioned above, the optimal-MF returns the elements of the input set where $\varepsilon \in \left\{y_i^{(n_r)}(k)\right\}_{k=0}^{K-1}$, that minimizes the cost function in equation (3.30). Then, the new expression of the cost function in equation (3.30) becomes:

$$\begin{aligned} \hat{\varepsilon} &= \text{optimal-MF}\left\{\varrho\ ;\ y_i^{(n_r)}(0), y_i^{(n_r)}(1), \ldots, y_i^{(n_r)}(K-1)\right\} \\ &= \arg\min_{\varepsilon \in \left\{y_i^{(n_r)}(k)\right\}_{k=0}^{K-1}} \prod_{k=0}^{K-1}\left(\varrho^2 + \left(y_i^{(n_r)}(k) - \varepsilon\right)^2\right) \\ &= \arg\min_{\varepsilon \in \left\{y_i^{(n_r)}(k)\right\}_{k=0}^{K-1}} \prod_{k=0}^{K-1}\left(\varrho^2 + \left|y_i^{(n_r)}(k) - \varepsilon\right|^2\right) \end{aligned} \tag{3.31}$$

The filtered signal $\tilde{\mathbf{y}}_i^{(n_r)}$ is then expressed as:

$$\tilde{\mathbf{y}}_i^{(n_r)} = \text{optimal-MF}\left\{\varrho;\ y_i^{(n_r)}(0), y_i^{(n_r)}(1), \ldots, y_i^{(n_r)}(K-1)\right\} \tag{3.32}$$

To obtain quasi-optimal filtering, it is necessary to adjust ϱ depending to α and γ. It can use one of the most approximations to optimize ϱ [15] as:

$$\varrho = \sqrt{\left(\frac{\alpha}{2-\alpha}\right)}\gamma^{1/\alpha} \tag{3.33}$$

A. *Estimator of the location parameter* δ: For the estimation of δ, we suggest using the median of the observations:

$$\hat{\delta} = \text{median}\left\{y_i^{(n_r)}(0), y_i^{(n_r)}(1), \dots, y_i^{(n_r)}(K-1)\right\} \tag{3.34}$$

B. *Estimator of the stability parameter and the scale parameter:* To estimate the two parameters α and γ of $\upsilon \sim S\alpha S_\alpha(\gamma, 0)$ process, we can use the estimators in [106]. Then these estimators of α and γ are :

$$\begin{cases} \hat{\alpha} = \psi_1\left(\frac{\upsilon_{0.95}-\upsilon_{0.05}}{\upsilon_{0.75}-\upsilon_{0.25}}, 0\right) \\ \hat{\gamma} = \frac{\upsilon_{0.75}-\upsilon_{0.25}}{\phi_3(\hat{\alpha},0)} \end{cases} \tag{3.35}$$

where $\psi_1(.,.)$ and $\phi_3(.,.)$ are the mapping tables, and υ_q is the quantile q of the process υ. Using the estimates of α and γ in equation (3.35), we calculate the linearity parameter as:

$$\hat{\varrho} = \sqrt{\left(\frac{\hat{\alpha}}{2-\hat{\alpha}}\right)}\hat{\gamma}^{1/\hat{\alpha}} \tag{3.36}$$

Algorithm 1. Blind selective-myriad filtering of received signal $\mathbf{y}_i$ at the n_r-th antenna [102].

Input : Sampled received signal $y_i(mT_s)$. The algorithm requires prior temporal synchronization of the receivers, as well as the estimation of T.

1 : $n \leftarrow 0$

2 : Based on the set $\left\{\Re\left(y_i(mT_s)\right)\right\}_{m=0}^{Tf_s-1}$, estimate $\hat{\alpha}$ and $\hat{\gamma}$ using (3.35) {by substituting the set $\left\{\Re\left(y_i(mT_s)\right)\right\}_{m=0}^{Tf_s-1}$ for the process a}

3 : $\hat{\gamma}_0 \leftarrow \hat{\gamma}^{1/\hat{\alpha}}$

4 : **Estimate** $\hat{\varrho}_n$ using (3.36)

5 : **For** $m = 0$ until the index of the last sample of $y_i(mT_s)$ **do**

6 : **Estimate** $\tilde{y}_i(mT_s)$ using (3.32), where $\varrho = \varrho_n$ and $N = Tf_s$

7 : **If** $(m+1)T_s > (n+1)T$ **then** {Updating $\hat{\varrho}_n$ for each T}

8 : $n \leftarrow n+1$

9 : Based on the set $\left\{\Re\left(y_i(mT_s)\right)\right\}_{m=nTf_s}^{(n+1)Tf_s-1}$, update the estimates $\hat{\alpha}$ and $\hat{\gamma}$ Using (3.35) {by substituting the set $\left\{\Re\left(y_i(mT_s)\right)\right\}_{m=nTf_s}^{(n+1)Tf_s-1}$ for the process a}

10 : $\hat{\gamma}_0 \leftarrow \hat{\gamma}^{1/\hat{\alpha}}$

11 : Updating $\hat{\varrho}_n$ using (3.36)

12 : **End If**
13 : **End For**
Output : Filtered signal $\tilde{y}_i(mT_s)$

3.3.3.3 Generalized-SNR

In order to determine the SNR, higher order moments are used to measure the signal and noise power (Gaussian case). However, this distortion metric is not valid in the presence of impulsive noise (α-stable), since these noise processes do not have finite higher-order statistics. One of the most commonly used signal distortion measures in the context of α-stable processes is the generalized-SNR (GSNR). The GSNR is the ratio between the average signal power and the average dispersion of α-stable noise [107-108], such that:

$$\mathrm{GSNR_{dB}} = 10\log_{10}\frac{E\left[\|\mathbf{y}(n)-\boldsymbol{\eta}(n)\|^2\right]}{N_r\gamma} \tag{3.37}$$

Therefore, direct comparison between existing methods (which assume Gaussian noise) and methods developed under the assumption of impulsive noise is not possible. However, it is interesting to note that the equivalence between the SNR and the GSNR is possible in a particular case where $\alpha = 2$ [11].

In the presence of impulsive noise, the DMC process is the same as that proposed in [11, 25]. Here we assume perfect CSI at the receiver. Otherwise, the channel estimation must be performed. In our study, the impact of the channel estimation error on the DMC process is examined. Consequently, the channel considered is modeled as:

$$\widehat{\mathbb{H}}^{(n_r)} = \mathbb{H}^{(n_r)} + \sigma_e \mathbb{H}_e^{(n_r)} \tag{3.38}$$

where $\left[\mathbb{H}_e^{(n_r)}\right]_{m,n}$ are zero-mean complex circular Gaussian variables i.i.d with unit-variance, and σ_e^2 is the variance of channel estimation error.

After decoding, the estimated vector $\hat{\mathbb{s}}_i$ is sent to the following subsystem to extract the features.

In figure 3.13 the performance of optimal-MF is examined with Gaussian and impulsive noises. The performance is evaluated by the $\mathrm{P_{ci}}$ versus GSNR. We observe that the $\mathrm{P_{ci}}$ improves as the value of α increases from 1.2 to 2. $\mathrm{P_{ci}}$ is the best for $\alpha = 2$, which corresponds to a

Gaussian channel. The mitigation of impulsive noise by MF has no effect on P_{ci} for GSNR inferior to 10dB.

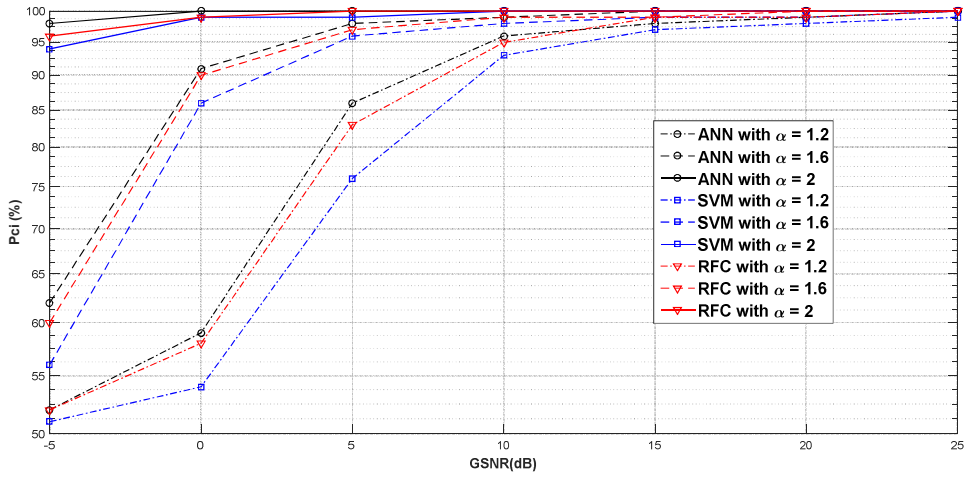

Figure 3.13- Probability of correct identification versus GSNR in STBC-OFDM system with presence of impulsive noises. $N_t = 2, N_r = 4, N = 64$.

ANN based classifier outperform always the one based on all classifiers.

3.4 DMC in SFBC-OFDM systems

In the case of frequency-selective MIMO channels, there is an additional source of diversity, which is frequency diversity. By combining OFDM modulation with MIMO systems, space-frequency block codes (SFBC) have been proposed to exploit spatial and frequency diversity in frequency-selective MIMO channels [109-111]. The strategy of SF coding is to distribute the channel coefficients on different transmit antennas and on all the sub-carriers within the same OFDM block. The SF coding mapping is based on ST codes (see table 3.1), replacing the time domain with the frequency domain [112-113].

The digital modulation identification in MIMO-OFDM systems using SF coding has aroused considerable research interest.

In this section, we have applied our modulation identification algorithm in SFBC-OFDM system. The identification process in SFBC-OFDM system is similar as we explained previously, and is composed of four subsystems: **(1)** The equalization/decoding subsystem **(2)** The features extraction subsystem using HOS estimates, **(3)** pattern recognition using two classifiers ANN and SVM, and **(4)** the decisions fusion center.

We consider a MIMO-OFDM system with N_t transmitting antennas, N_r receiving antennas, and N-IFFT subcarriers. At the transmitter, the data symbols are taken from a QPSK or

16QAM constellation. For the i-th data block, we consider the data vector $\mathbf{s}_i = [s_i(0),\ s_i(1), \ldots,\ s_i(N_d-2), s_i(N_d-1)]^T$ and consists of N_d symbols. The SF coding is obtained by linearly transforming the precoded data of vector $\mathbf{s}_i$. In the case of an Alamouti coding, the symbol vector $\mathbf{s}_i$ is coded by SF encoder SF of Alamouti type into two vectors $\mathbf{c}_i^{(1)}$ and $\mathbf{c}_i^{(2)}$ of size N_d as:

$$\begin{cases} \mathbf{c}_i^{(1)} = [s_i(0),\ -s_i^*(1), \ldots,\ s_i(N_d-2), -s_i^*(N_d-1)]^T \\ \mathbf{c}_i^{(2)} = [s_i(1), s_i^*(0), \ldots, s_i(N_d-1), s_i^*(N_d-2)]^T \end{cases} \tag{3.39}$$

The vectors elements represent the frequency domain data symbols transmitted respectively by the first and the second antenna. In the spatial multiplexing (SM) system, the i-th data vector $\mathbf{x}_i = [x_i(0),\ x_i(1), \ldots,\ x_i(2N_d-2), s_i(2N_d-1)]^T$ of length $2N_d$ is multiplexed into two vectors ($N_t = 2$), giving two independent vectors of the frequency domain of length N_d :

$$\begin{cases} \mathbf{b}_i^{(1)} = [x_i(0),\ x_i(2), \ldots,\ x_i(2N_d-2),]^T \\ \mathbf{b}_i^{(2)} = [x_i(1), x_i(3), \ldots, x_i(2N_d-1),]^T \end{cases} \tag{40}$$

The SFBC coder maps the data symbol vector into an SF coding matrix of size $N_d \times N_t$, denoted $\mathcal{G}_{\mathrm{SFBC}}$. The table 3.1 presents different SF code matrices used in literatures. Each codeword is presented by an coding rate, denoted R_{SF}.

Table 3.1. Different types of SF code matrices with different coding rates "R_{SF}".

$\mathcal{G}_{\mathrm{SFBC}}(s_1, s_2, s_3)$ **[114]**	$\mathcal{G}_{\mathrm{SFBC}}(s_1, s_2, s_3, s_4)$**[49]**	$\mathcal{G}_{\mathrm{SFBC}}(s_1, s_2, s_3, s_4)$ **[114]**	$\mathcal{G}_{\mathrm{SFBC}}(s_1, s_2, s_3, s_4)$**[49]**
$\begin{bmatrix} s_1 & s_2 & s_3 \\ -s_2^* & s_1^* & 0 \\ s_3^* & 0 & -s_1^* \\ 0 & s_3^* & -s_2^* \end{bmatrix}$	$\begin{bmatrix} s_1 & s_2 & s_3 \\ -s_2 & s_1 & -s_4 \\ -s_3 & s_4 & s_1 \\ -s_4 & -s_3 & s_2 \\ s_1^* & s_2^* & s_3^* \\ -s_2^* & s_1^* & -s_4^* \\ -s_3^* & s_4^* & s_1^* \\ -s_4^* & -s_3^* & s_2^* \end{bmatrix}$	$\begin{bmatrix} s_1 & s_2 & s_3 & s_4 \\ -s_3^* & -s_4^* & s_1^* & s_2^* \\ -s_2^* & s_1^* & -s_4^* & s_3^* \\ s_4 & -s_3 & -s_2 & s_1 \end{bmatrix}$	$\begin{bmatrix} s_1 & s_2 & s_3 & s_4 \\ -s_2 & s_1 & -s_4 & s_3 \\ -s_3 & s_4 & s_1 & -s_2 \\ -s_4 & -s_3 & s_2 & s_1 \\ s_1^* & s_2^* & s_3^* & s_4^* \\ -s_2^* & s_1^* & -s_4^* & s_3^* \\ -s_3^* & s_4^* & s_1^* & -s_2^* \\ -s_4^* & -s_3^* & s_2^* & s_1^* \end{bmatrix}$
$N_t = 3, K = 3, R_{\mathrm{SF}} = \frac{3}{4}$	$N_t = 3, K = 4, R_{\mathrm{SF}} = \frac{1}{2}$	$N_t = 4, K = 4, R_{\mathrm{SF}} = 1$	$N_t = 4, K = 4, R_{\mathrm{SF}} = \frac{1}{2}$

The operation of SF encoder and decoder can be described in terms of the even and odd components of the vector $\mathbf{s}_i$. Let $\mathbf{s}_i^o$ and $\mathbf{s}_i^e$ two vectors of length $\left({}^{N_d}/_{2}\right)$ simultaneously designating the odd and even vectors of $\mathbf{s}_i$. Then we define [109]:

$$\begin{cases}\mathbf{s}_i^o = [s_i(1), s_i(3), \dots, s_i(N_d-3), s_i(N_d-1)]^T \\ \mathbf{s}_i^e = [s_i(0), s_i(2), \dots, s_i(N_d-4), s_i(N_d-2)]^T\end{cases} \tag{3.41}$$

Using the equations of (3.41), we can write:

$$\begin{cases}\left(\mathbf{c}_i^{(1)}\right)^o = -(\mathbf{s}_i^o)^* \\ \left(\mathbf{c}_i^{(1)}\right)^e = \mathbf{s}_i^e \\ \left(\mathbf{c}_i^{(2)}\right)^o = (\mathbf{s}_i^e)^* \\ \left(\mathbf{c}_i^{(2)}\right)^e = \mathbf{s}_i^o\end{cases} \tag{3.42}$$

From equation (3.42), we can conclude that SFBC can be represented by a transmission matrix as:

$$\begin{aligned}\mathcal{G}_{\text{SFBC}}(\mathbf{s}_i) &= \begin{bmatrix}\mathbf{c}_i^{(1)} & \mathbf{c}_i^{(2)}\end{bmatrix} \\ &= \begin{bmatrix}\mathbf{s}_i^e & \mathbf{s}_i^o \\ -(\mathbf{s}_i^o)^* & (\mathbf{s}_i^e)^*\end{bmatrix} \Rightarrow \mathcal{G}_{\text{SFBC}}^{\mathcal{H}}(\mathbf{s}_i)\mathcal{G}_{\text{SFBC}}(\mathbf{s}_i) = \|\mathbf{s}_i\|_F^2 \mathbf{I}_{N_t}\end{aligned} \tag{3.42}$$

After the coding matrix generation, the N_{vsc} virtual subcarriers are added to each vector $\mathbf{c}_i^{(n_t)}$ to form the vector $\bar{\mathbf{v}}_i^{(n_t)}$. Then, N-points of the IFFT matrix ($\mathbf{F}_N^{\mathcal{H}}$), are applied to the vector $\bar{\mathbf{v}}_i^{(n_t)}$ and the CP is inserted by multiplication with an appropriate matrix $\mathbf{T}_{cp} = \left[\mathbf{I}_{N_{cp}\times N}^T, \mathbf{I}_N^T\right]^T$. We note here that the CP is strictly greater than the channel length ($N_{cp} \gg L$). The resulting signal sent by N_t antennas passes through a Rayleigh channel and received by N_r antennas. $h^{(n_r,n_t)}(l)$ with $l \in [0, L-1]$ denotes the L-th channel coefficients between the n_t-th transmit antenna and the n_r-th receive antenna.

Using an appropriate matrix $\mathbf{R}_{cp} = \left[\mathbf{0}_{N\times N_{cp}}, \mathbf{I}_N\right]$, to remove the CP from the received signal. We assume that the synchronization between the oscillators of the transmitter and receiver is perfect (absence of CFO), the i-th received signal by the n_r-th antenna after the application of FFT is written in the following form:

$$\tilde{\mathbf{y}}_i^{(n_r)} = \frac{1}{N}\sum_{n_t=1}^{N_t} \mathbf{D}_N\left(\tilde{\mathbf{h}}^{(n_r,n_t)}\right)\bar{\mathbf{v}}_i^{(n_t)} + \tilde{\boldsymbol{\eta}}_i^{(n_r)} \tag{3.43}$$

where $\tilde{\mathbf{y}}_i^{(n_r)} = \mathbf{F}_N \mathbf{y}_i^{(n_r)}$, and $\tilde{\boldsymbol{\eta}}_i^{(n_r)} = \mathbf{F}_N \boldsymbol{\eta}_i^{(n_r)}$ of size $(N \times 1)$ is the zero-mean AWGN vector and variance $\sigma_\eta^2\, \mathbf{I}_N$.

The identification system begins after the equalization/decoding operations. The DMC process is the same as that proposed in the STBC-OFDM system.

Here we assume perfect CSI at the receiver. Therefore, for the SFBC-OFDM system, we examine the impact of the channel estimation error on the DMC process. The channel considered is modeled as :

$$\widehat{\mathbf{H}}^{(n_r)} = \mathbf{H}^{(n_r)} + \sigma_e \mathbf{H}_e^{(n_r)} \tag{3.44}$$

where $\left[\mathbf{H}_e^{(n_r)}\right]_{m,n}$ are zero-mean complex circular Gaussian variables and i.i.d with unit-variance, and σ_e^2 is the variance of channel estimation error.

After decoding, the estimated vector $\hat{\mathbf{s}}_i$ is sent to the following subsystem to extract the features.

The simulation results show the performance of our proposed algorithm and the identification capacity for the pool $\Theta = \{\text{QPSK}, \text{16QAM}\}$, in the presence of transmission degradations, with relatively low SNR values. These favorable results are obtained with an acceptable calculation cost.

Figure 3.14 shows the probability of correct identification for different numbers of subcarriers N. The performance of the proposed algorithm improves with the increase of N but involves a great computation complexity.

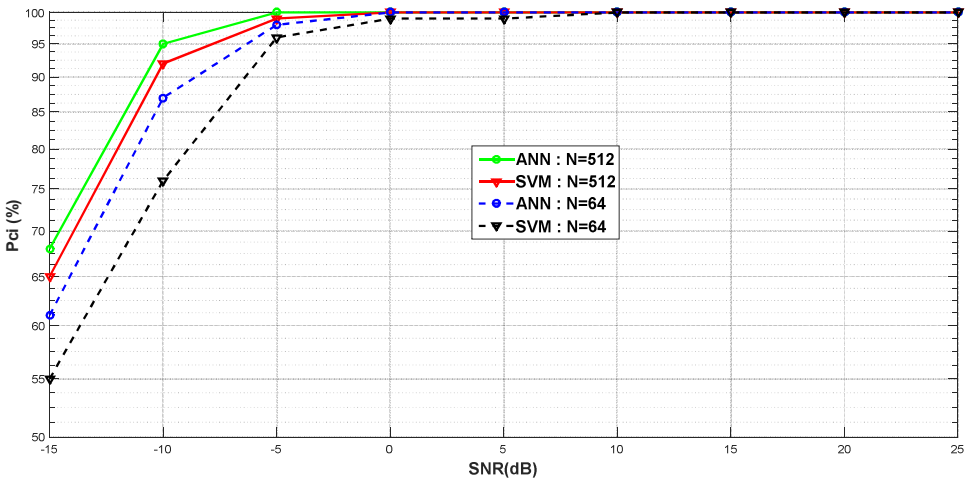

Figure 3.14- Probability of correct identification versus SNR in SFBC-OFDM system for different values of N. $N_t = 2, N_r = 4$.

Figure 3.15 shows the probability of correct identification versus SNR by applying two types of classification ANN and SVM in SFBC-OFDM system with and without the channel estimation error.

The addition of estimation errors degrades the performance of our identification process. However, this degradation is small compared to the results achieved without these errors (the variance of the channel estimation errors is $\sigma_e^2 = 0{,}1$).

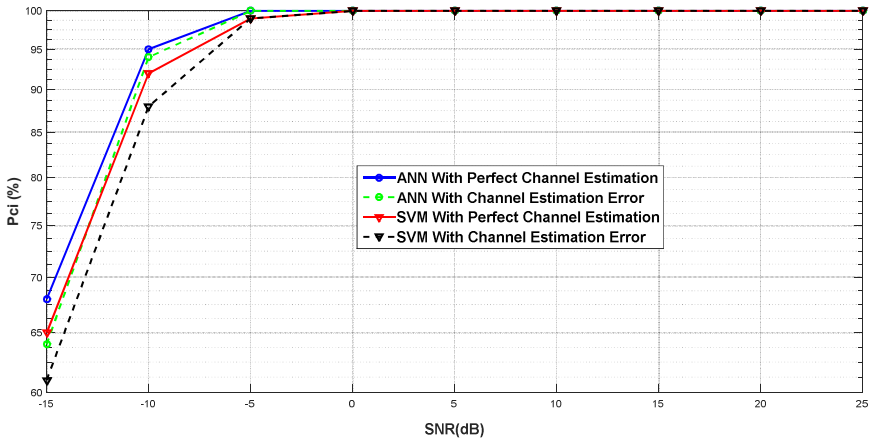

Figure 3.15- Probability of correct identification versus SNR in SFBC-OFDM system with and without the channel estimation error. $\sigma_e^2 = 0{,}1$, $N_t = 2$, $N_r = 4$.

In figure 3.16, the P_{ci} and P_{fa} for each modulation in pool Θ are evaluated by the classification process in SFBC-OFDM system. We use an ANN classifier to show the performance of our DMC process with perfect CSI at the receiver side. We can see that the probabilities for the two modulations are very close with a superiority of the QPSK modulation. The results indicate that the performance of P_{ci} augmentent avec un $SNR_{dB} \geq -10$ et lorsque le P_{fa} s'approche de 0.01.

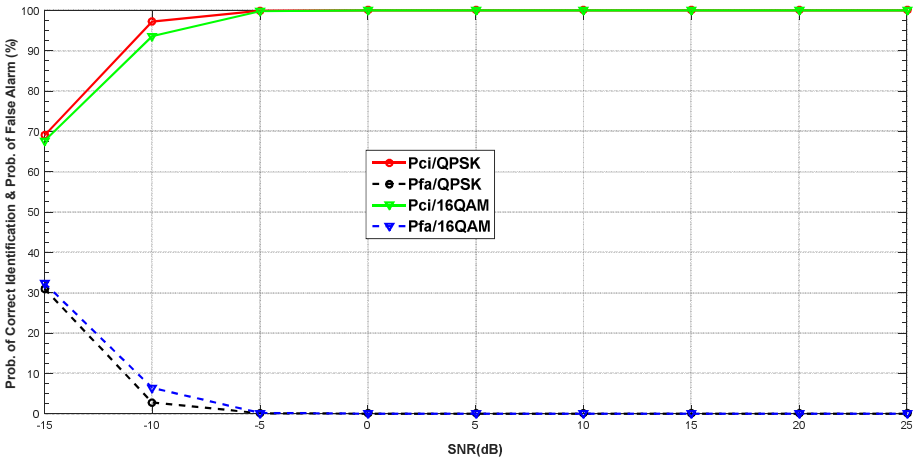

Figure 3.16- P_{ci} and P_{fa} versus SNR in SFBC-OFDM system. $N_t = 2$, $N_r = 4$, $N = 512$, and ANN classifier.

Of all the classification results compared, ANN obtained the highest overall classification accuracy, followed by the SVM classifier in different scenarios. Analysis of the results stability allowed us to conclude that all the classifiers presented small variances in terms of overall

precision even with the presence of the channel degradations. This proves the effectiveness of our classification algorithm.

3.5 Conclusion

In this last part, we present a brief study on digital modulations identification algorithms in MIMO-OFDM systems.

We show that, by taking advantage of the redundancy in space, time and frequency, thus the different phases of the received signals filtering, the digital modulations identification can be performed by exploiting the features extraction of the filtered signals using HOS from different antennas and the differents classifiers. Due to this functionality, we develop differents tests for decision-making. The proposed processes do not require a priori recognition of the channel coefficients, the nature of the noise, the modulation schemes, or the frequency offset. The simulation results thorough allowed us to verify the effectiveness of the proposed methods.

To solve the degradation problems of BDMC performances due to CFO and channel estimation errors, we have proposed joint blind and semi-blind estimation methods for CFO and channels.

In this work, the effect of impulsive noise on the digital modulations identification for MIMO-OFDM system is considered. The MIMO-OFDM system is very sensitive to impulsive noise and to reduce these effects, pulsive noise, a filtering based on the optimal Myriad filter is proceeded and implemented to estimate the parameters of this noise type.

To recognize the digital modulation type, the DMC algorithm uses HOS for the features extraction. After that, different classifiers (ANN, SVM, RFC, KNN) are applied to solve the pattern recognition problem. This steps-end with a decisions fusion in order to improve the accuracy of desired modulations identification. The simulation results showed that our BDMC algorithm is robust to CFO, channel estimation errors and impulsive noise, and that it works with a high identification probability at low SNR. The two classifiers SVM and ANN can achieve, for all settings, a classification rate of **97.6%** for SNR greater than or equal to 0dB and up to **90%** for GSNR greater than 5dB.

Conclusion

This thesis presents one of the applications of cognitive radio, that is the digital modulations identification for STBC-MIMO and MIMO-OFDM systems operating in multipath environment and in presence of impulsive noise and frequency offset. So, the identification is affected by the harmful effects of this channel, hence the need to its estimation. For that, blind and semi-blind estimation algorithms of channels, CFO and impulsive noise were used. At the receiver side, and based on these estimates, CFO compensation, channel equalization (ZF or SCMA), and Myriad filtering are applied in order to reducing errors which degrade identification. Then, the blind modulation identification started. First, the HOS are to be extracted from the received signal. These features are exploited by the pattern recognition algorithms (ANN, SVM, KNN and RFC), to be able to achieve the final classification after the passage by a decisions fusion center. This center of fusion used to reinforce the identification capacity of all modulations types under inappropriate transmission conditions, and for medium and low SNR levels.

Indeed, in the second chapter, we have done the blind digital modulation identification for spatially correlated STBC-MIMO systems based on the HOS and the different classifiers (ANN, SVM, ... etc.). Here all classifiers are subjected to the same conditions of training and test and are evaluated in the sense of the average probability of correct identification. Intensive simulations show that ANN classifier have the best average probability of correct identification for all simulated SNR range and MIMO system configurations. Additionally, we note that, globally, all classifiers have close performances; this can be explained by their good deployment after leading them to their best completion.

According to the simulation results, the ZF-DMC method is a best semi-blind algorithm when we assume a perfect CSI, and deploy before the features extraction process. However, the ZF-DMC algorithm is sensitive to channel estimation errors. The presence of these errors leads to rapid performance degradation and leads to upper bound of the probability of identification. To solve this problem, the SCMA-DMC algorithm is assumed to blindly separate symbols and offer best performances when any prior information on the channel is required at the receiver. The proposed algorithms are examined through a correlated MIMO channels and they prove capable of identifying different digital modulation schemes with great precision.

The use of multi-carriers systems is constantly growing either for 4G or for the future 5G, this is why we have opted it in the third chapter for the STBC-OFDM and SFBC-OFDM systems,

firstly. On the other hand and to the best our knowledge, modulation identification for MIMO-OFDM systems has not discussed in detail previously in the literature. For this, we considered the identification problem for MIMO-OFDM systems operating in a hostile environment, the same that used in chapter 2 (impulsive noise, CFO and channel errors). By following the same modulation identification process, that is: HOS features extraction, then applications of the ANN, SVM, KNN, and RFC algorithms followed by decision fusion, we were able to demonstrate the reliability of the proposed algorithms. Indeed, the simulation results showed that our BDMC algorithm is robust to CFO, to channel estimation errors and to impulsive noise, and that it works with a high probability of identification at low SNR. The modulation classification process can achieve, for all settings, a best classification rate ($\geq$ 97% for SNR $\geq$ 0dB and > 90% for GSNR > 5dB).

Note that, the classification performance is directly related to the quality of learning phase of each classifier, and that better learning can be achieved by including a wider range of data in a predefined interval of SNRs.

Appendices

A1. SNR in Rayleigh fading channels

In any communication system, the SNR is a very important parameter for describing and measuring the reception sensitivity of an information signal. It is the ratio between the maximum signal power and the noise power, present at the receiver. However, the communication channel noise is not often the ultimate disadvantage. Considering a system subject to the influence of fading, modeled by a Rayleigh distribution, a more appropriate measure to describe the the receiver sensitivity is the SNR calculation. In a MIMO-SC system, the output of ZF equalizer at the receiver side is given by:

$$\hat{\mathbf{s}} = \widehat{\mathbf{B}}(\mathbf{H}\mathbf{s} + \boldsymbol{\eta}) \tag{A.1}$$

where $\widehat{\mathbf{B}} = \widehat{\mathbf{H}}^{\#} = (\mathbf{H} + \sigma_e\boldsymbol{\Omega})^{\#}$ and the coefficients of $\boldsymbol{\Omega}$ are zero-mean complex circular Gaussian variables and i.i.d with unit-variance. Suppose $\sigma_e \ll 1$, then the pseudo-inverse of the estimated channel matrix can be approximated by the linear part of the Taylor expansion as $\widehat{\mathbf{B}} = \mathbf{H}^{\#}\left(\mathbf{I}_{N_r} - \sigma_e\boldsymbol{\Omega}\mathbf{H}^{\#}\right)$. Consequently, the estimated signal can be written as $\hat{\mathbf{s}} = \mathbf{s} + \hat{\boldsymbol{\eta}}$ where $\hat{\boldsymbol{\eta}}$ is given by:

$$\hat{\boldsymbol{\eta}} = \mathbf{H}^{\#}\boldsymbol{\eta} - \sigma_e\mathbf{H}^{\#}\boldsymbol{\Omega}\mathbf{s} - \sigma_e\mathbf{H}^{\#}\boldsymbol{\Omega}\mathbf{H}^{\#}\boldsymbol{\eta} \tag{A.2}$$

The last two terms in equation (A.2) are additional noise introduced by the channel estimation error. To calculate the effective post-processing SNR for each estimated stream, we must calculate the covariance matrix of the effective post-processing noise, i.e. $E[\hat{\boldsymbol{\eta}}\hat{\boldsymbol{\eta}}^{\mathcal{H}}]$. This covariance matrix is calculated as:

$$\begin{aligned}
E[\hat{\boldsymbol{\eta}}\hat{\boldsymbol{\eta}}^{\mathcal{H}}] &= E[(\mathbf{H}^{\#}\boldsymbol{\eta} - \sigma_e\mathbf{H}^{\#}\boldsymbol{\Omega}\mathbf{s} - \sigma_e\mathbf{H}^{\#}\boldsymbol{\Omega}\mathbf{H}^{\#}\boldsymbol{\eta}) \times (\mathbf{H}^{\#}\boldsymbol{\eta} - \sigma_e\mathbf{H}^{\#}\boldsymbol{\Omega}\mathbf{s} - \sigma_e\mathbf{H}^{\#}\boldsymbol{\Omega}\mathbf{H}^{\#}\boldsymbol{\eta})^{\mathcal{H}}] \\
&= \sigma_\eta^2\mathbf{H}^{\#}(\mathbf{H}^{\#})^{\mathcal{H}} - \sigma_e\sigma_\eta^2E[\mathbf{H}^{\#}(\mathbf{H}^{\#})^{\mathcal{H}}\boldsymbol{\Omega}^{\mathcal{H}}(\mathbf{H}^{\#})^{\mathcal{H}}] + \sigma_e^2\sigma_s^2\mathbf{H}^{\#}E[\boldsymbol{\Omega}\boldsymbol{\Omega}^{\mathcal{H}}](\mathbf{H}^{\#})^{\mathcal{H}} \\
&\qquad - \sigma_e\sigma_\eta^2E[\mathbf{H}\mathbf{H}^{\#}\boldsymbol{\Omega}(\mathbf{H}^{\#})^{\mathcal{H}}] + \sigma_e^2\sigma_\eta^2\mathbf{H}^{\#}E[\boldsymbol{\Omega}\mathbf{H}^{\#}(\mathbf{H}^{\#})^{\mathcal{H}}\boldsymbol{\Omega}^{\mathcal{H}}](\mathbf{H}^{\#})^{\mathcal{H}} \\
&= \sigma_\eta^2(\mathbf{H}^{\mathcal{H}}\mathbf{H})^{-1} + \sigma_e^2\sigma_s^2\mathbf{H}^{\#}N_t\mathbf{I}_{N_r}(\mathbf{H}^{\#})^{\mathcal{H}} + \sigma_e^2\sigma_\eta^2\mathbf{H}^{\#}E[\boldsymbol{\Omega}(\mathbf{H}^{\mathcal{H}}\mathbf{H})^{-1}\boldsymbol{\Omega}^{\mathcal{H}}](\mathbf{H}^{\#})^{\mathcal{H}} \\
&= \left[\sigma_\eta^2 + N_t\sigma_e^2\sigma_s^2 + \sigma_e^2\sigma_\eta^2\mathrm{tr}((\mathbf{H}^{\mathcal{H}}\mathbf{H})^{-1})\right](\mathbf{H}^{\mathcal{H}}\mathbf{H})^{-1}
\end{aligned} \tag{A.3}$$

where $E[\mathbf{s}\mathbf{s}^{\mathcal{H}}] = \sigma_s^2\mathbf{I}_{N_t}$, $E[\boldsymbol{\eta}\boldsymbol{\eta}^{\mathcal{H}}] = \sigma_\eta^2\mathbf{I}_{N_r}$, $E[\boldsymbol{\Omega}\boldsymbol{\Omega}^{\mathcal{H}}] = N_t\mathbf{I}_{N_r}$, $\mathbf{H}^{\#}(\mathbf{H}^{\#})^{\mathcal{H}} = (\mathbf{H}^{\mathcal{H}}\mathbf{H})^{-1}$, and $E[\boldsymbol{\Omega}(\mathbf{H}^{\mathcal{H}}\mathbf{H})^{-1}\boldsymbol{\Omega}^{\mathcal{H}}] = \mathrm{tr}((\mathbf{H}^{\mathcal{H}}\mathbf{H})^{-1})\mathbf{I}_{N_r}$.

Based on the above equation, the post-processing SNR by symbol of the n-th stream can be expressed as [1]:

$$\varrho_n = \frac{\varrho_0}{\left[1+N_t\sigma_e^2\varrho_0+\sigma_e^2\mathrm{tr}\left((\mathbf{H}^{\mathcal{H}}\mathbf{H})^{-1}\right)\right]\left[(\mathbf{H}^{\mathcal{H}}\mathbf{H})^{-1}\right]_{n,n}} \tag{A.4}$$

where $\varrho_0 = \frac{\sigma_s^2}{\sigma_\eta^2}$ is the average normalized SNR at each receiving antenna. The probability of $[(\mathbf{H}^{\mathcal{H}}\mathbf{H})^{-1}]_{n,n}$ to be large is still small. The term $\sigma_e^2\mathrm{tr}((\mathbf{H}^{\mathcal{H}}\mathbf{H})^{-1})$ in the above equation can be neglected. Finally, the post-processing SNR for each estimated stream is approximated by:

$$\varrho_n = \frac{\varrho_0}{\left[1+N_t\sigma_e^2\varrho_0\right]\left[(\mathbf{H}^{\mathcal{H}}\mathbf{H})^{-1}\right]_{n,n}} = \frac{\varrho_0\kappa_n}{\lambda_e} \tag{A.5}$$

where κ_n is a random variable following a weighted chi-square distribution and $\lambda_e = 1 + N_t\sigma_e^2\varrho_0$ is the degradation of SNR due to imperfect CSI. For large SNR ($\varrho_0 \to \infty$) the ratio $\frac{\varrho_0}{\lambda_e} \to \frac{1}{N_t\sigma_e^2}$, which leads to an upper bound for correct identification contrary to the perfect CSI case [1, 115].

A2. Derivation of moments and cumulants expressions

The cumulants κ_n are defined by the cumulants generating function $g(t)$ as:

$$g_{\mathbf{x}}(t) = \ln\left(E(e^{t\mathbf{x}})\right) = \sum_{n=1}^{\infty}\kappa_n\frac{t^n}{n!} = \mu t + \sigma^2\frac{t^2}{2!} = \cdots \tag{A.6}$$

This function is therefore linked to the moment generating function and to the features function of variable $\mathbf{x}$. The cumulants are given by the derivatives in "0" of $g(t)$.

As indicated in equation (A.6), the cumulants and the moments of a distribution are linked. With independent variables $\mathbf{x}$ and $\mathbf{y}$, the generator function is more practical in the measurement of cumulants:

$$g_{\mathbf{x}+\mathbf{y}}(t) = \ln\left(E\left(e^{t(\mathbf{x}+\mathbf{y})}\right)\right) = \ln\left(E(e^{t\mathbf{x}})\right) + \ln\left(E(e^{t\mathbf{y}})\right) = g_{\mathbf{x}}(t) + g_{\mathbf{y}}(t) \tag{A.7}$$

Whereas with the moments generating function $m_{\mathbf{x}}$, we obtain:

$$m_{\mathbf{x+y}}(t) = E\left(e^{t(\mathbf{x+y})}\right) = E(e^{t\mathbf{x}}) \cdot E(e^{t\mathbf{y}}) = m_{\mathbf{x}}(t) \cdot m_{\mathbf{y}}(t) \tag{A.8}$$

For a stationary random process with complex values $s(n)$, the second order moments and cumulants can be defined in two different ways. Likewise, fourth-order moments and cumulants can be written in three ways. Thus, second, fourth and sixth order cumulants can be defined as [4, 64, 116]:

$$\begin{cases} \kappa_{2-}: \begin{cases} \kappa_{20} = E[s^2(n)] = \mu_{20} \\ \kappa_{21} = E[|s(n)|^2] = \mu_{21} \end{cases} \\ \kappa_{4-}: \begin{cases} \kappa_{40} = cum\big(s(n), s(n), s(n), s(n)\big) = \mu_{40} - 3\kappa_{20}^2 \\ \kappa_{41} = cum\big(s(n), s(n), s(n), s^*(n)\big) = \mu_{41} - 3\kappa_{20}\kappa_{21} \\ \kappa_{42} = cum\big(s(n), s(n), s^*(n), s^*(n)\big) = \mu_{42} - |\kappa_{20}|^2 - 2\kappa_{21}^2 \end{cases} \\ \kappa_{6-}: \begin{cases} \kappa_{60} = \mu_{60} - 15\kappa_{20}\mu_{40} + 30\kappa_{20}^3 \\ \kappa_{61} = \mu_{61} - 5\kappa_{21}\mu_{40} - 10\kappa_{20}\mu_{41} + 30\kappa_{20}^2\kappa_{21} \\ \kappa_{62} = \mu_{62} - 6\kappa_{20}\mu_{42} - 8\kappa_{21}\mu_{41} - \mu_{22}\mu_{40} + 6\kappa_{20}^2\mu_{22} + 24\kappa_{21}^2\kappa_{20} \\ \kappa_{63} = \mu_{63} - 9\mu_{42}\kappa_{21} - 3\kappa_{20}\mu_{43} - 3\mu_{22}\mu_{41} + 18\kappa_{20}\kappa_{21}\mu_{22} + 12\kappa_{21}^3 \end{cases} \end{cases} \tag{A.9}$$

The theoretical values of moments and cumulants for different orders and for all the modulations constellations used in our studies are given in table A1. These values are calculated for noise-free constellations with equiprobable symbols and unit-variances [5, 64]. These values clearly show how each modulation constellation is characterized by a set of these HOS, which means each modulation constellation comprises a distinct set of HOS values.

Table A1. Some theoretical statistical values of moments and cumulants for different modulation schemes [4-5].

	BPSK	QPSK	8-PSK	4-ASK	8-ASK	16-QAM	64-QAM
μ_{20}	1	0	0	1	1	0	0
μ_{40}	1	1	0	1.64	1.77	-0.67	-0.18
μ_{41}	1	0	0	1.64	1.77	0	0
μ_{42}	1	1	1	1.64	1.77	1.32	1.34
κ_{40}	-2	1	0	-1.36	-1.24	-0.68	-0.62
κ_{41}	-2	0	0	-1.36	-1.24	0	0
κ_{42}	-2	-1	-1	-1.36	-1.24	-0.68	-0.62
μ_{60}	1	0	0	2.92	3.62	0	0
μ_{61}	1	-1	0	2.92	3.62	-1.32	0.38
μ_{63}	1	1	1	2.92	3.62	1.96	2.08
κ_{60}	16	0	0	8.32	7.19	0	0
κ_{61}	16	-4	0	8.32	7.19	2.08	1.8
κ_{62}	16	0	0	8.32	7.19	0	0
κ_{63}	16	4	4	8.32	7.19	2.08	1.8

Bibliography

[1] K. HASSAN, "*Contributions to Cognitive Radio Awareness for High Mobility Applications*," Ph.D Thesis, Université De Valenciennes et du Hainaut-Cambresis, no. 12/32, pp. 16-17, France, 2012.

[2] Y. D. Huang, P. P. Liang, Q. Zhang, and Y.-C. Liang, "*A Machine Learning Approach to MIMO Communications*," in IEEE International Conference on Communications (ICC), Kansas City, MO, USA, pp. 1-6, 20-24 May 2018.

[3] Q. Zhang, H. Guo, Y.-C. Liang, and X. Yuan, "*Constellation Learning Based Signal Detection for Ambient Backscatter Communication Systems*," IEEE Journal on Selected Areas in Communications, vol. 37, no. 2, pp. 452-463, February. 2019.

[4] A. Swami and B. M. Sadler, "*Hierarchical Digital Modulation Classification Using Cumulants*," IEEE Transactions on Communications, vol. 48, no. 3, pp. 416-429, March 2000.

[5] O. A. Dobre, A. Abdi, Y. Bar-Ness, and W. Su, "*Survey of Automatic Modulation Classification Techniques: Classical Approaches and New Trends*," IET Communications, vol. 1, no. 2, pp. 137-156, April 2007.

[6] M. S. Muhlhaus, M. Oner, O. A. Dobre, and F. K. Jondral, "*A Low Complexity Modulation Classification Algorithm for MIMO Systems*," IEEE Communications Letters, vol. 17, no. 10, pp. 1881-1884, October 2013.

[7] K. Hassan, I. Dayoub, W. Hamouda, C. N. Nzeza, and M. Berbineau, "*Blind Digital Modulation Identification for Spatially-Correlated MIMO Systems*," IEEE Transactions on Wireless Communications, vol. 11, no. 2, pp. 683-693, February 2012.

[8] X. Yuan, Y. Li, M. Gao, T. Li, and H. Zhang, "*Automatic Modulation Classification for MIMO-OFDM Systems with Imperfect Timing Synchronization*," in IEEE 86th Vehicular Technology Conference (VTC-Fall), Toronto, ON, Canada, 24-27 September. 2017.

[9] Y. Liu, O. Simeone, A. M. Haimovich and W. Su, "*Modulation Classification for MIMO-OFDM Signals via Approximate Bayesian Inference*," IEEE Transactions on Vehicular Technology, vol. 66, no. 1, pp. 268-281, January 2017.

[10] T. Hirakawa ; M. Fujii ; M. Itami ; K. Itoh, "*A Study on Iterative Impulse Noise Reduction in OFDM Signal by Recovering Time Domain Samples*," in IEEE International Symposium on Power Line Communications and Its Applications, Orlando, FL, USA, 26-29 March 2006.

[11] K. Hassan, R. Gautier, I. Dayoub, M. Berbineau, and E. Radoi,"*Multiple-Antenna-Based Blind Spectrum Sensing in the Presence of Impulsive Noise*," IEEE Transactions on Vehicular Technology, vol. 63, no. 5, pp. 2248-2257, June 2014.

[12] A. El-Mahdy, "*Classification of MFSK Signals over Time-Varying Flat Correlated Fading Channels Under Class-A Impulsive Noise Environment*," IEEE Proceedings-Communications, vol. 151, no. 6, pp. 619–626, December. 2004.

[13] W. Wei and J. Mendel, "*A Fuzzy Logic Method for Modulation Classification in Non-Ideal Environm*ents," IEEE Transactions on Fuzzy Systems, vol. 7, no. 3, pp. 333–344, June 1999.

[14] J. Ferrer-Coll, S. Ben Slimane, J. Chilo, P. Stenumgaard, "*Detection and Suppression of Impulsive Noise in OFDM Receiver*," Springer Wireless Personal Communications, vol. 85, no. 4, pp. 2245-2259, December 2015.

[15] J. Gonzalez and G. Arce, "*Optimality of the myriad filter in practical impulsive-noise environments*," IEEE Transactions on Signal Processing, vol. 49, no. 2, pp. 438–441, February 2001.

[16] Y. A. Eldemerdash, O. A. Dobre, and M. oner, "*Signal Identification for Multiple-Antenna Wireless Systems: Achievements and Challenges*," IEEE Communications Surveys & Tutorials, vol. 18, no. 3, pp. 1524–1551, thirdquarter 2016.

[17] H. Agirman-Tosun, Y. Liu, A. M. Haimovich, O. Simeone, W. Su, J. Dabin, and E. Kanterakis, "*Modulation Classification of MIMO-OFDM Signals by Independent Component Analysis and Support Vector Machines*," in Conference Record of the Forty Fifth Asilomar Conference on Signals, Systems and Computers (ASILOMAR), Pacific Grove, CA, USA, pp. 1903–1907, 6-9 November 2011.

[18] J. Mitola, G. Q. Maguire, "*Cognitive Radio: Making Software Radios More Personal*," IEEE Personal Communications, vol. 6, no. 4, pp. 13–18, August 1999.

[19] R. H. Nangare, S. H. Rajput., "*Security Against Pue Attack in Cognitive Radio Network*," International Conference on Industrial Applications of Signal Processing, DACOE, Karad, India, 2013.

[20] C. E. Shannon, "*A Mathematical Theory of Communications*," Bell Systems Technical Journal, vol. 27, no. 7, pp. 379–423, 623-656, 1948.

[21] J. Palicot., "*Radio Engineering: From Software to Cognitive Radio*," ISTE Ltd and John Wiley & Sons, Great Britain and the United States, 2011.

[22] S. Haykin, "*Cognitive Radio : Brain-Empowered Wireless Communications*," IEEE Journal on Selected Area in Communications, vol. 23, no. 2, pp. 201–220, February 2005.

[23] T. W. Rondeau, C. W. Bostian, D. Maldonado, A. Ferguson, S. Ball, B. Le, and S. Midkiff, "*Cognitive Radios in Public Safety and Spectrum Management*," in Telecommunications Policy and Research Conference, vol. 33, September 2005.

[24] N. Baldo and M. Zorzi, "*Learning and Adaptation in Cognitive Radios Using Neural Networks*," in IEEE Consumer Communications and Networking Conference (CCNC), Las Vegas, USA, pp. 998–1003, January 2008.

[25] A. Amanna, M. G. M. J. Price, J. H. Reed, W. P. Siriwongpairat, and T. K. Himsoon, "*Railway Cognitive Radio, Future Wireless Communication Systems for Railways*," IEEE Vehicular Technology Magazine, vol. 5, no. 3, pp. 8289, 2010.

[26] S. Russell and P. Norvig, "*Artificial Intelligence: A Modern Approach*," 2nd Ed. Prentice-Hall, 1995.

[27] T. W. Rondeau, "*Application of Artificial Intelligence to Wireless Communications*," Ph.D. dissertation, Virginia Polytechnic Institute and State University, September 2007.

[28] B. A. Fette, "*Cognitive Radio Technology*," 2nd Ed., Academic Press, Elsevier Inc., 2009.

[29] H. Arslan, Ed., "*Cognitive Radio, Software Defined Radio, and Adaptive Wireless Systems*," Springer, 2007.

[30] G. Ghosh, P. Das, S. Chatterjee, "*Simulation and Analysis of Cognitive Radio System Using MATLAB*," International Journal of Next-Generation Networks (IJNGN), vol. 6, no. 2, India, June 2014.

[31] S. Barve, A. Akotkar, A. Chavan, A. Kumar and M. Dhaigude, "*Open Source Software Defined Radio Using GNU Radio and USRP*," International Journal of Scientific and Technology Research, vol. 3, no. 5, pp. 305-308, 2014.

[32] I. F. Akyildiz, W.-Y. Lee, M. C. Vuran and S. Mohanty, "*Next Generation/Dynamic Spectrum Access/Cognitive Radio Wireless Networks: A Survey*," Elsevier, Computer Networks, vol. 50, no. 13, pp. 2127-2159, September 2006.

[33] T. Charles Clancy, "*Dynamic Spectrum Access in Cognitive Radio Networks*," Ph.D Thesis, Faculty of the Graduate School of the University of Maryland, 2006.

[34] A. Bansal, Ms. R. Mahajan, "*Building Cognitive Radio System Using Matlab*," IJECSE, vol. 1, no. 3, pp. 1555-1560, June 2012.

[35] J. Mitola, "*The Software Radio Architecture*," IEEE Communications Magazine, vol. 33, no. 5, pp. 26–38, May 1995.

[36] S. Kharbech, I. Dayoub, M. Zwingelstein-Colin, E. P. Simon, and K. Hassan, "*Blind Digital Modulation Identification for Time-Selective MIMO Channels*," IEEE Wireless Communications Letters, vol. 3, no. 4, pp. 373-376, August 2014.

[37] E. Krouk, S. Semenov, "*Modulation and Coding Techniques in Wireless Communications*," John Wiley & Sons Ltd, 2011.

[38] A. Paulraj, R. Nabar, and D. Gore, "*Introduction to Space-Time Wireless Communications*," Cambridge University Press, May 2003.

[39] M. Chryssomallis, "*Smart Antennas*," IEEE Antennas and Propagation Magazine, vol. 42, no. 3, pp. 129–136, June 2000.

[40] S. M. Alamouti, "*A Simple Transmit Diversity Technique for Wireless Communications*," IEEE Journal on Selected Areas in Communications, vol. 16, no. 8, pp. 1451–1458, October 1998.

[41] V. Tarokh, N. Seshadri, and A. R. Calderbank, "*Space-Time Codes for High Data Rate Wireless Communication: Performance Criterion and Code Construction*," IEEE Transactions on Information Theory, vol. 44, no. 2, pp. 744–765, March 1998.

[42] Gerard J. Foschini, "*Layered Space-Time Architecture for Wireless Communication in a Fading Environment when using Multi-Element Antennas*," Bell Labs Technical Journal, vol. 1, no. 2, pp. 41–59, Autumn 1996.

[43] I. Emre Telatar, "*Capacity of Multi-Antenna Gaussian Channels*," European Transactions on Telecommunications, vol. 10, no. 6, pp. 585–595, April 2000.

[44] S. Wyne, A. Molisch, P. Almers, G. Eriksson, J. Karedal, and F. Tufvesson, "*Statistical Evaluation of Outdoor-to-Indoor Office MIMO Measurements at 5.2 GHz*," in IEEE 61st Vehicular Technology Conference, Stockholm, Sweden, 30 May-1 June 2005.

[45] D. Shiu, G. J. Foschini, M. J. Gans, and J. M. Kahn, "*Fading Correlation and its Effect on the Capacity of Multielement Antenna Systems*," IEEE Transactions on Communications, vol. 48, no. 3, pp. 502–513, March 2000.

[46] S. L. Loyka, "*Channel Capacity of MIMO Architecture Using the Exponential Correlation Matrix*," IEEE Communications Letters, vol. 5, no. 9, pp. 369–371, September 2001.

[47] A. van Zelst and J. S. Hammerschmidt, "*A Single Coefficient Spatial Correlation Model for MIMO Radio Channels*," in General Assembly of the International Union of Radio Science, 2002.

[48] I. Ouachani, "*Analyse de Performance de Systèmes de Communications Sans Fils Exploitant Micro et Macro Diversité*," Ph.D Thesis, Univerité de Paris-Sud, U.F.R. Scientifique d'Orsay, 28 Juin 2005.

[49] V. Tarokh, H. Jafarkhani, and A. R. Calderbank. "*Space-Time Block Codes From Orthogonal Designs*," IEEE Transactions on Information Theory, vol. 45, no. 5, pp. 1456–1467, July 1999.

[50] E. G. Larsson and P. Stoica, "*Space-Time Block Coding for Wireless Communication*," Cambridge Press, 2003.

[51] V. Choqueuse, M. Marazin, L. Collin, G. Burel, "*Blind Recognition of Linear Space–Time Block Codes: A Likelihood-Based Approach*," IEEE Transactions on Signal Processing, vol. 58, no. 3, March 2010.

[52] J. G. Gonzalez, "*Robust Techniques for Wireless Communications in Non-Gaussian Environments*," Ph.D. dissertation, University of Delaware, 1997.

[53] V. Choqueuse, "*Interception des Signaux Issus de Communications MIMO*," Ph.D Thesis, Traitement du signal et de l'image, Université de Bretagne Occidentale - Brest, France, 2008.

[54] V. Choqueuse, S. Azou, K. Yao, L. Collin, and G. Burel, "*Modulation Recognition for MIMO Systems*," Military Technical Academy Review, vol. 19, no. 2, pp. 183-196, June 2009.

[55] V. Choqueuse, L. Collin, K. Yao, and G. Burel, "*Reconnaissance Aveugle de Codages OSTBC Basée sur les Propriétés Matricielles des Statistiques d'Ordre 2*," in 21° Colloque GRETSI, pp. 249-252, Troyes, France, September 2007.

[56] A. Belouchrani, K. Abed-Meraim, J. F. Cardoso, and E. J. C. Moulines, "*A Blind Source Separation Technique using Second-Order Statistics*," IEEE Transactions on Signal Processing, vol. 45, no. 2, pp. 434-444, February 1997.

[57] A. T. James, "*Tests of Equality of Latent Roots of the Covariance Matrix*," in P. R. Krishnaiah Ed., Multivariate Analysis, vol. II, pp. 205-218, Academic Press, New York, 1969.

[58] T. W. Anderson, "*Asymptotic Theory for Pincipal Component Analysis*," Annals of Mathematical Statistics, vol. 34, no. 1, pp. 122-148, 1963.

[59] D. N. Lawley, "*Tests of Significance for the Latent Roots of Covariance and Correlation Matrices*," Biometrika, vol. 43, no. 1/2, pp. 128-136, 1956.

[60] H. Bolcskei, and A. Paulraj, "*Multiple-Input Multiple-Output (MIMO) Wireless Systems*," Communications Handbook, CRC Press, 2001.

[61] A. Ikhlef and D. Le Guennec, "*A Simplified Constant Modulus Algorithm for Blind Recovery of MIMO QAM and PSK Signals: A Criterion with Convergence Analysis*," EURASIP Journal on Wireless Communications and Networking, J. Wireless Commun. and Networking, vol. 2007, article ID 90401, 13 pages, December 2007.

[62] C. Papadias, "*Globally Convergent Blind Source Separation Based on A Multiuser Kurtosis Maximization Criterion*," IEEE Transactions on Signal Processing, vol. 48, no. 12, pp. 3508–3519, December 2000.

[63] S. C. Douglas, "*Combined Subspace Tracking, Pre-Whitening, and Contrast Optimization for Noisy Blind Signal Separation*," in Workshop Independent Component Analysis Source Separation, pp. 579–584, 2000.

[64] H. C. Wu, M. Saquib, and Z. Yun, "*Novel Automatic Modulation Classification using Cumulant Features for Communications via Multipath Channels*," IEEE Transactions on Wireless Communications, vol. 7, no. 8, pp. 3098–3105, August 2008.

[65] S. Kharbech, I. Dayoub, E. Simon, and M. Zwingelstein-Colin, "*Blind Digital Modulation Detector for MIMO Systems over High-Speed Railway Channels*," in International Workshop on Communication Technologies for Vehicles. Springer, pp. 232–241, May 2013.

[66] P. McCullagh, "*Tensor Methods in Statistics*," Chapman & Hall/CRC Monographs on Statistics & Applied Probability, vol. 161, London, August 1987.

[67] I. T. Jolliffe, "*Principal Component Analysis*," 2nd Ed., Springer, 2002.

[68] Z. Zhu, and A. K. Nandi, "*Automatic Modulation Classification: Principles, Algorithms and Applications*," Brunel University London, UK, John Wiley & Sons Ed., 2015.

[69] E. E. Azzouz, A.K. Nandi, "*Automatic Modulation Recognition of Communication Signals*," 1996th Ed., Springer, November 30, 1996.

[70] M. L. D. Wong and A. K. Nandi, "*Automatic Digital Modulation Recognition using Artificial Neural Network and Genetic Algorithm*," Elsevier, Signal Processing, pp. 351-365, 2004.

[71] D. Wang, M. Zhang, J. Li, Z. Li, J. Li, C. Song, and X. Chen, "*Intelligent Constellation Diagram Analyzer using Convolutional Neural Network-Based Deep Learning*," Optics Express, vol. 25, no. 15, pp. 17150–17166, 2017.

[72] Vladimir N. Vapnik, "*The Nature of Statistical Learning Theory*," 1st Ed., Springer-Verlag, New York, 1995.

[73] Vladimir N. Vapnik, "*The Nature of Statistical Learning Theory*," 2nd Ed., Statistics for Engineering and Information Science, Springer-Verlag, New York, 2000.

[74] A. Shigeo, "*Support Vector Machines for Pattern Classification*," Springer-Verlag, London, pp.21-26, 2010.

[75] L. Breiman, "*Random Forests*," Machine Learning, Springer, vol. 45, no. 1, pp. 5-32, 2001.

[76] M. Kubat, and M. Cooperson, "*A Reduction Technique for Nearest-Neighbor Classification: Small Groups of Examples*," Journal of Intelligent Data Analysis, vol. 5, no. 6, pp. 463–476, 2001.

[77] R. O. Duda, "*Pattern Classification*," 2nd Ed., John Wiley & Sons, 2001.

[78] Y. Song, J. Huang, D. Zhou et *al.*, "*Informative K-Nearest Neighbor Pattern Classification*," in European Conference on Principles of Data Mining and Knowledge Discovery (PKDD 2007), Springer-Verlag, pp. 248–264, Amsterdam, 2007.

[79] Erik G. Larsson, Petre Stoica, "*Space-Time Block Coding for Wireless Communications*," Cambridge University Press, 2003.

[80] Y. S. Cho, J. Kim, W. Y. Yang, and C. G. Kang, "*MIMO-OFDM Wireless Communications with MATLAB*," John Wiley & Sons, 2010.

[81] Paul H. Moose, "*A Technique for Orthogonal Frequency Division Multiplexing Frequency Offset Correction*," IEEE Transaction on Communications, vol. 42, no. 10, pp. 2908–2914, October 1994.

[82] M. L. Doelz, E. T. Heald, D. L. Martin, "*Binary Data Transmission Techniques for Linear Systems*," Proceedings of the IRE, vol. 45, no. 5, pp. 656–661, May 1957.

[83] G. A. Franco, G. Lachs, "*An Orthogonal Coding Technique for Communications*," IRE International Convention Record, vol. 9, pp. 126–133, 1961.

[84] Robert W. Chang, "*Synthesis of Band-Limited Orthogonal Signals for Multichannel Data Transmission*," The Bell System Technical Journal, vol. 45, no. 10, pp. 1775–1796, December 1966.

[85] B. R. Saltzberg, "*Performance of an Efficient Parallel Data Transmission System*," IEEE Transactions Communication Technology, vol. 15, no. 6, pp. 805–811, December 1967.

[86] R. Van Nee, R. Prasad, "*OFDM for Wireless Multimedia Communications*," Artech House Publisher, 2000.

[87] A. Goldsmith, "*Wireless Communications*," Cambridge University Press, New York, USA, 2005.

[88] A. Peled, and A. Ruiz, "*Frequency Domain Data Transmission using Reduced Computational Complexity Algorithms*," in ICASSP '80. IEEE International Conference on Acoustics, Speech, and Signal Processing, vol. 5, pp. 964–967, Denver, Colorado, USA, 9-11 April 1980.

[89] M. Marey, O. A. Dobre, R. Inkol, "*Blind STBC Identification for Multiple-Antenna OFDM Systems*," IEEE Transactions on Communications, vol. 62, no. 5, May 2014.

[90] X. Ma, M. K. Oh, G. B. Giannakis and D. J. Park, "*Hopping Pilots for Estimation of Frequency-Offset and Multiantenna Channels in MIMO-OFDM*," IEEE Transactions on Communications, vol. 53, no. 1, pp. 162-172, January 2005.

[91] T. Pollet, M. Van Bladel, and M. Moeneclacy, "*BER Sensitivity of OFDM Systems to Carrier Frequency Offset and Wiener Phase Noise*," IEEE Transactions on Communications, vol. 43, no. 2/3/4, pp. 191-193, February/March/April 1995.

[92] J. Lee, H. Lou, D. Toumpakaris, and J. M. Cioffi, "*Effect of Carrier Frequency Offset on OFDM Systems for Multipath Fading Channels*," IEEE Global Telecommunications Conference, GLOBECOM '04, Dallas, TX, USA, 29 November – 3 December 2004.

[93] A. Gangwar, M. Bhardwaj, "*An Overview: Peak to Average Power Ratio in OFDM System and its Effect*," International Journal of Communication and Computer Technologies, vol. 01, no.2, pp. 22-25, September 2012.

[94] M. Besseghier, and A. B. Djebbar, "*New Design of Pilot Patterns for Joint Semi-Blind Estimation of CFO and Channel for OFDM Systems*," International Journal of Electronics and Communications (AEU), vol. 69, no. 4, pp. 759–764, April 2015.

[95] U. Mengali, and Aldo N. D'Andrea, "*Synchronization Techniques for Digital Receivers*," Applications of Communications Theory Series, Springer, 1997.

[96] M. Button, J. Gardiner, and I. Glover, "*Measurement of the Impulsive Noise Environment for Satellite-Mobile Radio Systems at 1.5 GHz*," IEEE Transactions on Vehicular Technology, vol. 51, no. 3, pp. 551–560, May 2002.

[97] D. Middleton, "*Non-Gaussian Noise Models in Signal Processing for Telecommunications: New Methods and Results for Class A and Class B Noise Models*," IEEE Transactions in Information Theory, vol. 45, no. 4, pp. 1129–1149, May 1999.

[98] John P. Nolan, "*Numerical Calculation of Stable Densities and Distribution Functions*," Communications in Statistics: Stochastic Models. vol. 13, no. 4, pp. 759–774, 1997.

[99] John P. Nolan, "*Stable Distributions Models for Heavy Tailed Data*," Springer, Mathematical & Statistics, New York, 2016.

[100] O. E. Barndorff-Nielsen, T. Mikosch, S. I. Resnick, "*Levy Processes: Theory and Applications*," Springer Science & Business Media, New York, 2001.

[101] John P. Nolan, "*Multivariate Elliptically Contoured Stable Distributions: Theory and Estimation*," Computational Statistics, vol. 28, no. 5, pp. 2067–2089, January 2013.

[102] S. Kharbech, I. Dayoub, M. Zwingelstein-Colin, E. P. Simon, "*Blind Digital Modulation Identification for MIMO Systems in Railway Environments with High-Speed Channels and Impulsive Noise*," IEEE Transactions on Vehicular Technology, vol. 67, no. 8, pp. 7370-7379, August 2018.

[103] S. V. Zhidkov, "*Impulsive Noise Suppression in OFDM Based Communication Systems*," IEEE Transactions on Consumer Electronics, vol. 49, no. 4, pp. 944–948, November 2003.

[104] S. V. Zhidkov, "*Performance Analysis and Optimization of OFDM Receiver with Blanking Nonlinearity in Impulsive Noise Environment*," IEEE Transactions on Vehicular Technology. vol. 55, no. 1, pp. 234–241, January 2006.

[105] G. A. Tsihrintzis and C. L. Nikias, "*Fast Estimation of the Parameters of Alpha-Stable Impulsive Interference*," IEEE Transactions on Signal Processing, vol. 44, no. 6, pp. 1492-1503, June 1996.

[106] J. H. McCulloch, "*Simple Consistent Estimators of Stable Distribution Parameters*," Communications in Statistics-Simulation and Computation, vol. 15, no. 4, pp. 1109–1136, 1986.

[107] C. L. Nikias, and M. Shao, "*Signal Processing With Alpha-Stable Distribution and Application*," John Wiley & Sons, Inc, New York, USA, 1995.

[108] R. J. Barton, and H. V. Poor, "*On Generalized Signal-to-Noise Ratios in Quadratic Detection*," Springer-Verlag, Mathematics of Control, Signals and Systems, vol. 5, no. 1, pp. 81–91, New York, March 1992.

[109] King F. Lee, and Douglas B. Williams, "*A Space-Frequency Transmitter Diversity Technique for OFDM Systems*," in IEEE Global Telecommunications Conference. Conference Record (Cat. No.00CH37137), Globecom'00, San Francisco, CA, USA, vol. 3, pp. 1473–1477, 27 November – 1 December 2000.

[110] Y. Gong and K. B. Letaief, "*An Efficient Space-Frequency Coded Wideband OFDM System for Wireless Communications*," in IEEE International Conference on Communications. Conference Proceedings. ICC 2002 (Cat. No.02CH37333), New York, NY, USA, vol. 1, pp. 475–479, 28 April – 2 May 2002.

[111] W. Su, Z. Safar, M. Olfat, and K. J. R. Liu, "*Obtaining Full-Diversity Space-Frequency Codes from Space-Time Codes via Mapping*," IEEE Transactions on Signal Processing (Special Issue on MIMO Wireless Communications), vol. 51, no. 11, pp. 2905–2916, November 2003.

[112] H. Bölcskei, and A. J. Paulraj, "*Space-Frequency Coded Broadband OFDM Systems*," in IEEE Wireless Communications and Networking Conference. Conference Record (Cat. No.00TH8540), Chicago, IL, USA, pp. 1–6, September 23-28 2000.

[113] H. Bölcskei; A. J. Paulraj, "*Space-Frequency Codes for Broadband Fading Channels*," in IEEE International Symposium on Information Theory (IEEE Cat. No.01CH37252), Washington, DC, p. 219, June 24–29 2001.

[114] O. Oguz, U. Aygolu, and E. Panayirci, "*A Novel Space-Time-Frequency Coded System Design for OFDM over Fast Fading Channels*," Proceedings of the IEEE 12th Signal Processing and Communications Applications Conference in IEEE, Kusadasi, Turkey, April 30-30 2004.

[115] C. Wang et *al.*, "*On The Performance of the MIMO Zero-Forcing Receiver in the Presence of Channel Estimation Error*," IEEE Transactions on Wireless Communications, vol. 6, no. 3, pp. 805-810, March 2007.

[116] M. R. Mirarab, M. A. Sobhani, "*Robust Modulation Classification for PSK/QAM/ASK Using Higher Order Cumulants*," in 6th International Conference on Information, Communications & Signal Processing, Singapore, December 10-13 2007.

Université de Djillali Liabès - Sidi Bel Abbès -
Faculté de Génie Électrique
Département de Télécommunications
Laboratoire de Télécommunications et de Traitement Numérique du Signal (LTTNS)

Abstract

Research in the field of cognitive radio (CR) has emerged to meet both the military's communication and the public safety sector needs. The CR often share the same requirements as civilian radio-mobile telecommunication operators.

One of the main features of a CR device is to be aware of its radio environment and to detect available bands. The objective of the research work in this doctoral thesis is to develop a blind digital modulation identification algorithm that can be used for STBC-MIMO and STBC-OFDM systems.
The modulation identification process requires four steps: 1- The extraction of higher order statistics (HOS) from the signal; 2- HOS processing (normalization and use of PCA to keep only a subset of HOS with large variance); 3- The use of Pattern Recognition tools (ANN, SVM, RF and KNN) for modulation classification; 4- The improvement of classification using a decision fusion center. The results obtained show the effectiveness of the proposed algorithm.
Keywords: Multi-carrier, Cognitive radio, spectral sounding, blind waveform identification, multiple antennas, multiple-input multiple-output systems.

Résumé

Les recherches dans le domaine de la radio cognitive (CR) ont vu le jour afin de répondre aux besoins de communication de l'armée ainsi qu'aux besoins dans les secteurs de la sécurité publique. La CR partage souvent les mêmes exigences que les opérateurs de télécommunication radio-mobile civile.

Une des principales fonctionnalités d'un dispositif de radio cognitive est de prendre conscience de son environnement radioélectrique et de détecter les bandes disponibles. L'objectif du travail effectué dans le cadre de cette thèse de doctorat est de développer un algorithme qui sera utiliser pour l'identification aveugle de modulations numériques pour les systèmes STBC-MIMO et STBC-OFDM. Le processus d'identification de modulation exige quatre étapes : 1- L'extraction des statistiques d'ordre supérieur (HOS) à partir du signal ; 2- Le traitement des HOS (normalisation et utilisation de la PCA pour ne garder qu'un sous ensemble de HOS à grande variance) ; 3- L'utilisation des outils de Pattern Recognition (ANN, SVM, RF et KNN) pour la classification de modulation ; 4- L'amélioration la classification en utilisant un centre de fusion des décisions. Les résultats obtenus montrent l'efficacité de l'algorithme proposé.
Mots Clef: Multi-porteuses, Radio cognitive, sondage spectral, identification aveugle de la forme d'onde, antennes multiple, Systèmes multiple-input multiple-output.

ملخص

ظهرت الأبحاث في مجال الراديو الادراكي أو المعرفي (CR) لتلبية كل من الاتصالات العسكرية واحتياجات قطاع السلامة العامة. غالباً ما يتشارك CR نفس المتطلبات مع مشغلي الاتصالات اللاسلكية.

تتمثل إحدى السمات الرئيسية لجهاز CR في الانتباه إلى بيئته الكهرورادیویة واكتشاف النطاقات أو الترددات المتاحة. الهدف من العمل البحثي في أطروحة الدكتوراه هذه هو تطوير خوارزمية يمكن استخدامها لمعرفة التعديل الرقمي في أنظمة STBC-MIMO وSTBC-OFDM تتطلب عملية تحديد التعديل إلى أربع خطوات: 1)- إستخدام الإشارة المقدرة لاستخراج الإحصائيات برتبة أعلى (HOS) ؛ 2)- معالجة HOS (تحسين واستخدام PCA للحفاظ على مجموعة فرعية فقط من HOS مع تباين كبير)؛ 3)- استخدام أدوات التعرف على الأشكال (ANN، SVM، RFC، و KNN) لتصنيف التعديل، 4)- تحسين التصنيف باستخدام مركز دمج التصنيفات الفرعية. تُظهِر النتائج التي تم الحصول عليها فعالية الخوارزمية المقترحة.
كلمات مفتاحية: الموجات الحاملة المتعددة، الراديو الادراكي أو المعرفي، السبر الطيفي، التحديد الأعمى لشكل الموجة، هوائيات متعددة، أنظمة متعددة المخرجات متعددة المدخلات.